RHIC Multi-Year Beam Use Request
For Run 9 – Run 13

The STAR Collaboration
April 21, 2008

RHIC Multi-Year Beam Use Request
For Runs 9 – 13

The STAR Collaboration

April 21, 2008

1. Executive summary

The STAR Collaboration, in order to achieve its spin and relativistic heavy ion physics goals on a timescale consistent with intense international interest and competition in these areas, as well as to utilize RHIC beams effectively, taking full advantage of planned improvements in machine and detector capability as a function of time, makes the following five year beam use proposal:

Table 1: 25 cryo-weeks FY09 run, 18 weeks production with two species.

Run	Energy (GeV)	System	Time	Goal
9[1]	$\sqrt{s} = 200$	$p_\rightarrow p_\rightarrow$	12 weeks[a]	50 pb^{-1} P^{4}L 6.5 pb^{-1}
	$\sqrt{s} = 500$	$p_\uparrow p_\uparrow$	2 weeks[b]	Commissioning
	$\sqrt{s} = 200$	$p_\uparrow p_\uparrow$	½ week	pp2pp
	$\sqrt{s_{NN}} = 200$	Au + Au	3 weeks	0.3B minbias, 0.5 nb^{-1}
	$\sqrt{s_{NN}} = 5$	Au + Au	½ week[c]	Commisioning
10[2]	$\sqrt{s_{NN}} = 39 – 6.1$	Au + Au	14 weeks	1st energy scan
	$\sqrt{s_{NN}} = 5$	Au + Au	1 week[d]	Commisioning
	$\sqrt{s_{NN}} = 200$	Au + Au	2 weeks	200M central
	$\sqrt{s_{NN}} = 200$	Au + Au	1 week[e]	50M central
	$\sqrt{s} = 200$	$p_\rightarrow p_\rightarrow$	½ week	pp2pp
	$\sqrt{s} = 500$ or 200	$p_\uparrow p_\uparrow$ or $p_\rightarrow p_\rightarrow$	4 ½ weeks	Spin studies
11[2]	$\sqrt{s} = 200$	$p_\uparrow p_\uparrow$ or $p_\rightarrow p_\rightarrow$	6 weeks	20-30 pb^{-1}
	$\sqrt{s} = 500$	$p_\uparrow p_\uparrow$ or $p_\rightarrow p_\rightarrow$	15 weeks	150 pb^{-1}
	$\sqrt{s_{NN}} = 200$	U + U	2 weeks[f]	Commissioning
12[3]	$\sqrt{s_{NN}} = 200$	Au + Au	12 weeks	0.5B minbias, 5 nb^{-1}
	$\sqrt{s_{NN}} = 39 – 5$	Au + Au	13 weeks	2nd energy scan
13[3]	$\sqrt{s} = 200$	$p_\uparrow p_\uparrow$ or $p_\rightarrow p_\rightarrow$	13 weeks	2B minbias, 100 pb^{-1}
	$\sqrt{s} = 500$	$p_\uparrow p_\uparrow$ or $p_\rightarrow p_\rightarrow$	12 weeks	300 pb^{-1}

(1) 25 cryo-weeks, 18 weeks production with two species
(2) 30 cryo weeks, 23 weeks production with two species.
(3) 30 cryo weeks, 25 weeks production with one species.

(a) 60% or higher polarization at both yellow and blue rings is needed. Spin flipper development desirable.
(b) Contingent on C-AD achieving efficiencies in accelerator and beam set-up.
(c) C-AD low energy test, contingent on achieving goals with transverse stochastic cooling.
(d) C-AD test for higher luminosity at the lowest energy.
(e) photon converter HBT test program.
(f) HFT fingers prototyping.

Table 2: 16 cryo-weeks, FY09 run, 11 weeks for production with one species.

Run	Energy (GeV)	System	Time	Goal
$9^{(1)}$	$\sqrt{s} = 200$	$p_\rightarrow p_\rightarrow$	11 weeks[a]	50 pb^{-1}, P^{4}L 6.5 pb^{-1}
	$\sqrt{s} = 200$	$p_\uparrow p_\uparrow$	½ week[b]	pp2pp
$10^{(2)}$	$\sqrt{s_{NN}} = 39 - 6.1$	Au + Au	12 weeks	1st energy scan
	$\sqrt{s_{NN}} = 5$	Au + Au	1 week[c]	Commissioning
	$\sqrt{s_{NN}} = 200$	Au + Au	3 ½ weeks	0.5B events, 0.5 nb^{-1}
	$\sqrt{s_{NN}} = 200$	Au + Au	1 week[d]	50M central
	$\sqrt{s} = 500$	$p_\uparrow p_\uparrow$ or $p_\rightarrow p_\rightarrow$	5 weeks[e]	Commissioning
	$\sqrt{s} = 200$	$p_\uparrow p_\uparrow$ or $p_\rightarrow p_\rightarrow$	½ week	pp2pp
$11^{(2)}$	$\sqrt{s} = 200$	$p_\uparrow p_\uparrow$ or $p_\rightarrow p_\rightarrow$	6 weeks	20-30 pb^{-1}
	$\sqrt{s} = 500$	$p_\uparrow p_\uparrow$ or $p_\rightarrow p_\rightarrow$	15 weeks	150 pb^{-1}
	$\sqrt{s_{NN}} = 200$	U + U	2 weeks[f]	Commissioning
$12^{(3)}$	$\sqrt{s_{NN}} = 200$	Au + Au	12 weeks	0.5B minbias, 5 nb^{-1}
	$\sqrt{s_{NN}} = 39 - 5$	Au + Au	13 weeks	2nd energy scan
$13^{(3)}$	$\sqrt{s} = 200$	$p_\uparrow p_\uparrow$ or $p_\rightarrow p_\rightarrow$	13 weeks	2B minbias, 100 pb^{-1}
	$\sqrt{s} = 500$	$p_\uparrow p_\uparrow$ or $p_\rightarrow p_\rightarrow$	12 weeks	300 pb^{-1}

(1) 16 cryo weeks, 11 weeks production with one species.
(2) 30 cryo weeks, 23 weeks production with two species.
(3) 30 cryo weeks, 25 weeks production with one species.
(a) 60% or higher polarization at both yellow and blue rings is needed. Spin flipper development desirable.
(b) Contingent on achieving goals with longitudinal running
(c) C-AD test for higher luminosity at the lowest energy
(d) photon converter HBT test program
(e) Contingent on C-AD achieving efficiencies in accelerator and beam set-up
(f) HFT fingers prototyping

Upgrade	Completion	Key physics measurements
FMS	Fall 2007 Ready for Run 08	(a)Transverse asymmetry at forward rapidity (b) CGC
TPC DAQ (DAQ1000)	Summer 2008 Ready for Run 09	Large data set, minimal dead time
MRPC TOF	Summer 2009 Full TOF ready for Run 10	Full PID in full azimuthal acceptance
FGT	Summer 2010 Ready for Run 11	Forward $W^\pm$ for flavor separated quark polarization
HFT	Summer 2011 Ready for Run 12	(a) Precision hadronic ID for Charm and Bottom hadrons (b) Charm and Bottom hadron energy loss and flow

Table 3: Timeline for STAR major upgrade and key physics measurements.

In this proposed physics-driven plan, the STAR Collaboration intends to make the most efficient use of RHIC beam time and upgrades in order to make timely progress in determining the properties of the new state of matter produced at RHIC, to map the x dependence of the gluon polarization in the proton, $\Delta G(x)$, and to perform a definitive search for the phase boundary and the existence and location, if it exists, of the QCD critical point.

The primary goals of the proposed program are:

Run 9#: 25 cryo-weeks, 18 weeks for physics production with two species:
a) Initial map at $\sqrt{s} = 200$ GeV of the x dependence of gluon polarization in the proton, $\Delta G(x)$
b) C-AD commissioning of $\sqrt{s} = 500$ GeV pp collisions to study the environment at the the new energy with polarized beams
c) Qualitative advance in the study of transversely polarized pp elastic scattering
d) C-AD development of transverse stochastic cooling for 200 GeV Au+Au collisions

Run 9##: 16 cryo-weeks, 11 weeks for physics production with one species::
a) Initial map at $\sqrt{s} = 200$ GeV of the x dependence of gluon polarization in the proton, $\Delta G(x)$

Run 10#: 30 cryo-weeks, 23 weeks for physics production:
a) Search for the existence and location of the QCD Critical point. First energy scan from $\sqrt{s_{NN}} = 39$ to 6.1 GeV Au+Au collisions, combined with C-AD test to increase luminosity for $\sqrt{s_{NN}} = 5$ GeV Au+Au collisions
b) 200 GeV Au+Au low material run with full Time-of-Flight
c) First measurement of photon HBT with 10% absorberr

d) Complete the pp elastic scattering program with longitudinally polarized collisions
e) Further spin studies, guided by progress achieved in Run 9

Run 10##: 30 cryo-weeks, 23 weeks for physics production:
    a) Search for the existence and location of the QCD Critical point. First energy scan from $\sqrt{s_{NN}}$ = 39 to 6.1 GeV Au+Au collisions, combined with C-AD test to increase luminosity for $\sqrt{s_{NN}}$ = 5 GeV Au+Au collisions
    b) C-AD development of transverse stochastic cooling for 200 GeV Au+Au collisions, combined with low material run with full Time-of-Flight
    c) First measurement of photon HBT with 10% absorber
    d) Qualitative advance in the study of polarized pp elastic scattering with pp2pp program
    e) C-AD commissioning of $\sqrt{s}$ = 500 GeV pp collisions to study the environment at the new energy with polarized beams

Run 11: 30 cryo-weeks, 23 weeks for physics production:
    a) Complete the map at $\sqrt{s}$ = 200 GeV of the x dependence of gluon polarization in the proton, $\Delta G(x)$; starts on any transverse spin milestones.
    b) First measurement of flavor dependence of sea quark / anti-quark polarization in the proton at $\sqrt{s}$ = 500 GeV
    c) HFT prototyping in $\sqrt{s_{NN}}$ = 200 GeV U+U collisions

Run 12: 30 cryo-weeks, 25 weeks for physics production:
    a) First HFT physics measurements of charm hadron $v_2(p_T)$ and $R_{CP}(p_T)$ in $\sqrt{s_{NN}}$ = 200 GeV Au+Au collisions
    b) Second energy-scan measurements in the search for the QCD critical point. Accelerator development is crucial for the measurement at $\sqrt{s_{NN}}$ = 5 GeV

Run 13: 30 cryo-weeks, 25 weeks for physics production:
    a) HFT physics reference measurement of charm hadron spectra in $\sqrt{s}$ = 200 GeV pp collisions; complete any remaining sqrt(s) = 200 GeV spin milestones.
    b) Measurement of the x dependence of gluon polarization and W production at $\sqrt{s}$ = 500 GeV

#: Corresponding to a relatively long run in FY09: 25 cryo-week
##: Corresponding to a short run in FY09: 16 cryo-week

In the period from Run 9 to 10, our top priorities are:
(1) Measurements using longitudinally polarized pp collisions at $\sqrt{s}$ = 200 GeV, allowing a significant map of the *x*-dependence of the gluon polarization from approximately 0.03 < *x* < 0.3. Smaller values of *x* will subsequently be probed in 500 GeV running. Contingent on C-AD achieving efficiencies in accelerator and beam set-up, we propose commissioning time dedicated to preparing for a future $\sqrt{s}$ = 500 GeV polarized proton run.
(2) Energy Scan in Au+Au collisions starting at $\sqrt{s_{NN}}$ = 39 − 6.1* GeV. (* The lowest collision energy at this period is determined by the collision rates. We plan to scan lower energies later, when luminosities are improved significantly.) This energy region

corresponds to a range in baryon chemical potential from 130 - 400 MeV and freeze-out temperature from 170 – 120 MeV in the QCD phase diagram.

(3) Development of transverse stochastic cooling for Au beams at $\sqrt{s_{NN}}$=200 GeV, which is critical for the future of the RHIC program. We propose to test it in Run 9 if possible. However, if the run is only 16 weeks long, the overhead involved is too large to permit two species. In that case, the transverse stochastic cooling test should occur during Run 10.

The DAQ1000 upgrade to the TPC readout electronics will be complete in Run 9, and the full barrel of the MRPC Time-of-Flight upgrade will be complete in Run 10. Coupled with DAQ1000, the possibility of on-line tracking is under consideration in the collaboration.

In the period from Run 11 to 13, the highest priorities will be to:

(1) Complete the minimum goal of 50 pb^{-1} sampled in longitudinal spin running to map the x-dependence of ΔG at $\sqrt{s}$ = 200 GeV no later than Run 11;

(2) Continue the energy scan program with the beam energy down to $\sqrt{s_{NN}}$ = 5 GeV, the most crucial step in the searching for the QCD critical point;

(3) Make significant measurements of the flavor-identified q and q-bar contributions to the spin of the proton via the longitudinal-spin asymmetry of W production at $\sqrt{s}$ = 500 GeV, using the FGT upgrade;

(4) Start the physics program with heavy flavor hadrons, enabled by the HFT upgrade, and the program with the high luminosities of RHIC II, enabled by stochastic cooling in Au+Au collisions at 200 GeV and sufficient reference data in p+p at 200 GeV;

(5) Search for evidence of repulsive color-charge interactions in the Sivers effect in correlations between forward photons and mid-rapidity jets.

In this period, both the upgrades FGT, for W measurements, and the HFT, for Charm and Bottom hadrons, will be completed

2. Report on data taking in Run 8

A primary scientific goal for STAR during Run 8 was to determine whether or not gluon saturation is the origin of the particle suppression that has been observed in d+Au in the forward region. The primary spin goal during the pp part of the run stated in the Run 8 STAR Beam Use Request was to obtain the first significant measurement of the x dependence of the gluon polarization in the proton. The severely curtailed duration of Run 8 made it impossible to accomplish this spin goal. Therefore, STAR chose to pursue one of the other goals described in the Run 8 Beam Use Request, extending the x_F and p_T range of the transverse single-spin asymmetries that we have observed in forward π^0 production and embarking on direct photon transverse-spin asymmetry measurements in the forward direction. Other goals that STAR hoped to accomplish included performing non-photonic electron measurements in both p+p and d+Au systems with very little material in the center of the STAR detector and measuring Upsilon and D-meson yields in d+Au collisions. Finally, STAR hoped to record a few thousand good events during the brief low-energy Au+Au test run.

The data acquisition targets for Run 8 are shown in Table 4. As seen in the Table, the goals for the d+Au run were all met, as was that for the Au+Au low-energy test. STAR also did well on the luminosity-based goals for the p+p run, but fell well short of the transverse polarization figure-of-merit goal.

Table 4: Data acquisition goals for Run 8.

System	Trigger	Goal	Acquired
d+Au	FMS	Original: 60 nb^{-1} Reduced: 30 nb^{-1}	49 nb^{-1}
d+Au	BEMC High Tower	30 nb^{-1}	36 nb^{-1}
d+Au	Minimum bias	30 M usable events	46 M usable events
p+p	FMS integrated luminosity	9 pb^{-1}	7.8 pb^{-1}
p+p	FMS integrated figure-of-merit (P^2L)	3.8 pb^{-1}	1.6 pb^{-1}
p+p	BEMC High Tower	4.5 pb^{-1}	3.1 pb^{-1}
Low-energy test Au+Au	Minimum bias	Few thousand good events	Few thousand good events

STAR approached the original goal that we set for integrated sampled luminosity with the FMS during the d+Au run and exceeded the reduced goal that was established when it was decided that the d+Au run would end ~10 days sooner than had been expected. These data will be analyzed in conjunction with the FMS data that were recorded under identical

conditions during the p+p run to provide an in-depth search for forward mono-jets in d+Au, as predicted in the Color Glass Condensate model.

STAR exceeded the goals that we set for d+Au BEMC high-tower triggered events. They will be used to perform a measurement of the non-photonic electron spectrum in d+Au with much reduced background from conversion electrons when compared to Run 3. The high-tower triggered events will also provide a measurement of the Upsilon yield in d+Au with statistics that are comparable to the measurements STAR has performed in p+p and Au+Au. In p+p, STAR sampled 3.1 pb^{-1} with our BEMC high-tower triggers or 69% of our goal. This overall slow detector luminosity goal was missed due to a priority decision to record data in p+p with significantly lower prescale factors at any given p_T than were used in d+Au enhancing those specific triggers. Hence, the event yields that were recorded during the d+Au and p+p runs are comparable. The d+Au and p+p data sets should help to resolve the current difference between STAR and PHENIX regarding the magnitude of the open charm cross section.

STAR exceeded the goal that we set for usable minimum bias events in d+Au. They will be used to measure the D-meson spectrum, thereby providing an important reference for the measurements that are currently underway in Cu+Cu (Run 5) and Au+Au (Run 7). The same events will provide reference data for a broad range of correlation measurements that are underway in heavy-ion collisions.

The only major shortfall during Run 8 was that the integrated transverse figure-of-merit for the FMS was only 1.6 pb^{-1} or 43% of our goal. This number has been calculated using the blue beam polarization values as reported by the CNI polarimeter, scaled down by a factor of 1.14 to account for the calibration of the CNI asymmetries that was reported to the RHIC Spin Collaboration by the polarized jet group. The blue beam polarization is relevant for FMS measurements. These data will permit a significant extension of the x_F and p_T range of the STAR π^0 forward single-spin asymmetries, but that extension will fall well short of what we had intended to achieve. The data will also permit studies of direct photon detection with the FMS, but the low figure-of-merit means that direct photon transverse-spin asymmetry measurements probably will not be practical. The integrated figure-of-merit would have been even smaller if calculated using the yellow beam polarizations, as appropriate for measurements with the Forward Pion Detector on the east end of STAR.

The Forward Meson Spectrometer played a central role in STAR's data acquisition goals during Run 8. The FMS is a new Pb-glass electromagnetic calorimeter that spans the pseudorapidity interval $2.5 < \eta < 4.0$ and the full azimuth. Consequently, it is sensitive to a broad mass range of particles that decay to $\gamma\gamma$ or e^+e^- and are produced at large Feynman x in ion collisions at RHIC. Large x_F physics at RHIC energies remains a frontier, with little known. Earlier RHIC runs have clearly established striking transverse spin effects, and particle suppression in heavy ion collisions that may signal the onset of gluon saturation. There is intrinsic interest in large-x_F J/ψ production. Clear understanding of the large pair mass region is also a requirement of a future measurement of transverse single spin asymmetries for the Drell Yan production of dilepton pairs.

The preliminary results of FMS are shown in Figure 2-1. The analysis is applied to events where the total energy deposited in the FMS is Etot>20 GeV and $20 < p$z,tot$ < 25$ GeV/c. The $\pi^0 \rightarrow \gamma\gamma$ peak is being used to calibrate the energy scales of individual FMS cells. The tail of the pair mass distribution extends to large mass. Peak positions, widths and signal-to-background ratios will be strongly influenced by the ongoing calibration efforts.
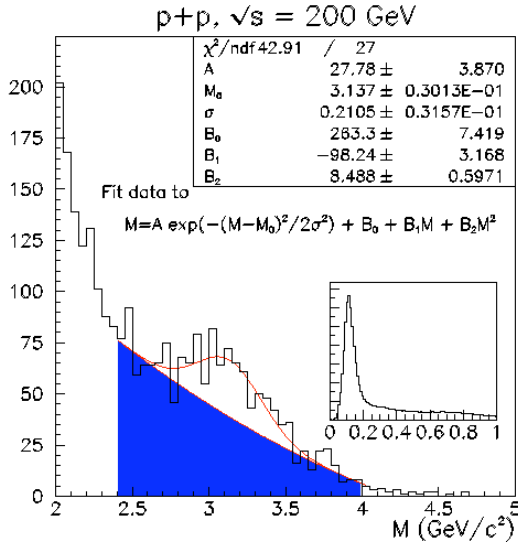

Figure 2-1: Clustering and shower-shape analysis that were developed for the forward peon detector have been adapted and applied to Run 8 data from the Forward Meson Spectrometer. (Inset) Mass distribution from all pairs after clustering and shower shape analysis

The last two days of Run 8 were devoted to a low-energy Au+Au test at $\sqrt{s_{NN}} = 9$ GeV. Previously, it had been determined that STAR recorded essentially no real collisions during the short Au+Au low-energy test in Run 7. The goal for this test run was to observe real collisions to establish the RHIC luminosity scaling at low $\sqrt{s_{NN}}$ and to collect a few thousand good events. Several different triggers were tried. Preliminary analysis indicates that we succeeded in recording at least a few thousand good events, but the precise number is not yet known.

In addition to our data acquisition goals, STAR was very successful during Run 8 in commissioning new detectors for the future. One entire sector of the TPC (out of 24) was instrumented with DAQ1000 electronics prior to Run 8. They were commissioned early in the run, then used in normal data-taking through the last 6 weeks of the d+Au run and all of p+p. During p+p, the DAQ1000 sector was read out at a typical rate of 250 Hz. A special test demonstrated operation at 1000 Hz with only 5-7% dead time, meeting specifications. Preliminary analysis of the data also indicates that DAQ1000 is achieving good *dE/dx*-based particle identification, as illustrated in Figure 2-2 and Figure 2-3. The entire DAQ1000 system will be installed before Run 9.

Five Time-of-Flight trays, instrumented with the final TOF electronics, were installed outside the DAQ1000 sector of the TPC. The TOF system was commissioned during the d+Au run. It was then included in the normal data stream during the p+p run. A total of 78 M minimum bias p+p events were recorded with TOF+DAQ1000. Figure 2-3 shows a preliminary analysis of a small fraction of the data. Very good π-*K*-*p* separation is seen,

which implies that both the DAQ1000 tracking and the TOF time measurements are performing as expected. At least half of the TOF trays will be installed before Run 9, and the entire system will be in place for Run 10.
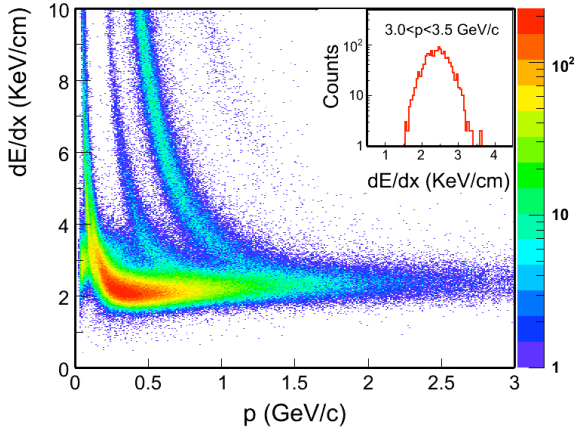

Figure 2-2: Preliminary results for TPC dE/dx vs. momentum measured with the DAQ1000 sector during the p+p run.
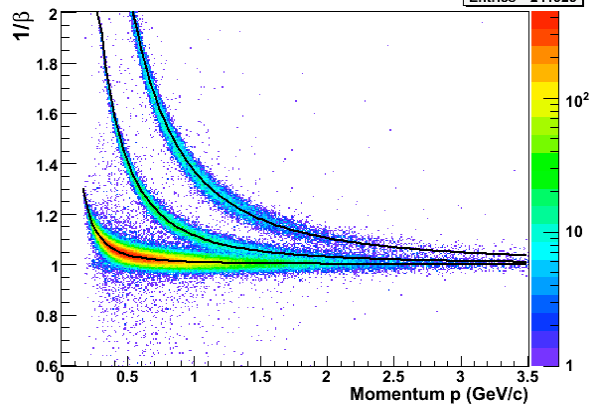
Figure 2-3: Preliminary results for particle identification with TOF combined with DAQ1000 tracking. The solid lines show the expected locations for the pion, kaon, and proton bands.

The Collider-Accelerator Division installed the pp2pp Roman pot systems east and west downstream of STAR prior to Run 8. Over the course of Run 8, pp2pp was integrated into the STAR trigger and data acquisition systems. The Roman pots were then inserted into the beam pipes and used to trigger STAR during the last 2 hours of the p+p run. The trigger rates in pp2pp were as expected, and no impact was seen on the background levels in the STAR mid-rapidity detectors.

3. Polarized proton results and proposed running for Run 9

3.1. Report on data taking in Run 6

STAR sampled a total luminosity of approximately 8.5 pb^{-1} with longitudinal beam polarization and approximately 3.4 pb^{-1} with slow detectors and 6.8pb^{-1} with fast detectors with transverse beam polarization at √s = 200 GeV during Run 6. In addition, at the end of Run 6, STAR collected a total of 0.1 pb^{-1} at √s = 62 GeV using transversely polarized beams. The longitudinal data sample was split between an initial sample of 2.1 pb^{-1} during the beginning of Run 6 and 6.4 pb^{-1} at the end of the 200 GeV data taking period. These two samples were separated by data taken with transversely polarized beams. Beginning with the start of the transverse running period at √s = 200 GeV, the average beam polarization in both RHIC beams was approximately 60%. The longitudinal data sample taken during Run 6 was the last data sample taken up to this point at longitudinal beam polarization. The original beam use request for Run 8 asked for a longitudinal data sample taken over 12 weeks with an anticipated total recorded luminosity of approximately 30pb^{-1}. Due to budget shortcomings, this data sample was not taken.

During Run 6, significant improvements in RHIC's capability as a polarized proton-proton collider as well as in STAR detector acceptance and trigger capability resulted in a dramatic change in the quality, magnitude, and richness of the spin data acquired. The simultaneous improvements in integrated luminosity and polarization in 2006 yielded at least a factor of 4 gain in the figure of merit LP^4 compared to 2005 for the measurement of any double spin asymmetry while allowing for significant running time with longitudinal polarization.

The result of these advances in the quality of the beam delivered and STAR's ability to mine the collisions was a Run 6 data set that far surpassed all previous polarized proton runs in terms of physics content. The combination of extended calorimetric coverage, reduction of the background trigger rate, and more intelligent triggering decisions increased the size the recorded di-jet sample by almost an order-of-magnitude per unit integrated luminosity compared to 2005. From these data, quantitative estimates of the magnitudes of the gluon and quark Sivers functions in several kinematic regions have been extracted and published. These data were compared to existing results from semi-inclusive DIS [1,2] and lead to an important understanding of the initial and final state interactions necessary to generate a Siver's affect. Data taken with the FPD have allowed STAR to map out the x_F and p_T dependences of the large neutral pion spin asymmetries observed earlier in STAR at high rapidity, recently submitted for publication, and to search for jets and direct photons in this regime. The longitudinally polarized runs have extended the existing STAR results on A_{LL} for inclusive jets and neutral pions to higher p_T, and, due to improvements in triggering and acceptance, they have provided the first substantial sample of di-jets. In particular A_{LL} preliminary results for inclusive jets have been released and already included in a new global analysis demonstrating important new constraints on ΔG. In addition the Run 6 data is crucial to the development of algorithms for identifying direct photons in the EMC's.

Further progress on the Run 6 published results, preliminary results and ongoing analyses will be discussed in the next sections.

3.2. Recent spin physics results

3.2.1. STAR transverse spin program

The study of transverse spin effects, both theoretically and experimentally, has received a great deal of attention in recent years. The ultimate goal of this effort is to extract transversity distribution functions and determine possible orbital angular momentum effects.

The first measurement of a transverse single-spin asymmetry, A_N, for forward neutral pion production at $3.3 < \eta < 4.1$ by the STAR collaboration[3] was found to increase with x_F and to be similar in magnitude to the measurement of A_N performed by the E704 experiment at $\sqrt{s} = 20$ GeV[4]. The STAR collaboration has performed cross-section measurements for forward neutral pion production at $<\eta>=3.3$, 3.8 and 4.0, which are in good agreement with next-to-leading order (NLO) perturbative QCD calculations[5]. This provides an important basis for the interpretation of the sizable measured asymmetries at forward rapidity. Several models beyond a conventional collinear perturbative QCD approach are able to account for the measured asymmetries. The essential idea is an extension to pQCD that introduces transverse momentum dependence (TMD) correlated with spin degrees of freedom. These models are based on three main correlation concepts: A correlation of the parton intrinsic transverse momentum k_T and the proton spin in the initial state ('Sivers effect')[6], a correlation between the quark spin and the hadron k_T in the final state ('Collins effect')[7] and a higher twist correlation in the initial and final state[8,9]. Spin-correlated TMD distribution functions ('Sivers effect'), in conjunction with initial- and final-state color-charge interactions, can explain large A_N effects. These functions describe parton orbital motion within the proton, and are therefore important to gain further insight into the spin structure of the proton. The STAR collaboration performed an upgrade of the Forward Pion Detector (FPD) for Run 6 as a prototype for the Forward Meson Spectrometer (FMS). The main goal is to disentangle different mechanisms responsible for the observed large transverse single-spin asymmetries in the forward direction.

New results for forward neutral pion production at higher precision are shown in Figure 3-1, which have recently been submitted for publication to Physical Review Letters[10]. These results are in good agreement with previous results, but have higher precision. The measured asymmetry A_N is found to be consistent with zero at negative x_F and grows from 0 at $x \sim 0.2$-0.3 up to 0.1 at $x_F \sim 0.6$. The figure also shows the results of two calculations at different $<\eta>$ values[11,12]. The measured asymmetries are precise enough to allow for a quantitative comparison with theory predictions. The measured x_F dependence in A_N is found to be in fair agreement with both a collinear twist-3 calculation and a calculation assuming factorization that attributes the spin effects to spin-correlated intrinsic transverse momentum of the quarks within the proton. The extended kinematic region in x_F and p_T and

the increase in the available data sample from Run 6 allow a mapping of A_N in x_F and p_T for the first time. Figure 3-1 (right) shows A_N as a function of p_T in fine bins of x_F. The current measured results for A_N do not support a decreasing behavior of A_N with p_T in all x_F bins as expected by various theoretical models, in particular those shown in the figure. Future measurements capable of disentangling TMD fragmentation and distribution function contributions to neutral pion spin effects, and measurements of A_N for real and virtual photon production sensitive to only Sivers contributions, are required to definitely establish if partonic motion is the correct explanation of these effects.
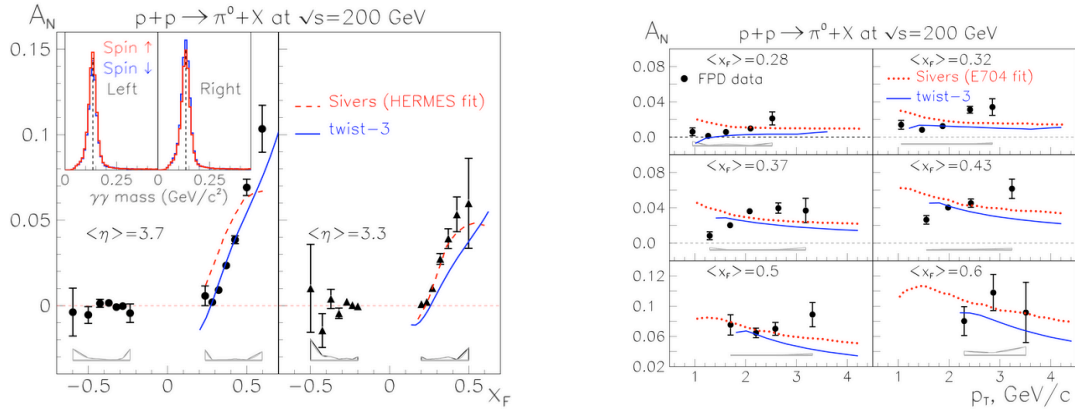

Figure 3-1: (Left) AN as a function of x_F for p+p $\rightarrow \pi^0$+X from Run 6. The error bars represent statistical errors only. Systematic uncertainties are indicated by the bands at the bottom of the plots. The solid blue line represents the result of a twist-3 calculation[11]; the dashed red line is the result of a calculation based on the Sivers effect[12]. (Right) A_N as a function of p_T for p+p $\rightarrow \pi^0$+X from Run 6 in bins of x_F in comparison to a calculation based on the Sivers effect[12] (dashed red line) and twist-3 calculation[11] (solid blue line).

The role of orbital angular momentum as represented by Siver's functions was also investigated and published as a Phys. Rev. Letter[13] in the past year. One possible manifestation of orbital angular momentum effects could be realized through a non-zero Sivers type correlation of the parton intrinsic transverse momentum k_T and the proton spin in the initial state. The HERMES collaboration recently reported a non-zero Sivers function in semi-inclusive DIS for π^+ production[14]. The Sivers function for π^- production has been found to be consistent with zero. This led to the interpretation that the Sivers functions are opposite in sign and different in magnitude for u quarks compared to d quarks. The study of Sivers type correlations in polarized proton-proton collisions has been considered in ref.[15]. The theoretical expectation is that the Sivers effect would be reflected in a spin-dependent side-ways boost observed as a corresponding spin-dependent asymmetry in the back-to-back di-jet opening angle. A measurement of the correlation between the spin direction and di-jet bi-sector direction was performed to search for this effect. A dedicated Level 2 di-jet trigger, utilizing the STAR Barrel and Endcap Electromagnetic Calorimeters (BEMC and EEMC), was implemented during Run 6 to provide a sufficient sample of di-jet events for the study.
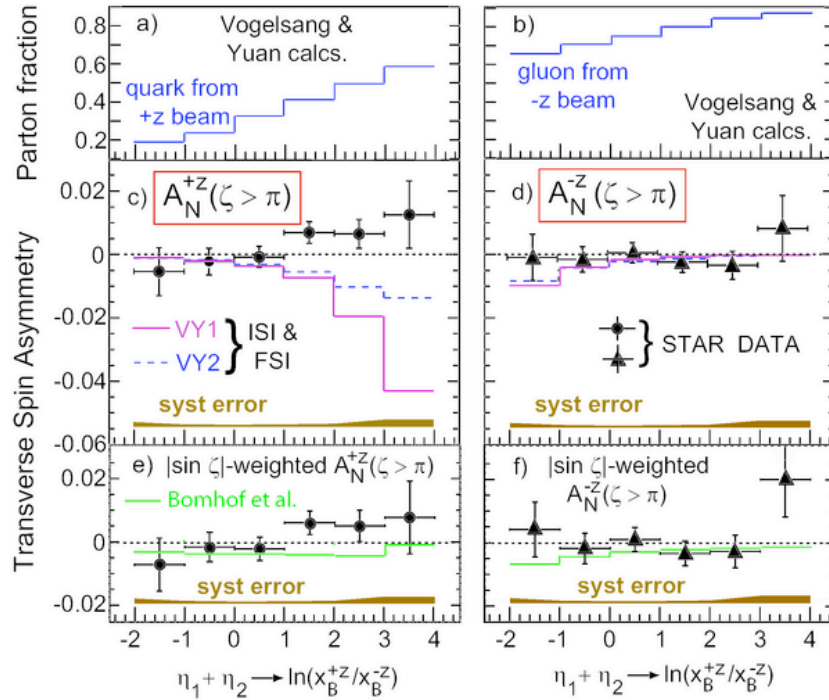
Figure 3-2: Transverse single-spin asymmetries for AN+z (left) and AN-z (right) as a function of $\eta_1+\eta_2$ for di-jet production at $\sqrt{s} = 200$ GeV from Run 6 in comparison to theoretical calculations[2,16] . (a,b): Fraction of the calculated di-jet cross section with a quark (gluon) from the +z (-z) beam. (c,d): Unweighted asymmetries compared with pQCD calculations for two models of quark Sivers functions fitted to SDIS results. (e,f): Asymmetries for weighted yields, compared with calculations based on twist-3 quark-gluon correlations.

Figure 3-2 shows the measured transverse single-spin asymmetry, A_N, for di-jet production as function[13] of $\eta_1+\eta_2$. The region of large $\eta_1+\eta_2$ values emphasizes quark (gluon) Sivers effects for +z (–z). In both cases, the measured transverse single-spin asymmetries are found to be consistent with zero. The measured results are compared to predictions based on u and d quark Sivers functions extracted from measured HERMES semi-inclusive DIS data, which assume a zero gluon-type Sivers function[2,16]. pQCD calculations can reconcile these results with sizeable SSA observed for forward hadron production in pp and for semi-inclusive deep inelastic scattering via canceling contributions from u and d quarks and from initial- and final-state interactions. These data constrain unified theoretical accounts for transverse SSA in hard pQCD processes, and their connection to parton orbital momentum.

3.2.2. STAR longitudinal spin program

The longitudinal STAR spin physics program profits enormously from the unique capabilities of the STAR experiment for large acceptance jet production, identified hadron production and photon production[17]. The measurement of the gluon polarization through

15

inclusive measurements such as jet production and π^0 production has so far been the prime focus of the physics analysis program of the Runs 3, 4, 5, and 6 data samples. The sensitivity of these inclusive measurements to the underlying gluon polarization in high-energy polarized proton-proton collisions has been discussed in detail[18]. Inclusive hadron production and jet production are strongly affected by the relative contributions from quark-quark, quark-gluon and gluon-gluon subprocesses. The low p_T region is dominated by gluon-gluon scattering, while at high p_T the quark-gluon contribution starts to become important. As a result, the sign of A_{LL} in this high p_T region indicates the sign of the gluon polarization. The fact that the inclusive photon channel is dominated by quark-gluon scattering results in a strong sensitivity to the underlying gluon polarization, despite the small production cross-section. Throughout the following discussion, four gluon polarization scenarios have been used as input to NLO perturbative QCD calculations of A_{LL}. The GRSV standard case refers to the best global analysis fit to polarized DIS data[19]. The case for a vanishing gluon polarization (GRSV-ZERO) and the case of a maximally positive (GRSV-MAX) or negative (GRSV-MIN) gluon polarization have been also considered. In addition, the global analysis result by the group of Gehrmann and Sterling (GS) has been used, specifically the set C of polarized parton distribution functions. In this set, the polarized gluon distribution function has a node in the measured kinematic region being negative at large x and positive at low x values, which results overall in a larger first moment value compared to the GRSV-STD scenario.

The first longitudinal double-spin asymmetry measurement for inclusive jet production and the associated inclusive jet cross-section measurement at mid-rapidity has been published[20] based on data taken during Runs 3 and 4. The measured asymmetries are consistent with NLO perturbative QCD calculations based on DIS polarized lepton-nucleon data, and disfavor a large positive value of the gluon polarization in the proton. In addition, the STAR collaboration has recently submitted the Run 5 longitudinal double-spin asymmetry measurement to Physical Review Letters[21]. The recently released Run 6 measurement of the longitudinal double-spin asymmetry provides a substantial improvement over previous measurements and clearly rules out extreme gluon polarization scenarios, suggesting that the gluon polarization in the measured kinematic region is rather small. Furthermore, an update of the preliminary result on neutral pion production based on Run 6 data has recently been released. The (unpolarized) cross-section measurements of inclusive jet and neutral pion production support applicability of perturbative QCD.

The following measurements of A_{LL} from Run 5 at at $\sqrt{s}$=200GeV for identified hadron production and inclusive jet production are based on an average beam polarization of approximately 50% and a data sample of approximately 3 pb^{-1}. The overall normalization uncertainty due to conservative error estimates on the preliminary polarization values amounts to ~40%. All A_{LL} analyses presented below make use of the STAR BEMC and EEMC system at the trigger and reconstruction level. A high-tower (HT1 / HT2) trigger is based on an energy threshold for a single tower ($\Delta\eta$ x $\Delta\phi$ = 0.05 x 0.05) whereas a jet-patch (JP1 / JP2) trigger is based on an energy threshold for a group of towers over a region in η and ϕ of $\Delta\eta$ x $\Delta\phi$ = 1.0 x 1.0. Both triggers are taken in coincidence with a minimum-bias condition using the STAR Beam-Beam Counter.

$\vec{p}+\vec{p} \rightarrow \pi^0 + X$ at $\sqrt{s}$ = 200 GeV and -.95 < η < .95
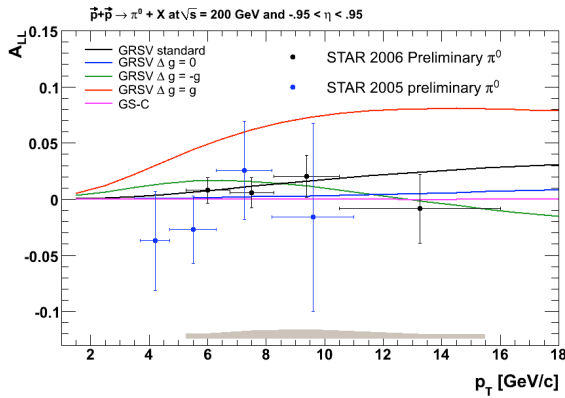
Figure 3-3: Longitudinal double-spin asymmetry A_{LL} for neutral pion production at $\sqrt{s}$ = 200 GeV as a function of p_T for Runs 5 and 6 in comparison to several gluon polarization scenarios.

Figure 3-3 shows the measured longitudinal double-spin asymmetry A_{LL} for neutral pion production as a function of p_T together with different gluon polarization scenarios as described above. The NLO calculations of A_{LL} make use of the recently released set of fragmentation functions based on a global analysis of ee, ep and pp data sets[22]. The error bars include statistical uncertainties only. The systematic error band includes contributions from the neutral pion yield extraction and background subtraction, possible non-longitudinal spin contributions and the relative luminosity uncertainty. The Run 5 data sample is based on a restricted pseudo-rapidity region of the STAR BEMC. The data from Run 6 includes the full acceptance of the STAR BEMC. This analysis allowed an extension of the p_T region towards larger values. The 2006 results exclude a large positive gluon polarization scenario.

In addition to the first neutral pion analysis of A_{LL} at mid-rapidity, the STAR collaboration has presented preliminary results for neutral pion production using the STAR EEMC in the pseudo-rapidity acceptance region of 1.086 < η <2.0 from Run 5[23] and Run 6[24]. The data are consistent with zero over the p_T range of 3 < p_T < 9 GeV/c. The systematic uncertainties during Run 5 were comparable to the statistical uncertainties and dominated by beam induced background. These background contributions were observed to be suppressed by a factor 20 during Run 6, profiting from the installation of shielding to reduce beam induced background between the runs. This resulted in an improved measurement for A_{LL} in the STAR EEMC acceptance region based on data taken during Run 6, which is shown in Figure 3-4. The EEMC based analysis provides an important baseline measurement for future prompt photon measurements in the STAR EEMC acceptance region.

The STAR collaboration has also presented the first measurement of the longitudinal double-spin asymmetry A_{LL} for inclusive charged pion production from Run 5. The asymmetries are calculated over the transverse momentum region 2 < p_T < 10 GeV/c and compared to several gluon polarization scenarios as described earlier. This analysis is unique in that the difference $A_{LL}(\pi^-)$ - $A_{LL}(\pi^+)$ tracks the sign of the gluon polarization, due to the opposite signs of the polarized distribution functions for up and down quarks. The STAR TPC offers robust reconstruction and identification of charged pions over the transverse momentum range 2 < p_T < 10 GeV/c. Particle identification in the TPC is accomplished using measurements of ionization energy loss of TPC hits. Figure 3-5 shows preliminary results during Run 5 for charged pion production. The measured asymmetries

are compared to theoretical predictions for A_{LL} based on different gluon polarization scenarios. The fragmentation functions for π^+ and π^- are based on the KKP fragmentation functions[25]. This first measurement of A_{LL} for charged pion production disfavors a large gluon polarization scenario. Several systematic checks have been performed. The leading systematic uncertainty is due to the bias introduced by the trigger used for this analysis. This trigger is based on a jet patch trigger, which introduces a bias towards jets with a large fraction of neutral energy. The impact of this trigger on the charge pion asymmetry analysis has been estimated using a MC sample. This uncertainty amounts to approximately 5×10^{-3}, which is comparable to the statistical uncertainty of the first p_T bin. In addition, asymmetries were calculated for trigger-jets in comparison to away-side jets. Both asymmetries have been found to be consistent within statistical uncertainties.
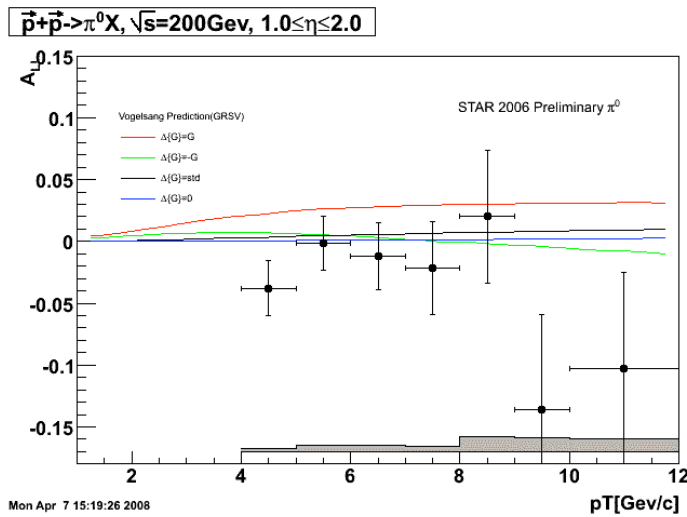

Figure 3-4: Double spin asymmetry for inclusive neutral pions in the EEMC region ($1 < \eta < 2$) from Run 6.

A first measurement of the longitudinal spin transfer D_{LL} in inclusive Λ ($\Lambda \rightarrow p\pi^-$) and $\overline{\Lambda}$ ($\overline{\Lambda} \rightarrow p\pi^+$) production in polarized proton-proton collisions at a center-of-mass energy of 200 GeV has also been carried out by STAR using data collected in Run-5. The data have 5-10% precision and cover transverse momenta (p_T) in the range of 1 to 4 GeV/c with a longitudinal momentum fraction of $x_F = 7.5 \times 10^{-3}$. At improved precision and larger p_T the measurement of D_{LL} for inclusive Λ and $\overline{\Lambda}$ production is sensitive to strange (anti) quark polarization[26] and polarized fragmentation functions[27].

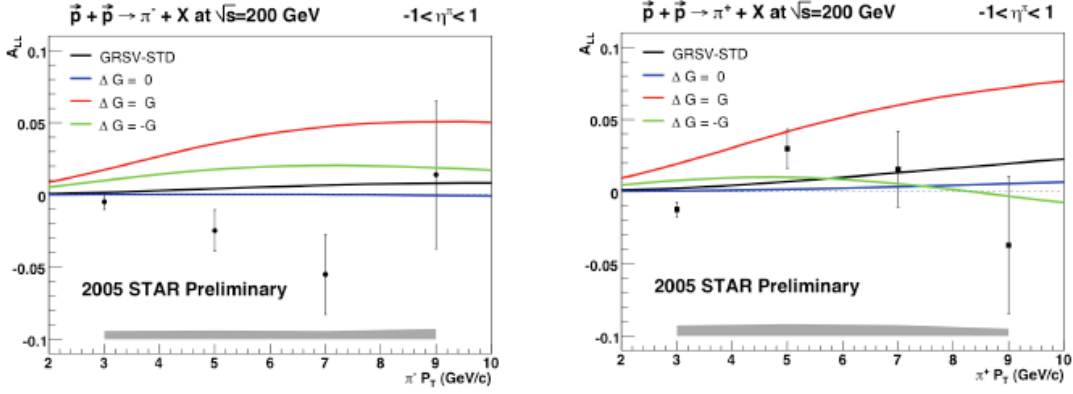**Figure 3-5: Longitudinal double-spin asymmetry ALL for charged pion production at** $\sqrt{s}$ = 200 **GeV as a function of pT (-1 < η < 1) for Run 5 in comparison to several gluon polarization scenarios.**

The STAR result for Run 5 of the measurement of the longitudinal double-spin asymmetry A_{LL} for inclusive jet production is shown in Figure 3-6 as a function of p_T for $5 < p_T < 30$ GeV/c in comparison to several gluon polarization scenarios as described earlier. Jets are reconstructed using a midpoint cone clustering algorithm using a cone radius of 0.4. This algorithm is fed in the case of STAR by reconstructed electromagnetic clusters in the STAR BEMC and tracks from the STAR TPC. Various systematic effects have been studied. The dominant contributions to the systematic uncertainties result from trigger bias and jet reconstruction bias, relative luminosity monitoring and backgrounds. The 2005 A_{LL} inclusive jet measurement is found to be in good agreement with the previous 2003/2004 measurements. The current measurement extends the p_T region to larger values, where the quark-gluon contribution starts to become important. This analysis rules out most GRSV fits with ΔG much larger than the GRSV std. solution. The most recent A_{LL} result for inclusive jet production is shown in Figure 3-7 which provides the most precise measurement to date to constrain the gluon polarization of the proton at RHIC. This analysis is based on a luminosity of 4.7pb^{-1} and an average polarization of approximately 60% which resulted together with the full STAR BEMC acceptance in a factor of 3-4 improvement in statistical precision for $p_T > 13$GeV/c compared to the Run 5 jet result.

Taking all current PHENIX and STAR A_{LL} measurements together in comparison to different NLO perturbative QCD predictions for A_{LL} yields a consistent picture which clearly rules out extreme gluon polarization scenarios and suggests that the gluon polarization on average in the measured kinematic region is rather small.

The first global analysis, incorporating polarized semi-inclusive DIS, polarized inclusive DIS and polarized proton-proton, data has recently been released[31]. Figure 3-8 shows a comparison of the STAR A_{LL} Runs 5 and 6 jet results in comparison to a calculation of A_{LL} using the extracted polarized gluon distribution function including the jet results from STAR. Good agreement is found between those measurements and the calculated A_{LL} value. The yellow band indicates a 2% variation of the χ^2 and provides a reasonable

measure of the experimental uncertainties. Figure 3-9 shows the extracted gluon polarization as a function of x at $Q^2 = 1\,0\,\text{GeV}^2$. The extracted gluon polarization is found to be rather small in the measured kinematic region with a node at an x value of approximately 0.1. The impact of the STAR jet result is shown in the bottom plot of Figure 3-9 showing the χ^2 variation as a function of the truncated first moment. The STAR jet results provided a substantial impact constraining the gluon polarization of the proton.
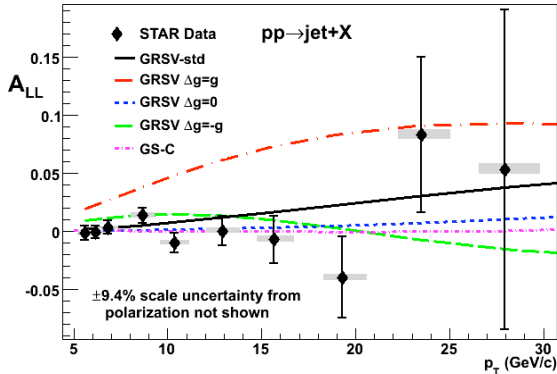

Figure 3-6: Longitudinal double-spin asymmetry A_{LL} for inclusive jet production $\sqrt{s} = 200\,\text{GeV}$ as a function of p_T ($0.2 < \eta < 0.8$) for Run 5 in comparison to several gluon polarization scenarios. The error bars are statistical. The gray bands show the systematic uncertainties in the measured A_{LL} and jet p_T.
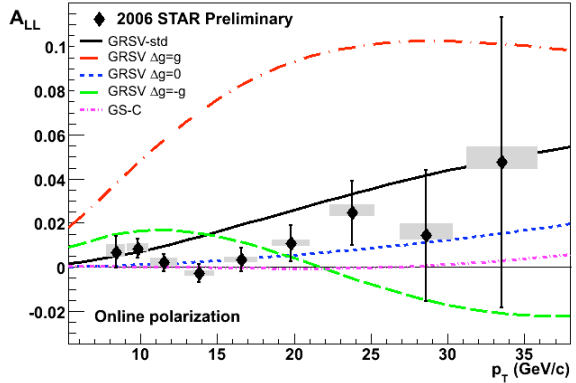

Figure 3-7: Longitudinal double-spin asymmetry A_{LL} for inclusive jet production at $\sqrt{s} = 200\,\text{GeV}$ as a function of p_T ($-0.7 < \eta < 0.9$) for Run 6 in comparison to several gluon polarization scenarios.
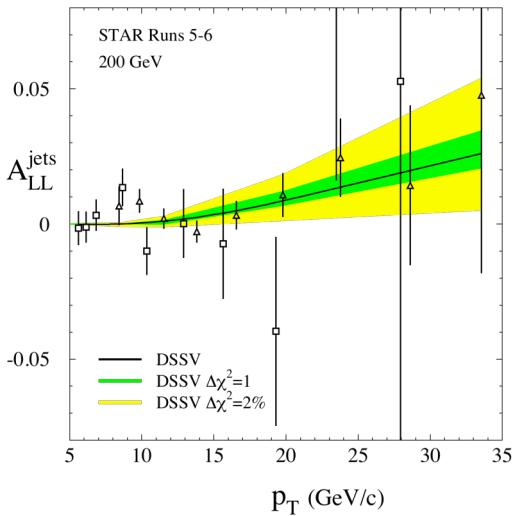

Figure 3-8: Longitudinal double-spin asymmetry ALL for inclusive jet production at $\sqrt{s} = 200\,\text{GeV}$ from STAR based on data taken during Run 5 and Run 6 in comparison to a calculation of A_{LL} using a polarized gluon distribution extracted from a global analysis[32] which includes the STAR jet result.

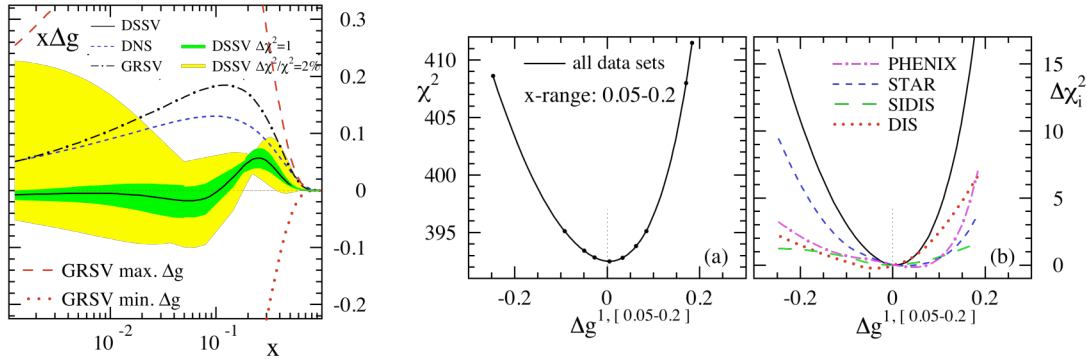**Figure 3-9: Gluon polarization as a function of x for Q2=10GeV2 for three different global analyses. The solid line indicates the recent global fit result by DSSV[32] including the STAR jet data (left). χ^2 variation as a function of the truncated first moment for the total χ^2 and the individual experiment contributions indicating a strong impact of the STAR jet result to constrain the polarized gluon distribution function (right).**

3.3. Ongoing studies

As the luminosity of RHIC grows, the already large STAR detector acceptance will allow measurements of jet-jet, hadron-hadron and photon-jet correlations. At leading order (LO) the hard scattering sub-process kinematics can be calculated on an event-by-event basis. This of course then leads to addressing the need to constrain the x-dependence of the polarized gluon distribution function. Such LO extractions must be followed up with a full global analysis incorporating correlation measurements beyond inclusive measurements, which has been the prime focus of the STAR longitudinal spin program so far. The theoretical framework to take advantage of those correlation measurements in a global analysis does exist. The reconstruction of di-jets and photon final states will play a critical role. The following section provides a brief overview of ongoing efforts towards a first di-jet and photon result from STAR.

3.3.1. Di-Jet analysis

Employing two-body kinematics of the underlying hard sub-process in di-jet production, the invariant mass M and rapidity y can be related to the x-values of both partons in the initial state: $M = \sqrt{x_1 x_2 s}$ and $y = (\eta_3 + \eta_4)/2 = (1/2)\ln(x_1/x_2)$.

Figure 3-10 shows a comparison of data taken during Run 5 and a PYTHIA MC simulation for a di-jet event sample showing distributions of the invariant mass M, the rapidity y, and the cosine of the partonic center-of-mass angle θ^*. Good agreement is found between data and MC in all three cases. The overall normalization is performed with respect to the invariant mass distribution, i.e. with only one normalization factor for all distributions shown. The Run 5 data sample is restricted to the pseudo-rapidity range of $0.2 < \eta < 0.8$. The full STAR BEMC together with the STAR EEMC and the STAR FMS will allow a

substantial extension of the overall kinematic coverage and points to a key strength of STAR to cover a wide kinematic region, selecting both symmetric partonic collisions at mid-rapidity at larger x values as well as asymmetric collisions to extend the kinematic region towards lower x values including in particular the STAR EEMC and STAR FMS in combination with the STAR BEMC coverage. The current di-jet analysis of Runs 5 and 6 is proceeding well.
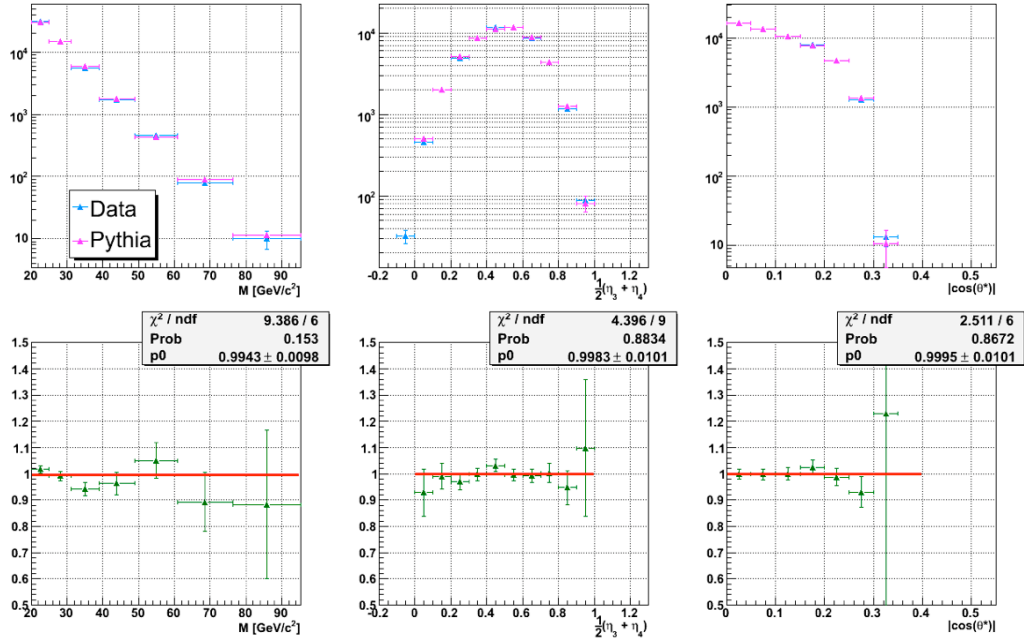

Figure 3-10: Comparison of data taken during Run 5 and a PYTHIA MC simulation for a di-jet event sample.

3.3.2. Photon analysis

The crucial experimental issue for the γ-jet program is to cleanly identify the direct photons in the presence of a much higher flux of neutral pions, and to do so with good efficiency. As can be seen in Figure 3-11. The yield of inclusive neutral pions is a factor of ~10 larger than that of photons at p_T =10 GeV and gets larger as one goes lower.
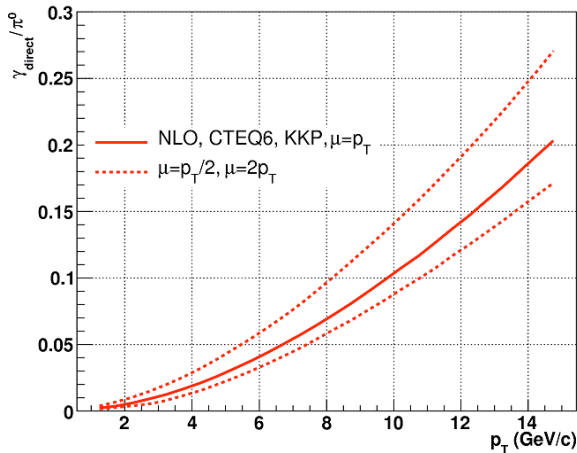
Figure 3-11: Inclusive γ/π^0 ratio as a function of p_T.

Initial simulations[34] have shown that the signal to background could be reduced to better than 1:1 by the combination of photon isolation cuts and selection on the shower shape in the shower maximum detector (SMD) for γ-jet coincident events. Such an analysis also identifies a background sample for subtraction. Over the past year, among the primary efforts of the photon reconstruction group has been repeating these and similar studies in the full Monte Carlo detector model of STAR and analyzing the sample data sets taken in the 2006 run. These studies hope to verify the early simulations and provide yield information from the data. In addition we are exploring the use of other observables in the calorimeter, e.g., pre and post-shower detectors, to see whether the analysis might be pushed to lower p_T given the expected integrated luminosity. Ultimately a composite analysis involving all observables and algorithms incorporated into linear discriminate or higher order analysis will likely be used and initial investigations along these lines have been developed.

Full STAR simulations have been carried out to explore the SMD shower shape cuts. The purpose is to try and select the single shower of a direct photon from the double shower of a π^0 (or other meson). Shown in Figure 3-12 is a shower shape analysis with full PYTHIA simulations of direct γ-jet events (upper left) and π^0's from hadronic events (upper right).
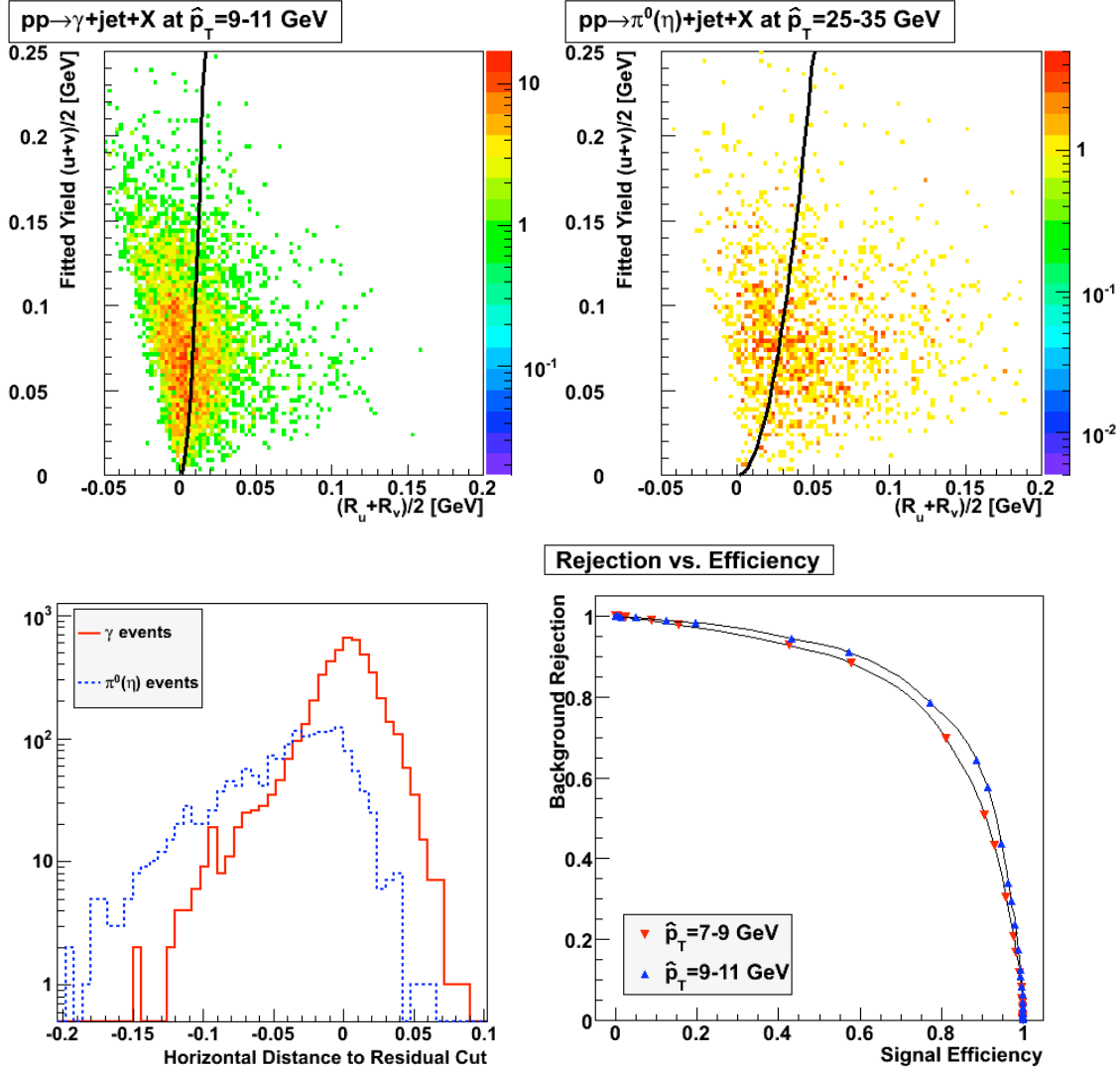
Figure 3-12: Shower shape analysis (described in the text) of Monte Carlo simulations of the full STAR detector using Pythia generated γ-jet (upper left) and hadronic backgrounds (upper right) are shown. In the lower left panel is shown the "distance" of events from the black curve separating direct gamma and background events in the upper panels. The signal efficiency and background rejection factor can then be extracted by considering sliding a vertical line along the x axis thus producing the 9-11 GeV plot at the lower right (included here is also a curve for the 7-9 GeV partonic p_T bin for comparison).

In this analysis a candidate γ peak is identified and a range of strips around it are fit with a canonical γ line shape. The maximum residual left or right of the peak in each of the 2 planes is summed to plot along the x-axis. An average of the peak areas is used to plot along the y axis. A nominal cut separating enriched direct photon vs. background events is shown as a black curve in the upper two figures. In the lower left panel we show the distance away from the cut line for the γ (solid red) and π^0/η (dashed blue) events. By considering the number of events to the left or right of a "vertical line" in the lower left

24

panel, and sliding it back and forth we can generate a plot of the efficiency of γ's surviving this cut vs. the rejection factor for π^0's as shown in the lower right panel. For the γ-jet partonic 9-11 GeV partonic p_T bin comparison about 2/3^{rds} of the background can be eliminated with this cut with about 90% of the γ's surviving. For the 7-9 GeV bin these efficiency/rejection values are slightly reduced but still quite encouraging. Evaluation of effects of other backgrounds - neutral (neutrons and K^0_L's) and charged hadrons, and from >2 photons, has begun. Similar shower shape analyses involving a chi-squared peak fitting approach are also under investigation.

The production of the above plot required some significant advances in the understanding of the calorimeters. In particular the transverse shower shapes in both BSMD and ESMD are not well reproduced by the Monte Carlo simulations. We find that the data shapes are somewhat wider and the fluctuations in tails of the shapes are greater than predicted by our GEANT model of the STAR detector. Monte Carlo and data from 2006 have been extensively studied in the EEMC. The deficiency in the Monte Carlo simulations has been addressed by selecting samples of isolated gammas. One such sample was generated by selecting identified η's decaying to two γ's where, due to the large η mass, the γ's are well separated in the SMD. Useful events were checked to be well isolated from other particles in the detector. These isolated γ's from η's were then used to define a more representative canonical line shape and also loaded in a library and used in the Monte Carlo to replace the generated shape with more realistic ones.

The shapes of the showers at the SMD from Run 6 data have been studied extensively by making full use of the EEMC's various detector subcomponents as shown for example in Figure 3-13. The information available is displayed on the right where in the lower 6 panels the energy deposited in η vs. ϕ is displayed for the tower (full energy deposition) and the energy deposited in the first two layers (preshower 1 & 2) as well as in the last layer (post shower) and SMD layers is shown. The shower shape for an isolated γ with highly selective cuts is shown in the upper two panels of the right side.
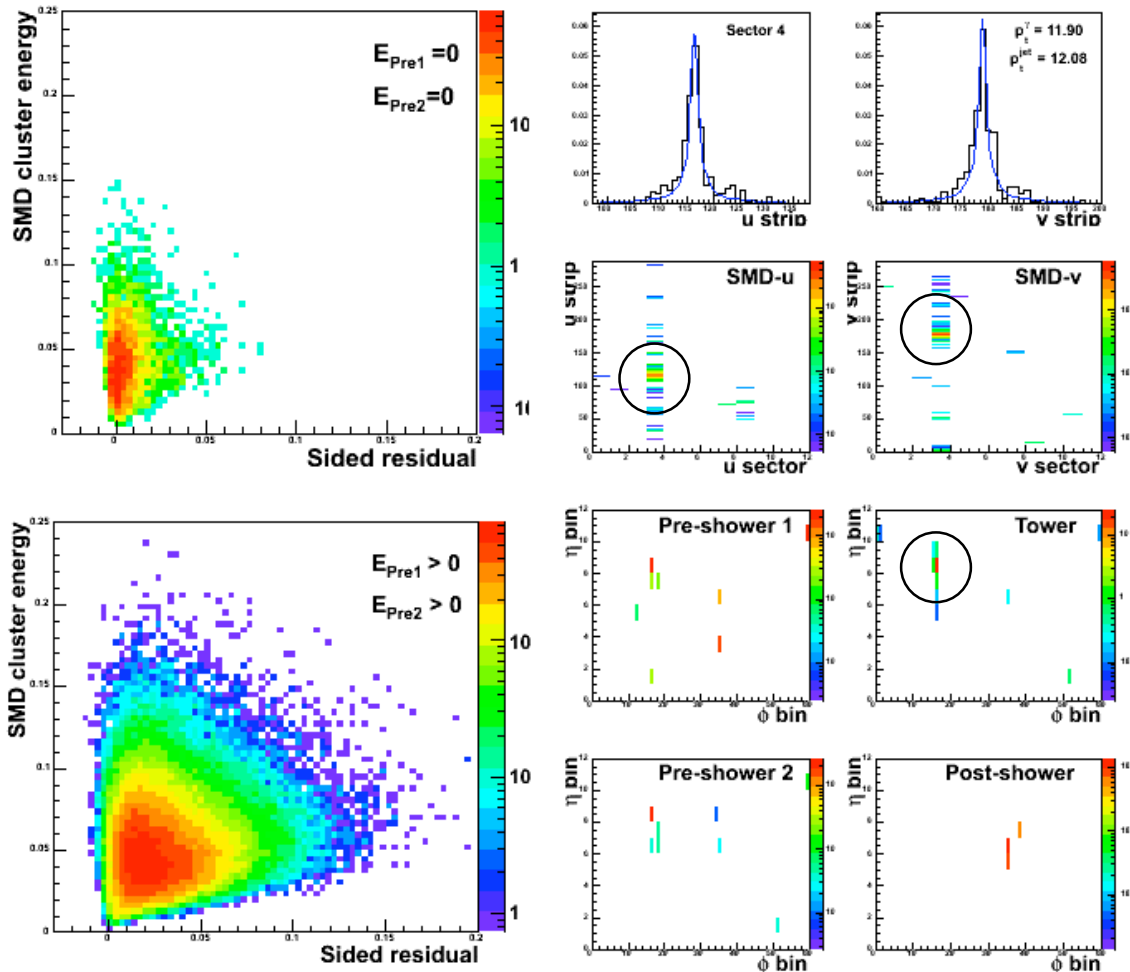
Figure 3-13: Shower shape analysis and example signals for γ candidate event in the EEMC. The lower 6 panels on the right show the signals available from the calorimeter as distributed in η vs. φ. The "tower" signal measures the full energy of the shower for the event ($p_T \sim 12$ GeV). The preshower detectors, measuring the energy deposited in the first two layers at the front of the calorimeter, here register little energy. The postshower detector measures the remaining energy at the back of the calorimeter (after 21 radiation lengths). The two panels in the upper right show the profile of what appears to be an electromagnetic shower. These profiles are analyzed against a canonical shape in a sided residual analysis described in the text. The upper left panel shows this analysis for an enriched sample of γ's, vetoed by both preshower layers and the lower left for a sample dominated by hadronic background where both preshowers are required to fire.

The full set of information as described above can be used for checking isolation of the signal under study as well as the shower development through the calorimeter. As an example, the pre-shower detectors were used to select an enriched sample of isolated γ's for

study from a sample already in coincidence with an away-side jet and the candidate containing 90% of the energy in an isolation cone of 0.7 radius in $\eta \times \phi$. There is approximately 1 radiation length of material in front of the calorimeter in 2006. In addition the first layer presents about 1 radiation length more. Thus by insisting that there is no signal in either pre-shower detector one enhances isolated γ's over the pairs one expects from π^0's. This sample was then compared to the sample generated from η's discussed above. In studying the systematics of these two samples we learned the following about the calorimeter: 1) While the width difference between data and Monte Carlo is not fully understood an insufficient amount of material in the model upstream of the calorimeter is suspected. In addition, there are indications that the generated width may be too narrow. We expect data from the 2008 run with limited material near the beam in STAR to provide important information on these questions. 2) We find the width of the distribution depends on the location of the SMD in the detector stack. The SMD planes are in one of 3 depths in the calorimeter (3 positions are shared by two planes and a blank alternating in adjacent sectors) and the width of the distribution detected is wider the deeper the SMD is in the detector stack. 3) The shape of the SMD distributions also depend on the depth at which conversion takes place, with those photons converting after the 2nd pre-shower having narrower shapes than those converting before it. Likewise photons converting after the 1st pre-shower detector have narrower shapes than those entering the calorimeter. These effects are now all modeled in a data driven way by the modified Monte Carlo and reflected in Figure 3-12 showing the shower shape analysis for the Monte Carlo. In Figure 3-13 in the left panels we see the shower shape analysis for data. The analysis is performed with the same data driven shape and in both cases we see that the presumed γ locus is centered on the vertical axis indicating that the shape on average well represents both the data and the Monte Carlo. The reasonable agreement between simulations for these crucial shower shape parameters at the SMD should greatly improve the reliability of estimates for efficiencies and backgrounds (purity).

In addition, we have learned to generate subsamples of the data with well controlled relationships with regard to their effect on single and double γ samples that can be used to check derived estimates of the efficiency and background. As one example, events that convert in the first Pb layer of the calorimeter, as evidenced by a veto in the first preshower and energy in the 2nd, can be used for a statistical separation of gamma's from π^0's and direct comparison to event-by-event separation. For the former, initial results indicate rough agreement of data yields and sample behavior as expected from Pythia and other detector data response.

Taken together this then provides most of the final tools necessary to complete an initial full analysis of γ-jet events from the 2006 run. By coupling the shower shape cuts described above with a selection of coincident away-side jets using the jet finder (instrumental to our inclusive and di-jet results) as well as an isolation cut around the candidate γ, we are selecting a strongly enhanced sample of direct γ-jet events. This analysis procedure has been an integral part of the effort above and is well underway. At the present, we are working toward the first full analysis results of the 2006 data and Monte Carlo to provide estimated yields, efficiencies and purities necessary to calculate the statistical and systematic errors from background subtraction in a given data set.

3.4. Polarized proton request in Runs 9 and 10

The STAR collaboration is requesting a polarized proton-proton run in Run 9 and/or Run 10. The primary goal is to collect a data sample at longitudinal polarization of 50pb^{-1} at 60% beam polarization, which translates into a Figure-of-Merit (FOM) of 6.5pb^{-1}. The detailed breakdown is shown in the executive summary for two different running scenarios of 25 and 16 cryo-weeks. Once this goal is met and sufficient time remains a switch should occur to transverse polarization to collect at least 6pb^{-1} during Run 9. The physics justification for both the longitudinal and transverse spin program is discussed in the following two sections. It is also important that development for 500 GeV polarized pp running occur in the next two years in order to be prepared for the first long production run in 2011. We thus reserve time for this development in the first two years of this beam use proposal under either scenario.

3.4.1. Longitudinal spin program

The primary goal of Run 9 is to advance our understanding of the gluon polarization based on three key measurements:

- Di-jet production over a wide kinematic region profiting from the large calorimetry coverage in STAR
- Precision inclusive measurements at large transverse momentum, in particular for the case of inclusive jet production, which had been so far the flagship of the STAR longitudinal spin program
- Embark on prompt photon measurements and photon-jet measurements

Di-jet production is a key element of the STAR longitudinal spin program. As discussed in the previous section, di-jet production provides sensitivity to the underlying partonic kinematics beyond inclusive measurements, which simply integrate over the measured kinematic region. The recent global analysis by DSSV[32] suggest a gluon polarization with a node around x=0.1 with a positive value for x>0.1 and a negative value for x<0.1. It would be extremely important to enhance those Bjorken-x regions through specific kinematic cuts. Di-jet (and gamma-jet) production in STAR does indeed allow such a selection. Figure 3-14 shows the longitudinal double-spin asymmetry A_{LL} for di-jet production as a function of the invariant mass M for different topological combinations of the STAR BEMC and STAR EEMC region. The projected uncertainties are shown for a luminosity of 50pb^{-1} and a beam polarization of 60% including detector effects. Those projected uncertainties are compared to a LO evaluation of A_{LL}. A full NLO calculation is in preparation. The A_{LL} curves at LO are shown for GRSV-STD and GRSV-ZERO, which have been both introduced in the longitudinal result section previously. In addition to those parton distribution functions, LO calculations based on GS-C and GRSV-m0.3 have been performed, where the latter refers to the case of a GRSV-type gluon polarization with a first moment of -0.3 at a scale of 1GeV^2. The projected uncertainties demonstrate the excellent discrimination that will be possible amongst different models that are fully compatible with the current RHIC data, such as GRSV-ZERO, GRSV-m0.3, and GS-C.

The di-jet data will provide access to $\Delta g(x)$ over a broad range of x values. In a leading-order picture, east barrel – east barrel, east barrel – endcap, and west barrel – west barrel di-jet events will sample $0.1 <\sim x_2 <\sim 0.2$ in collisions where x_1 is approximately $3x_2$. West barrel – endcap events will sample $0.04 <\sim x_2 < 0.1$ in collisions where x_1 is nearly $7x_2$. In these cases, the asymmetry is dominated by the scattering of highly polarized quarks off lower momentum gluons. This will provide a mapping of $\Delta g(x)$ over the region where the DSSV fit expects there to be a node. The east barrel – west barrel combination will provide complementary information about symmetric partonic collisions with x_1 and x_2 in the range 0.1 to 0.4, while the endcap – endcap region will involve collisions of very high x quarks with very low x gluons. Di-jet production in Run 9 with an anticipated luminosity of 50pb^{-1} and a beam polarization of 60% would allow a substantial improvement of our understanding of the gluon polarization.
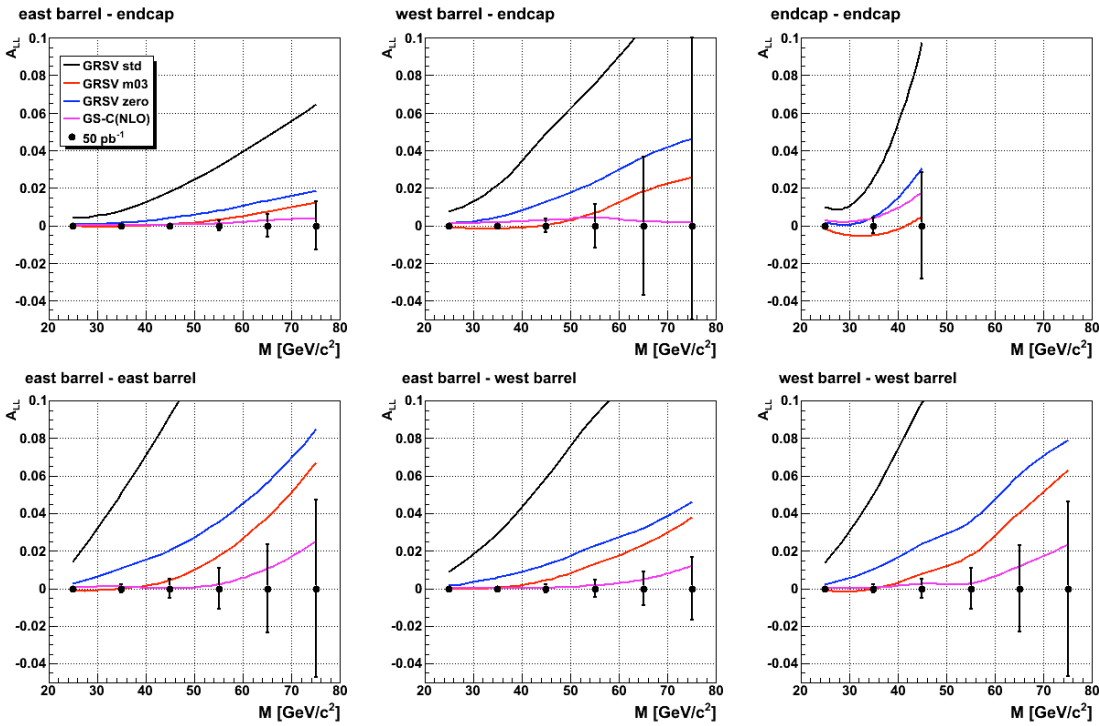

Figure 3-14: Longitudinal double-spin asymmetryA_{LL} for di-jet production as a function of the invariant mass M for different topological combinations of the STAR BEMC and STAR EEMC region. The projected uncertainties are shown for a luminosity of 50pb^{-1} and a beam polarization of 60%. Those projected uncertainties are compared to a LO evaluation of A_{LL}.

The potential for inclusive jet production for Run 9 can be understood in the context of the recent global analysis by DSSV[32]. Figure 3-15 shows the gluon polarization as a function of x including the inclusive jet result from STAR and the neutral pion result from PHENIX for Run 6 (top) and the projected performance for Run 9 (bottom) based on a data sample of 50pb^{-1} and a beam polarization of 60%. The uncertainty is substantially reduced which is shown as a variation of the total χ^2 by 1 unit in green and by a 2% variation of the total χ^2 in yellow. Figure 3-16 shows the individual contributions to the total χ^2 with the projected Run

9 results. This underlines the clear potential of the inclusive jet program of STAR in Run 9 to further reduce the actual uncertainty on the extracted gluon polarization. In practice, the gluon polarization will be even more precisely determined with the Run 9 results than illustrated in Figure 3-16 and Figure 3-19 because these projections do not include the additional knowledge that will be gained from the di-jet study described above.

In addition to the proposed measurements of inclusive jets and di-jets, we propose to make significant photon-jet coincidence measurements at $\sqrt{s}$ = 200 GeV and eventually $\sqrt{s}$ = 500 GeV. These measurements are sensitive mostly to quark-gluon scattering and thus allow the rather direct determination of the polarized gluon distribution ΔG as a function of gluon fractional momentum x.

Figure 3-15: Gluon polarization as a function of x for the inclusive jet result from STAR and the neutral pion result from PHENIX for Run 6 (top) and the projected performance for Run 9 (bottom) based on a data sample of 50pb^{-1} and a beam polarization of 60%.
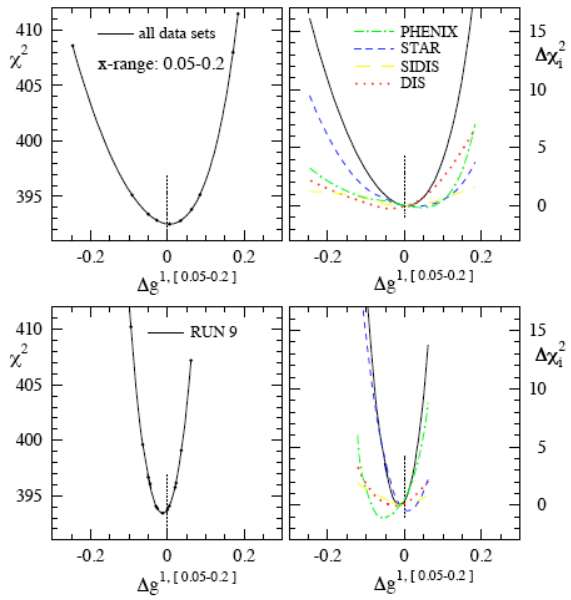

Figure 3-16: χ^2 as function of the truncated first moment (0.05, 0.2) including the inclusive jet result from STAR and the neutral pion result from PHENIX for Run 6 (top) and the projected performance for Run 9 (bottom) based on a data sample of 50pb^{-1} and a beam polarization of 60%.
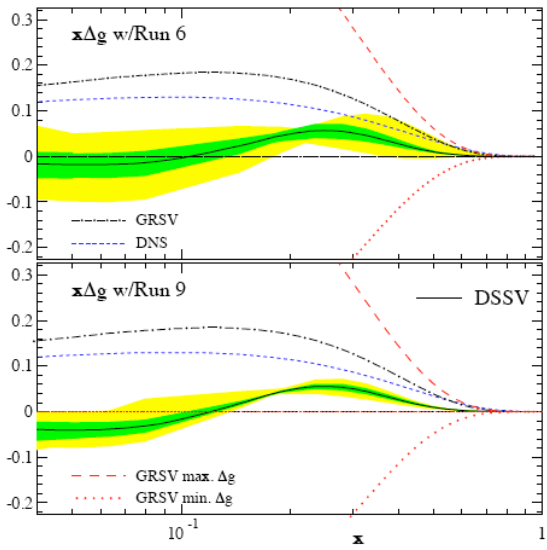
At the time of the writing of this beam use proposal, we have not yet completed a full evaluation of the sensitivities that STAR photon-jet measurements will yield. We have estimated sensitivities in the acceptance of the barrel and endcap calorimeters at the PYTHIA event generator level for the nominal integrated luminosity of 50 pb^{-1} and 60% beam polarization in Run 9. These projected sensitivities are shown in Figure 3-17, together with current world data from high-p_T hadron (pair) and open charm production in fixed-target polarized lepton-nucleon experiments by the COMPASS, HERMES, and SMC

collaborations. In addition representative polarized gluon distributions are shown at the scales typical of the STAR proposed measurements, $\mu^2 \approx 100$ GeV^2, and of the lepton-nucleon measurements of high p$_T$ hadron(s), $\mu^2 \approx 3$ GeV^2. The scale, $\mu^2 \approx 13$ GeV^2, of the COMPASS open charm measurement is in between the shown scales. Note that these COMPASS, HERMES, and SMC results were not included in the recent DSSV fit because corresponding NLO calculations are not yet available. In contrast, an NLO framework for photon+jet measurements already exists. We expect that the integrated luminosity of Run 9 will allow STAR to make a credible start on photon-jet measurements. These initial measurements at √s = 200 GeV are expected to probe resolved gluon momenta fractions down to x ≈ 0.03. In the region of kinematic overlap with existing data at higher x they probe at complementary harder perturbative scales. The accumulation of integrated luminosity at √s = 200 GeV and √s = 500 GeV beyond Run 9 is expected to improve the precision and extend the kinematic coverage of these measurements to x ≈ 0.01.

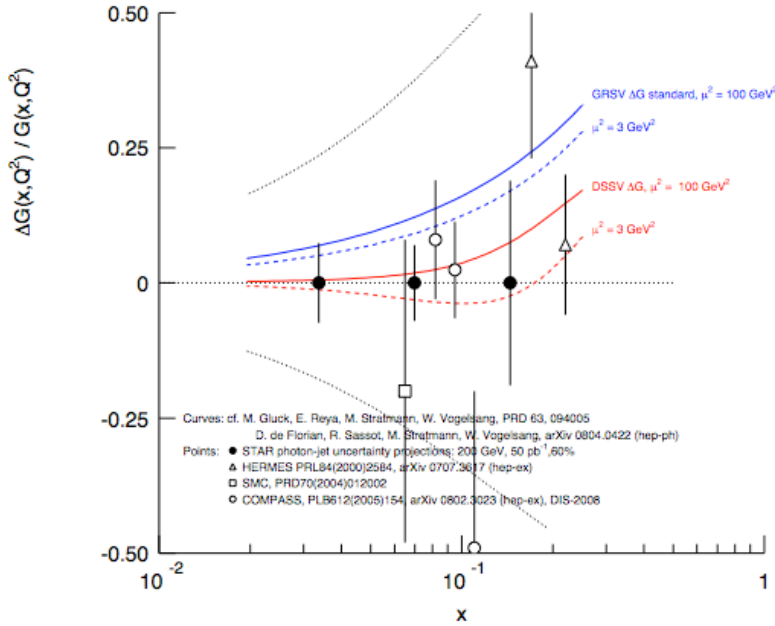**Figure 3-17: Projected uncertainties for Δg/g as a function of x for photon-jet measurements at √s = 200 GeV for an integrated luminosity of 50pb^{-1} and 60% beam polarization in Run 9. Experimental efficiencies are not yet taken into account. Also shown are current world data from high-p$_T$ hadron (pair) and open charm production in fixed-target polarized lepton-nucleon experiments by the COMPASS, HERMES, and SMC collaborations.**

3.4.2. Transverse spin program

The window on parton orbital motion at RHIC corresponds to the Sivers mechanism[35] as an explanation of transverse single spin asymmetries (SSA) for pion production at large Feynman x (x$_F$). Transverse SSA is suppressed in hard scattering in vector gauge theories in the massless limit[36], and the light quark sector of QCD is very nearly in that limit. The Sivers mechanism was proposed to explain striking experimentally observed spin effects in

polarized proton collisions at low collision energy ($\sqrt{s} < 20$ GeV)[37] that could not be generated in a naive leading-twist collinear pQCD description.

Many things have changed in the past six years. For example, there was a theoretical proof[7] that (naive) time reversal is violated by the Sivers mechanism, since it requires a (naive) T-odd spin and transverse momentum dependent distribution function, called the Sivers function. Along with this proof, another mechanism for explaining transverse SSA in p+p collisions producing pions was suggested by theorists[7]. In this mechanism, transversely polarized quarks must be present in a transversely polarized proton. The Bjorken-x dependence of the transverse spin asymmetry distribution is given by the transversity function. Moments of the transversity distribution have recently been computed in lattice QCD. The zeroth moment of transversity is the tensor charge of the proton, relevant to estimates of the electric dipole moment of the neutron, and so determination of the transversity distribution is of great importance. Transverse momentum (k_T) for hadrons produced in the fragmentation of a transversely polarized quark in the final state would have a sinusoidal variation on the azimuthal orientation of $\boldsymbol{k_T}$ in the Collins mechanism.

A theoretical proof that the Sivers function is zero has since been withdrawn[38] since final-state interactions[39], that are required by gauge invariance, spoil naive time reversal arguments that potentially could suppress the Sivers mechanism. Furthermore, a specific example was provided explicitly demonstrating how the Sivers mechanism produces a transverse SSA, thereby overcoming the naive time reversal arguments and supplying the requisite phase factor leading to the amplitude interference as needed for a transverse SSA.

These theoretical developments over the past six years have coincided with important experimental developments summarized below.

(1) Transverse SSA has been measured in semi-inclusive deep inelastic scattering (SIDIS) from a transversely polarized proton target by the HERMES collaboration[40]. A separation of the Collins and Sivers mechanisms from this data has been made.

(2) Zero asymmetries are observed in SIDIS from a transversely polarized deuterium target by the COMPASS collaboration[41]. The COMPASS results are consistent with present theoretical understanding that the Sivers functions for up and down quarks are opposite in sign and cancel for the isospin zero deuterium target. We eagerly await the results from COMPASS for transverse SSA from a transversely polarized proton target, although the Bjorken x range extends to much smaller values than probed by HERMES, where the spin effects may be smaller.

(3) Concurrent with the SIDIS measurements are measurements at RHIC that demonstrate that transverse SSA that are observed for pion production at $\sqrt{s} < 20$ GeV are present at $\sqrt{s} = 200$ GeV[42,10]. This is significant because measured cross sections at $\sqrt{s} = 200$ GeV are consistent with next-to-leading order pQCD calculations[5], meaning that theories that aim at a universal understanding of transverse SSA in hard scattering processes are supported by a good understanding of the spin averaged observables. This is not the case for pion production at lower $\sqrt{s}$, where observed cross sections are progressively larger than pQCD calculations

as $\sqrt{s}$ decreases, with very pronounced enhancements relative to theory in the forward direction[43].

(4) Finally, experimental observation of the Collins fragmentation function has been completed in (unpolarized) e^+e^- collisions by the Belle collaboration[44]. The Collins function corresponds to a harmonic dependence on the azimuthal angle relative to the thrust axis for fragmentation products from a transversely polarized quark.

The final-state interactions that spoil naive time-reversal symmetry for the Sivers mechanism have a simple intuitive explanation in SIDIS[45]. The absorption of a virtual photon by the current quark leads to a separation of equal and opposite colors, since the proton target is color neutral. Given this color separation, after the virtual photon is absorbed, the current quark does not propagate in free space, but rather propagates in the color field generated by the spectator quarks. The phase factor required for transverse SSA naturally arises in this mechanism, as in the case of Coulomb wave functions for the QED analogy of deep inelastic scattering on a hydrogen atom. This phase, as well as a spin- and k_T-dependent distribution function, is a requirement for the Sivers mechanism. It is clear that the final-state interaction is attractive in the case of SIDIS, because the proton is initially color neutral.

Model calculations have suggested that the x_F dependence of transverse SSA for $p_\uparrow + p \rightarrow \pi^0 + X$ at $\sqrt{s}=200$ GeV can be explained by the Sivers function[45] extracted from the HERMES data[46]. Current theory does not reliably predict the p_T dependence at fixed x_F for transverse SSA for pion production. A resolution to this may be in sight, invoking contributions from both Collins and Sivers mechanisms to the hadroproduction transverse SSA. First attempts at direct separation of these contributions will be made from data obtained with the FMS during RHIC Run 8.

If the Sivers function appears for both SIDIS and polarized proton collisions, then we can conclude that partons have orbital motion within the spinning proton. This is a significant development that requires further experimental and theoretical work to establish.

Further theoretical work has led to an even more interesting consequence of the Sivers mechanism. Namely, the color structure associated with present theoretical understanding of the Drell-Yan (DY) production of dilepton pairs, leads to the expectation that the Sivers function for transverse SSA in DY is exactly opposite in sign from the Sivers function that is extracted from SIDIS. This non-universality arises because the attractive color interactions in SIDIS are replaced by repulsive color interactions between like colors in DY. Experimental observation of this sign change would identify fundamental aspects of color charge interactions.

The RHIC experiments would need upgrades to complete a transverse SSA measurement for the DY process. For example, tracking upstream of the FMS is needed to discriminate like-sign from unlike-sign lepton pairs. At PHENIX, additional acceptance is required to allow isolation cuts to be included in $\mu^\pm$ identification to reduce backgrounds from open heavy flavor production. Furthermore, the integrated luminosity requirements mean that

this as a future effort, following sustained luminosity improvements for polarized proton collisions.

In the meantime, further theoretical work has proceeded. Specifically, there is a prediction that repulsive color charge interactions will produce a change in sign for forward photon +away-side jet in polarized proton collisions at $\sqrt{s}$=200 GeV[47]. There are two implications of this prediction:

(1) there is partonic orbital motion within the spinning proton, observable in a process dependent way in both SIDIS and polarized proton collisions;

(2) the sign difference between SIDIS and polarized proton collisions demonstrates the reality of attractive and repulsive color charge interactions.

The addition of the FMS prior to the start of Run 8, and the away-side jet detection capabilities in the central region at STAR, uniquely positions the STAR collaboration to complete this measurement. It should be mentioned that the simple explanations, based on abelian (QED) analogs, of why there is a sign change in forward photon + away-side jet is not as intuitive as for transverse SSA for the DY process. Observation of the predicted sign change would bolster the case for a future transverse spin DY measurement at RHIC.
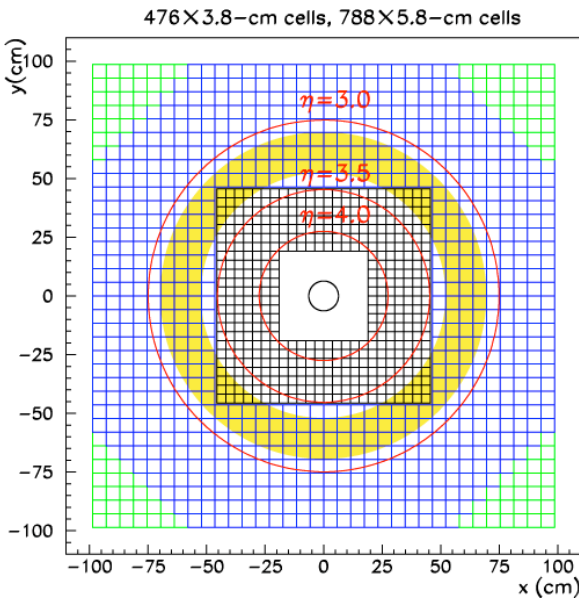

Figure 3-18: A schematic of the STAR forward meson spectrometer as seen from the interaction point. The Blue beam penetrates into the page at the center of the matrices. The yellow shaded area represents a conservative fiducial volume used for detection of direct γ candidates, with the remainder of the FMS used as a veto of photons arising primarily from π⁰ , η decay.

The STAR FMS (Figure 3-18) would be used for detecting direct photons at large rapidity. This device was built for studies of possible gluon saturation phenomena at RHIC. Run 8 results will address this question. Adaptation of cluster algorithms and shower shape analysis used for the STAR forward pion detector has been completed and applied to data from the FMS, after tuning the algorithms on full PYTHIA/GEANT simulations. Although final resolutions, energy scales and peak-to-background ratios await completion of offline calibration, first reconstructions of FMS data look quite promising, as shown by diphoton invariant mass distributions in Figure 3-19.

The FMS is a hermetic electromagnetic calorimeter, built from finely segmented lead-glass detectors, positioned west of the interaction point at STAR. It views particles produced in collisions through large holes in the poletips of the STAR magnet. The integrated number of radiation lengths between the calorimeter and the interaction point is dominated by crossing the beryllium beam pipe. The FMS is an outgrowth of the forward pion detector, corresponding to modular electromagnetic calorimeters built from finely segmented lead-glass detectors. Consequently, extensive experience with event reconstruction for both simulation and data exists from the FPD project, and can be carried over to the FMS. In general, full PYTHIA/GEANT simulations accurately account for what has been observed in the FPD. Single beam backgrounds are minimal, as confirmed in Run 8 by long dwell time vernier scans, due to shielding provided by the cryostats of the RHIC magnets. Comparison between simulation and data for the FMS awaits final calibrations.

For direct photon detection with a large-area hermetic electromagnetic calorimeter, the most effective method is to eliminate other sources of photons by direct detection. These other photons sources arise primarily from the decay of π^0 and η neutral mesons. Multiple aspects make this feasible with the FMS. First, because the calorimeter is at large rapidity, the typical photon energies are large ($E_\gamma > 35$ GeV) and the hadronic response of the FMS is small. Direct simulation of the detector response via GSTAR simulations employing the GEISHA hadronic simulation, applied to full PYTHIA events of collisions have demonstrated that the hadronic response of the lead glass detectors is minimal for energy depositions in excess of 25 GeV. Second, the large Lorentz factors result in significant spatial correlations for the decay products from π^0 and η mesons. For example, when there is a candidate direct photon having $E_\gamma = 25$ GeV, 95% of the phase space for all π^0 decays that could potentially be the source of this energetic photon are contained in a circle of radius 23 cm (approximately four large cells of the FMS) around the 25-GeV photon at the face of the FMS. Finally, π^0 and η mesons are most typically produced via fragmentation in p+p collisions at RHIC energies. This means that other hadrons share the energy of the fragmenting quark or gluon, softening the decay photon spectrum. The daughter photons from p and h decay then further divide this energy. In contrast, direct photons are produced in the hard scattering process. Their energy is not shared via fragmentation nor is it shared by particle decay. The energy where direct photon probabilities exceed decay photon probabilities is ~50 GeV for $\langle\eta\rangle \sim 3.2$, with no other conditions on the event. The π^0 and η backgrounds can be reduced, and this energy can be lowered to ~25 GeV, by subdivision of the FMS into two volumes. The fiducial volume, used for identifying direct photon candidates, is a small annular region within the outer calorimeter. The remainder of the FMS is used as a veto to establish that other photons from the decay of neutral mesons are not present. The effectiveness of the discrimination between direct and decay photons is demonstrated via full collision event simulations in Figure 3-20.

Restricting the measurement of the forward photon to $E_\gamma > 35$ GeV at $\langle\eta\rangle = 3.2$ produces a signal:background ratio of 2.1. Lower thresholds result in larger contamination, and so are undesirable. Substantial gains in yield can be realized by small changes in the fiducial volume towards smaller distance from the beam because of the very strong power law dependence on $p_{T,\gamma}$. A detailed optimization of signal magnitude and signal:background

ratio still must be completed and simulation of the weighted azimuthal moments is still required.
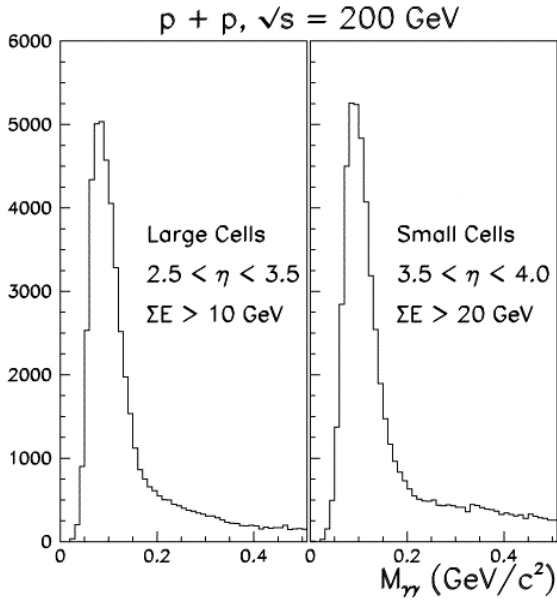

Figure 3-19: First reconstructions of events from the STAR Forward Meson Spectrometer. Clustering and shower shape analysis codes used for the forward pion detector were adapted to the FMS. Although final calibrations and efficiency corrections are still required, clear evidence for π^0 events is seen from the diphoton invariant mass distribution for both the large cell outer calorimeter and the small cell inner calorimeter (see Figure 3-18).
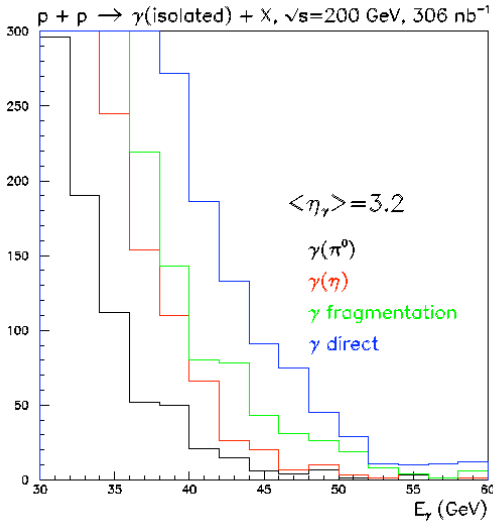

Figure 3-20: Simulation of inclusive forward photon spectrum. Direct photon candidates are detected in a small fiducial volume within the FMS as shown by the shaded region in Figure 3-18. Isolation of radius, $\Delta R = (\Delta\eta^2 + \Delta\phi^2)^{1/2}$, is then required around the photon candidate, where $\Delta\eta$ and $\Delta\phi$ refer to angular differences between near-side correlations with the direct photon candidate and potentially other particles.

Fragmentation photons are also a background for inclusive direct photon measurements that would require a careful study of jet asymmetries for forward jets that contain a fragmentation photon. The prediction for the sign change for transverse SSA is for a forward photon + recoil jet. The isolated fragmentation photon will have its momentum balanced by two jets, rather than one, as expected by the dominant *qg* Compton diagram. Consequently, the fragmentation photon contribution will be spread throughout a $\Delta\phi = \phi_{jet} - \phi_\gamma - \pi$ distribution, whereas the signal of interest is on the sides of the peak in the $\Delta\phi$ distribution, in the vicinity $\Delta\phi \approx 0$. More detailed simulations to quantify this argument are in progress.

An estimate of the luminosity necessary for this measurement has been made based on simulations of the $\Delta\phi$ distribution (Figure 3-21) for p+p $\rightarrow$ γ(forward)+jet at $\sqrt{s}$=200 GeV. The simulations use a simple clustering algorithm to define the midrapidity jet, requiring a seed with transverse energy of at least 0.5 GeV. A cone radius, $R = (\delta\phi^2 + \delta\eta^2)^{1/2} = 0.7$ is used in the clustering. Here, $\delta\phi(\delta\eta)$ refer to the deviation of a hadron from the thrust axis of the reconstructed jet. Jet reconstruction, even at $p_{T,jet} > 2$ GeV/c, is found robust by comparison to recoil parton kinematics and by comparison to a leading particle analysis. The result is that 10^4 useable forward photon + jet coincidences are expected in a 30 pb^{-1} data sample with 60% beam polarization. The γ(forward)+jet yield is sensitive to the jet-finding parameters and the fiducial volume requirement for the forward photon. A full optimization of the event selection to test the theoretical prediction is required, and possibly could result in robust sensitivity to the predicted sign change ($>4\sigma$) at smaller figure of merit. An initial sample of transverse spin γ(forward)+jet of 6 pb^{-1} recorded with beam polarization of 60% would be used to fine tune the figure of merit requirements for the measurement.
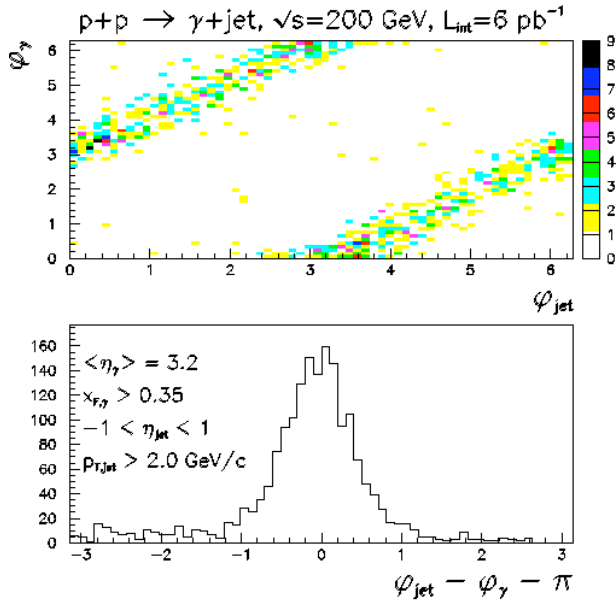

Figure 3-21: Simulation of forward photon + recoil jet for p+p collisions at $\sqrt{s}$=200 GeV.

The goal is to start this unique measurement in Run 9 with a continuation beyond to collect a total integrated luminosity of 30pb^{-1} at transverse beam polarization.

3.4.3. Polarized proton collisions at 500 GeV

Achieving the goals in 2011 of taking a data set for W production with physics impact cannot be met without further beam development at 500 GeV. In addition to important work on the CAD side of operations there is development at the experiments necessary as well. In particular we need to learn in a run before 2011 whether existing local polarimetry will work or not. This is essential for tuning of the spin rotators. In addition the higher

luminosities will provide new challenges to luminosity monitoring. These issues need to be addressed in development time before 2011 to allow for modifications of existing equipment or implementation of new techniques for the production run.

We hope that this can begin during Run 9. However, if Run 9 is significantly shorter than 25 weeks, this will need to be postponed until Run 10 because progress on $\Delta g(x)$ is a higher priority in the near term.

3.4.4 Polarized proton request in Runs 11-13

Beginning with year 11 it is expected that the focus of the STAR spin program will switch to W production with $\sqrt{s}$ =500 GeV polarized pp collisions. This channel has long been identified as a means to measure the polarization of sea quarks[48,49]. It can provide direct access to the difference between the polarizations of u-bar and d-bar quarks, a quantity sensitive to underlying mechanisms which produce the polarized sea[50]. In STAR, W detection will be primarily through W$^-$ $\longrightarrow$ e$^-\gamma$ and to e$^+$ for the W$^+$. Charge sign discrimination is essential to separate the u-bar and d-bar contributions. Construction of a Forward GEM Tracker to provide charge sign discrimination in the forward direction, $1 < \eta < 2$, has recently been approved at STAR and is expected to be installed for Run 11. In Figure 3-22 we show predictions for various underlying quark and anti-quark distributions based on GRSV-STD, GRSV-VAL[51] and GS-A[52] calculated with RHICBOS[53], a program that incorporates an NLO calculation of spin observables in W production. GRSV-VAL considers a flavor asymmetric scenario of Δu and Δd. It is qualitatively similar to the sea quark distributions in DSSV. In contrast, GRSV-STD is based on a flavor symmetric description. Since the cross section for W production is small, a large integrated luminosity is required. The calculations shows that 400pb^{-1} provides significant discrimination between these models setting the scale for goals in the $\sqrt{s}$ =500 GeV spin program.

An extensive effort to simulate electron - hadron discrimination in the forward direction covered by the EEMC are well underway. This analysis makes use of Pythia and GEANT simulations in the full STAR software framework. This effort is quite CPU intensive and special algorithms have been developed to preselect events capable of depositing significant energy in the EEMC. Still it has required the use of a Tier2 grid facility to generate sufficient hadronic background samples for the studies. It is expected that results from this effort including isolation cuts, awayside veto cuts and cuts based on the full segmentation of the EEMC will be released by the time of the PAC.

As the W program is carried out, the spin-dependent gluon distribution of the proton, $\Delta G(x)$, will be measured as well. Again, di-jets and γ-jets will be the most effective at providing a map of $\Delta G(x)$ while inclusive jets and other channels will provide the first results. A major portion of the available running time in Run 11 is assigned to collecting a substantial data set at 500 GeV. The listed goal of 150 pb^{-1} is estimated from current projections for Run 9 at 200 GeV and scaled by the increase in $\sqrt{s}$, i.e. by 2.5. A second running period in Run 13 is assumed to benefit from CAD upgrades and luminosity development which will enable a substantial step in integrated luminosity and physics reach for the W program.

However, given the amount of running time available in the preceding two years, it is expected that our 200 GeV longitudinal goal of 50pb^{-1} (6.5pb^{-1} F.O.M.) for mapping $\Delta G(x)$, and transverse measurements in γ-jet Sivers (30pb^{-1}) for exploring the color sign dependence of the strong force will require additional running time. For this reason a portion of Run 11 is set aside for these goals. In Run 13 there will need to be a substantial run with 200 GeV pp for comparison data for the previous year's Au-Au data with the newly installed HFT. This will provide an opportunity for the spin program to complete its 200GeV goals and hopefully extend its reach for rare probes like gamma-jet and heavy flavor.
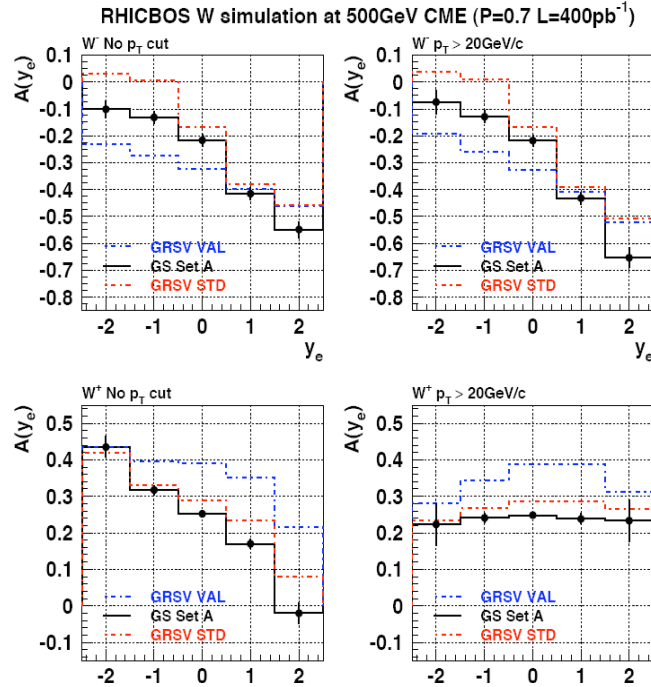

Figure 3-22: A NLO prediction for the single spin parity violating asymmetry for W production in proton - proton collisions at $\sqrt{s}$ =500 GeV from RHICBOS[53] for various underlying quark and anti-quark distributions.

3.5. Physics with tagged forward protons with STAR

By using the polarized proton beam, the STAR detector, and the pp2pp experiment's Roman Pots [54,55, 56], installed and debugged during Run 8, we propose to further extend our scientific program into the non-perturbative regime of QCD. Very forward protons are tagged using the Roman Pot detectors, thus selecting processes in which the proton stays intact and the exchange has quantum numbers of the vacuum i.e. the so-called Pomeron (IP) exchange process. In these processes the probability of measuring reactions where colorless gluonic matter dominates the exchange is enhanced. The use of polarized proton beams, unique at RHIC, will allow for the exploration of the unknown spin dependence of diffraction including both elastic and inelastic processes.

Physics Motivation: There are two main reactions that can be studied with tagged forward protons: Central Production (CP) in double Pomeron exchange (DPE); and polarized proton-proton elastic scattering, see 23.
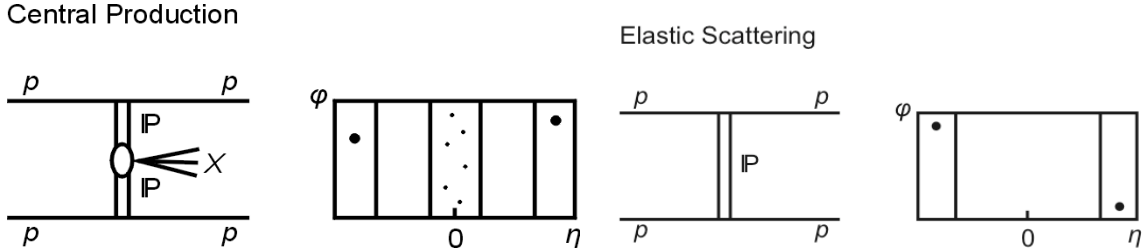

Figure 3-23: Central Production diagram (left) and Elastic Scattering diagram (right).

Central production of glueballs: The DPE processes are commonly characterized by using variables t, ξ, and M_X, where t is the square of the four-momentum transfer between the incoming and outgoing protons, $\xi = \Delta p/p$ is the momentum fraction carried off by the Pomeron and M_X is invariant mass of the system produced. In the case of double Pomeron exchange, separate t and ξ variables exist for each proton-Pomeron vertex.

Tagging and measuring forward protons is important since it removes the ambiguity of a (complementary) rapidity gap tag, which has a background due to the low multiplicity of diffractive events, and allows the full characterization of the event in terms of t, ξ and M_X.

The idea that the production of glueballs is enhanced in the central region in the process pp → pM_Xp was first proposed by[55] and was demonstrated experimentally[56]. The crucial argument here is that the pattern of resonances produced in the central region, where both forward protons are tagged, depends on the vector difference of the transverse momentum of the final state protons $\overline{k}_{T1}$, $\overline{k}_{T2}$, with $dP_T \equiv |\overline{k}_{T1} - \overline{k}_{T2}|$. The so-called dP_T filter argument is that when dP_T is large ($\geq \Lambda_{QCD}$) $\overline{q}q$ states are prominent and when dP_T is small the surviving resonances include glueball candidates. In quantifying the limit the WA102 experiment[56] found "small" $dP_T < 0.2$ GeV and "big" $dP_T > 0.5$ GeV.

The geometrical acceptance of our setup for both Singly Diffractive Dissociation (SDD) and DPE processes has been studied. Protons were generated with t and ξ uniformly distributed in the regions $0.003 < |t| < 0.04$ and $0.005 < \xi < 0.05$ respectively. It was further assumed that the Roman Pots (RPs) were at least 12σ of the beam size at the detection point. Figure 3-24 shows the geometrical acceptance as function of M_X, red dots are for the actual location of the RPs.

These simulations showed that there is good acceptance for measuring inelastic diffraction DPE with $\beta^* = 20$m. Thus, a large data sample of diffractive states can be obtained and analyzed as function of diffractive mass and t ($d^2\sigma/dM_X^2 dt$) for central production.
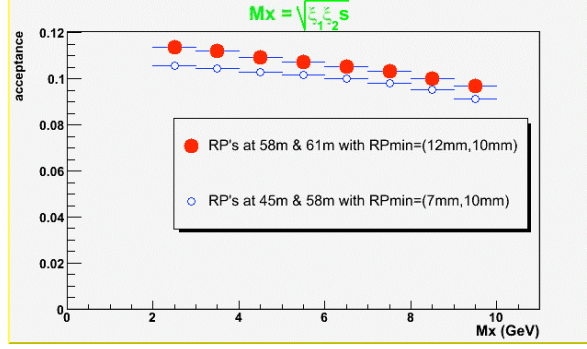
Figure 3-24: Mass geometrical acceptance for DPE processes, red dots are the simulation with final location of the RPs.

Elastic Scattering: The entire energy range of this study has been inaccessible to proton-proton (elastic) scattering in the past. Hence new results of high quality will be produced.

The measurement of the differential pp elastic cross section dσ/dt over the extended t-range will include the region at the lower |t| that is particularly sensitive to the ρ-parameter. Hence we will measure: 1) the ρ-parameter, 2) the nuclear slope parameter b in a combined fit to the differential cross section possible, and 3) the total cross section σ_{tot}.

An asymptotic difference between the differential and total cross sections for pp and $p\bar{p}$, if present, could be explained by a contribution of the Odderon to the scattering amplitude. The absence of an Odderon contribution would lead to identical cross sections, approaching each other roughly as $s^{1/2}$. Our measurement of the total cross section, σ_{tot}, will probe the prevalent assumption that the cross sections for pp and $p\bar{p}$ scattering are asymptotically identical.

Spin dependent observables: By measuring spin related asymmetries one will be able to determine elastic scattering at the amplitude level [57,58,59]. The availability of longitudinal polarization at STAR would allow measuring A_{LL} in addition to A_{NN}, A_{SS}, and A_N resulting in a significant improvement of our physics capabilities. Full azimuthal coverage of the elastic events that we are planning to have will assure high efficiency and small errors of the measurements.

One of the physics motivations to measure A_N is the possibility of the rise with energy of ratio of spin-flip to spin-nonflip amplitudes. In other words, it may occur that the small contribution from hadronic spin-flip to the spin single-spin asymmetry, measured with a polarized jet target at 100 GeV/c, could increase at √s=200 GeV. This will help to address the long standing problem of the energy dependence of the spin flip amplitude, which is best answered experimentally.

Reaching such a small |t|-value allows the measurement of the single spin analyzing power A_N close to its maximum at |t| =0.0024 $(GeV/c)^2$, where $A_{max} = 0.04$, at √s = 200 GeV. The A_N and its t-dependence in the covered range are sensitive to a possible contribution of the

single spin-flip amplitude, ϕ_5, from the interference between the hadronic spin-flip amplitude with the electromagnetic non-flip amplitude.

Forward Tagged Proton Beam Use Request Runs 9 and 10: To maximize physics output from the forward tagged physics running we are requesting a special period of 3 ½ days of beam time in Run 9 with transverse polarization and a separate special 3 ½ days of beam in Run 10 with longitudinal polarization. This would allow us take sizeable data samples with both transverse and longitudinal polarization respectively. The main reason for such runs is that in order to reach the t and ξ values needed for both diffractive and elastic data, beam scraping and special optics are needed. Our tests in Run 8 showed that both STAR and PHENIX could take data during our dedicated run.

We shall use elastic and inelastic trigger bits (ET, IT) based on scintillation counters in the Roman Pots. The CP trigger is from the Central Trigger Barrel and inelastic trigger. The physics reach can be expanded to study diffraction by using FMS and BBC triggers also. Some studies and optimization of those triggers will be required.

Using the capacity of existing power supplies optics of $\beta^* = 20$ m at $\sqrt{s} = 200$ GeV can be produced allowing the t coverage with 100% acceptance for elastic scattering for $0.003 < |t| < 0.024$ (GeV/c)^2. The setup time of the $\beta^*=20$ m optics is estimated by the C-AD to be 12 - 24 hours. Giving us 40 hrs data taking with transverse polarization during the 3½ day run. We are projecting higher efficiency as the lifetime of the beam is longer for our stores and we estimate that no more than two stores are needed for our data taking.

Given the achieved performance of RHIC, luminosity of $1.8\cdot10^{31}$ cm^{-2}sec^{-1}, and making the correction for scraping, which is needed to get close to the beam, and $\beta^*=20$m, luminosity at STAR of $3\cdot10^{29}$ cm^{-2}sec^{-1} for our special run can be obtained. The luminosity at PHENIX will be affected by the scraping only, thus lowered by about factor $1.3^2 = 1.69$, resulting in luminosity $1.1\cdot10^{31}$ cm^{-2}sec^{-1}, scaled from $1.8\cdot10^{31}$ cm^{-2}sec^{-1}. These estimates are based on RHIC projections of luminosity and beam polarization.

With the above conditions about $20\cdot10^6$ elastic events for each polarization could be collected. An estimated error on the slope parameter is $\Delta b=0.31$ (GeV/c)$^{-2}$ and on the ratio of real to imaginary part $\Delta\rho=0.01$, which is comparable to the existing measurements from the pp and p$\bar{\text{p}}$ data. The $\Delta\sigma_{tot} = 2\text{-}3$ mb, where the biggest contribution is from the error on luminosity measurement. This measurement of the total cross section, $\sigma_{\textbf{tot}}$ at the highest possible energy will probe the prevalent assumption that the cross sections for pp and p$\bar{\text{p}}$ scattering are asymptotically identical.

Our data sample of elastic events will allow statistically significant measurements of analyzing power for spin dependent processes. In four t subintervals we shall have $5\cdot10^6$ events in each resulting in corresponding errors $\delta An=0.0017$, $\delta A_{NN}=\delta A_{SS}=0.003$.

With the expected luminosity we can also collect about 450,000, triggered DPE events, for which the proton momentum is reconstructed for each beam polarization. One assumes a

10μbarn cross section within our acceptance for the DPE process, where it is required that two RPs on each side are used allowing reconstruction of the outgoing proton momentum. Number of events for which only one proton tag is used is factor of 4-5 higher or about $2.2 \cdot 10^6$ triggered DPE Central production events for each polarization.

4. RHIC beam energy scan and search for QCD critical point

4.1. Physics motivation

The RHIC PAC has given initial approval to a program of studying Au+Au collisions at energies well below those already explored. The primary goal of this program is to expand the study of the phase diagram of QCD. One particularly exciting possibility is the discovery of a critical point where the transition between the quark gluon plasma (QGP) and a hadron gas changes from a smooth cross-over to a first order phase transition. A detailed energy scan can also investigate how the properties of the created matter evolve as the initial conditions are varied.

A schematic QCD phase diagram is sketched in Figure 4-1. New phases of nuclear matter can be accessed by varying the temperature (T) and baryon chemical potential (μ_B). The QCD phase boundary, indicated by the solid and dashed curves, separates matter in the form of a hadron gas from the QGP. An important goal of nuclear physics is to map out the phase boundaries and understand the evolution of associated physical processes. Different regions of the phase diagram can be studied by varying the center of mass energy of the colliding nuclei. Collisions with higher energies lead to lower μ_B values. As the beam energy is decreased, the created matter enters regions of larger μ_B. Figure 4-2 shows the region of the phase diagram that can be accessed at the RHIC facility along with freeze-out data from previous heavy-ion measurements. Model simulations suggest that the nuclear matter is initially created at a point near the top of the shaded area. As the matter expands and cools, it evolves towards the phase transition and eventually to the freeze-out point. Experimental values for the freeze-out point are shown as open circles.
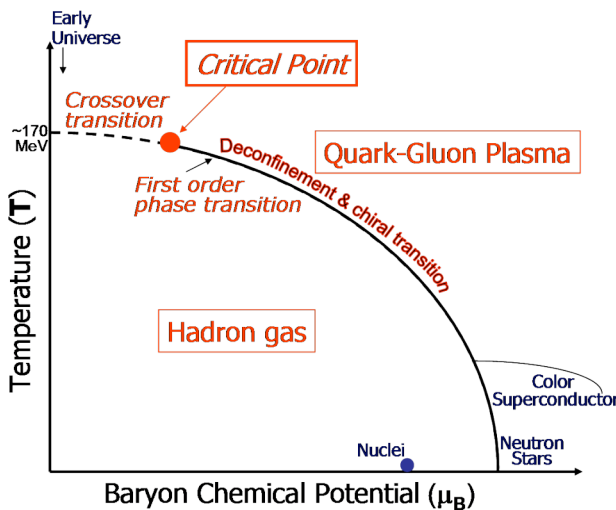

Figure 4-1: Schematic of QCD phase diagram of nuclear matter in terms of the temperature (T) and chemical potential (μ_B). The possible location of the Critical Point is indicated.

Critical Point Search: One of the important motivations for the RHIC energy scan is to search for the QCD critical point, an important landmark on the phase diagram. Model calculations suggest that at large chemical potentials, the boundary between hadron gas and the QGP is a first-order phase transition. Lattice QCD (LQCD) calculations show that at

zero baryon chemical potential, the transition is a smooth crossover. The point where the transition changes from an abrupt first order phase transition to a smooth crossover is called a critical point.

For technical reasons, LQCD calculations become unreliable at non-vanishing baryon chemical potential. Various methods have been devoloped to circumvent these problems but many uncertainties remain. Available LQCD calculations at non-zero baryon chemical potential suggest that as the baryon chemical potential increases, the fluctuations on the cross-over line increase dramatically, suggesting the existence of a Critical Point in the phase diagram. The Critical Point is obtained on a lattice using several methods and several different assumptions regarding the physical volume of the lattice, the lattice spacing, the number of quark flavors, as well as the chosen values for quark mass. None of the computations performed so far could satisfy all the required conditions and thus gave varying results for the location of the Critical Point. Figure 4-2 shows the QCD phase diagram with locations of three different estimations for the Critical Point. As seen in the figure, the different lattice predictions of the Critical Point location vary considerably, but all lie well within the region that will be explored in the RHIC Beam Energy Scan.
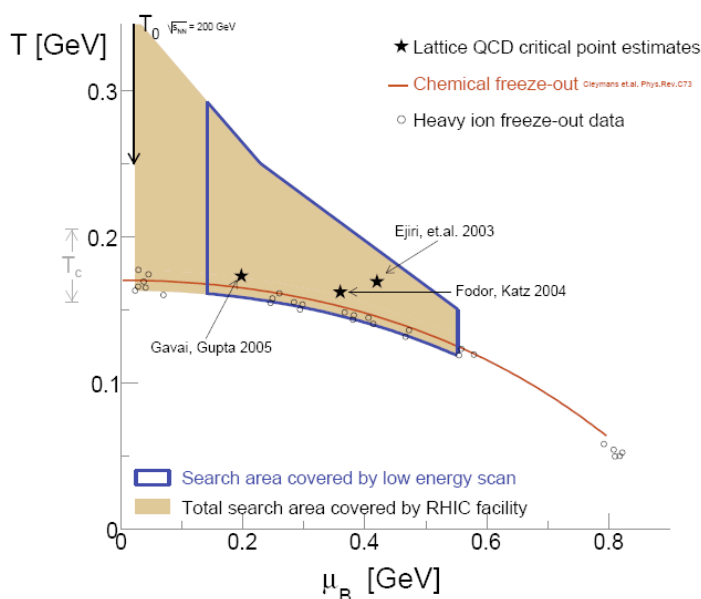

Figure 4-2: The phase diagram of nuclear matter in terms of the temperature (T) and chemical potential (μ_B). Possible locations of the Critical Point, estimated by three different lattice calculations, are indicated. The shaded area shows the parameter space accessible at RHIC; most of this region has yet to be explored, as indicated by the blue boundary line.

Verifying the existence of a Critical Point and fixing its location through experimental measurements would be a major step forward in the effort to determine the properties of QCD at high temperature and density. Specifically, discovery of the Critical Point would identify a crucial landmark in the QCD phase diagram, key to understanding the phases of QCD and their quasi-particles.

LQCD calculations confirm that, at the Critical Point, the baryon number susceptibility, the net charge susceptibility, and the specific heat diverge. In the vicinity of the Critical Point,

critical fluctuations occur in parameters such as the baryon number density, quark number, and charge. These fluctuations should be reflected in experimental observables such as hadronic yields and source size parameters, elliptic flow, fluctuations in net charge, $\langle p_T \rangle$, and particle ratios such as K/π, p/π, etc. The scale dependence of the fluctuations in these quantities may reveal the source of the signal.

The experimental search for the Critical Point must cover the range of temperatures and baryon chemical potentials suggested by the LQCD calculations. This can be achieved at RHIC with a beam energy scan. The experiment should be capable of making comprehensive measurements of all the signals related to the onset of deconfinement. As an example, let us consider one of the signals, the ratio of K^+ to π^+ and its comparison with the K^- to π^- ratio, as shown in Figure 4-3. The K^+/π^+ ratio shows a characteristic dramatic structure at a center-of-mass energy near 8 GeV, whereas the K^-/π^- ratio shows a smooth behavior as a function of the beam energy. The newly analyzed data from STAR at 19.6 GeV fits the systematic trend quite well. The RHIC energy scan includes a detailed study of this region with improved statistical and systematic errors, as well as extending the measurements somewhat farther below the observed structure.
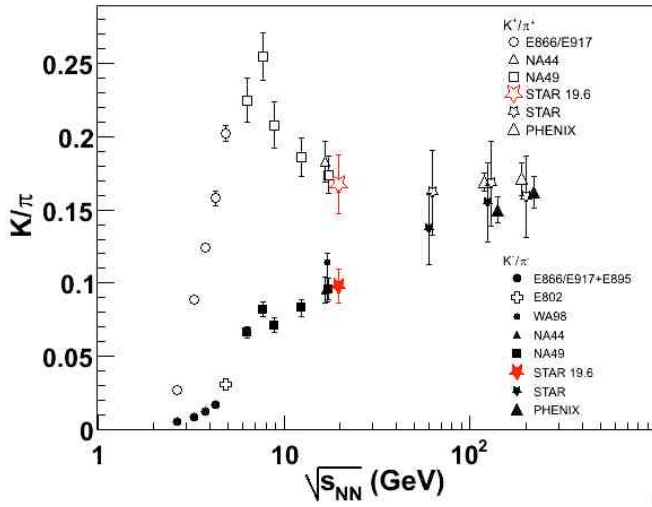

Figure 4-3: Beam energy dependence of the ratios of K^+/π^+ and K^-/π^-.

The STAR detector, as a consequence of its large, uniform acceptance, and excellent PID capability with the inclusion of the new TOF barrel, has superb capability for carrying out a search for the signatures outlined above, and for providing definitive results on the existence and location of the Critical Point. Detailed analyses from the STAR experiment have shown that large acceptance with full azimuthal coverage is essential for fluctuation measurements such as $\langle p_T \rangle$ fluctuations. The utility of such measures has already been demonstrated at available RHIC energies where the variance excess for $\langle p_T \rangle$ fluctuations in terms of $\langle \Delta p_{Ti} \Delta p_{Tj} \rangle$ has been inverted into p_T angular correlations, which are then used to characterize elliptic flow and the near- and away-side medium response (Figure 4-4). These have proved to be an important tool for understanding the role of elliptic flow, mini-jets, and medium response in producing the $\langle p_T \rangle$ fluctuations, forming an important baseline for the QCD critical point at lower energy as well.
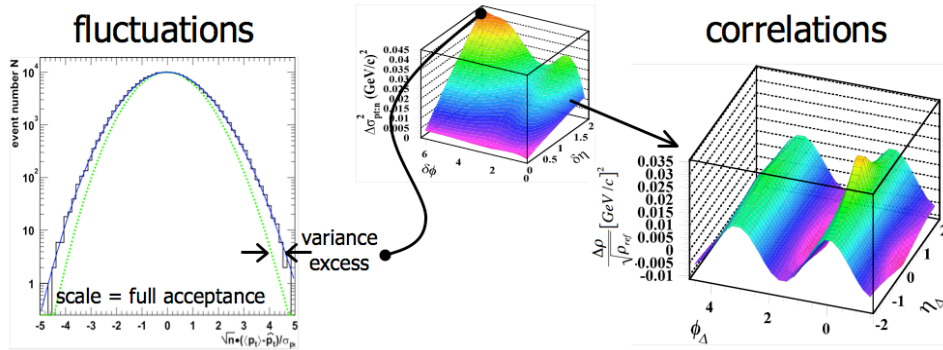
Figure 4-4: The variance excess from mean p_T fluctuations can be inverted to study the role of elliptic flow, mini-jets, and medium response to the correlations observed in Au+Au collisions.
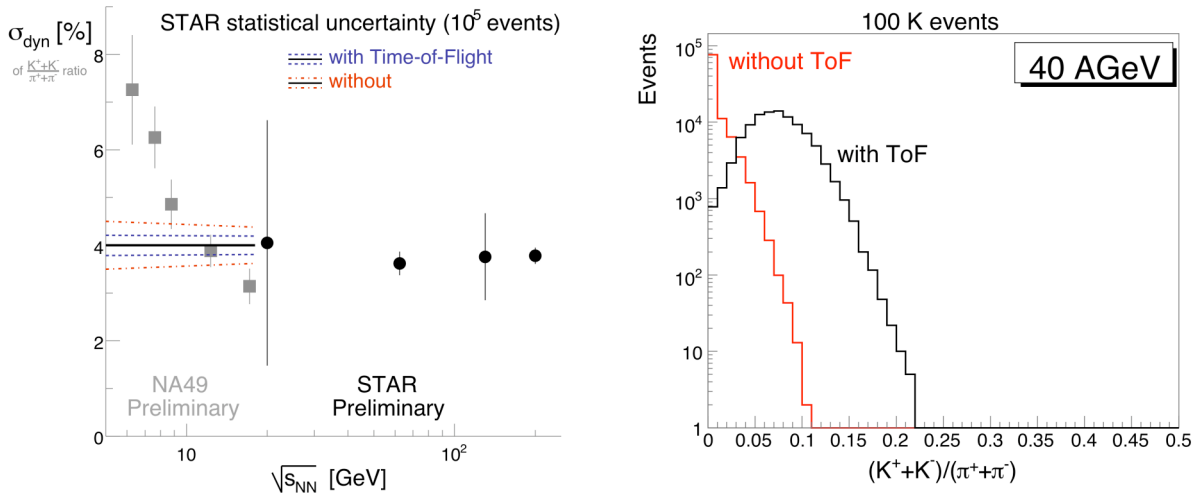

Figure 4-5: A study, based on 100,000 simulated events, of the statistical and systematic uncertainties with and without the PID capability of the STAR TOF. The left panel shows the capability for kaon identification with the inclusion of the Time-of-Flight detector. The right panel shows the beam energy dependence of the dynamic fluctuations associated with the ratio of kaons to pions. With the inclusion of the Time-of-Flight detector, the estimated error is reduced by a large factor.

As shown in Figure 4-5, it is essential to have comprehensive particle identification capability within STAR's acceptance to minimize the systematic error in searching for critical fluctuations, which might indicate the approach to the critical point. Systematic errors dominate the ultimate precision. As seen in Figure 4-5, based on simulation of 100,000 events at 40A GeV, the increase in the statistical error without the full-acceptance STAR TOF is very significant. A misidentification of only 1%, leading to a swapping of pions for kaons, reduces the width of the observed K/π fluctuation distribution by 10%. A misidentification of 2% leads to a reduction in width of 20%. The conclusion from our

simulations is that to optimize the potential to discover the QCD Critical Point, a large acceptance with 2π azimuthal coverage and excellent PID capability, which will be provided by the full-acceptance TOF barrel, is essential.

Energy Dependence of Near-side Correlations: STAR measurements of two-particle correlations either with or without minimum p_T cuts can be decomposed into a few analytic structures, each related to different mechanisms such as elliptic flow, HBT, and jets or mini-jets. This decomposition reveals a near-side correlation structure that extends over a large range in pseudo-rapidity, η. This large $\Delta\eta$ correlation is unique to A+A collisions and shows an abrupt variation with collision centrality. Figure 4-6 shows the correlation for d+Au and Au+Au collisions formed with intermediate-p_T particle pairs. The long-range $\Delta\eta$ correlation is only present in the Au+Au data.
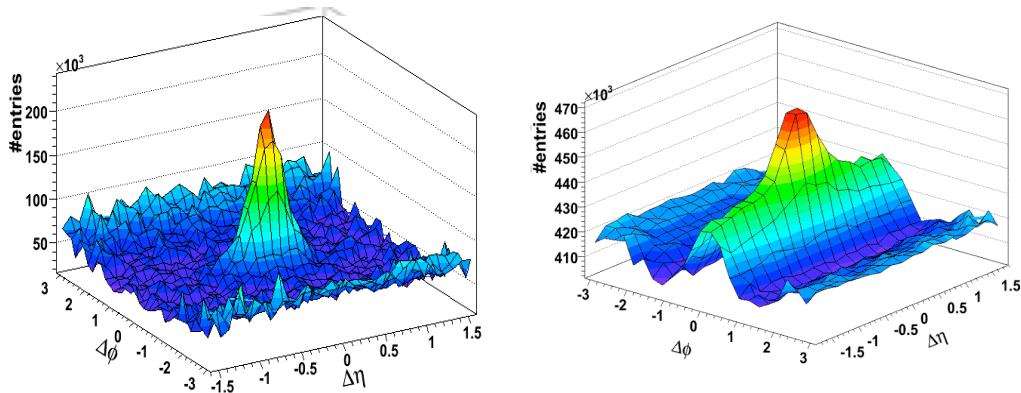

Figure 4-6: Correlations of intermediate-p_T particles in d+Au (left) and Au+Au (right) collisions at $\sqrt{s_{NN}}$ = 200 GeV.

The source of these correlations is under debate, but their extent to large values of $\Delta\eta$ indicates that they must arise earlier in the collision evolution, before the different η regions become causally disconnected. Figure 4-7 shows the amplitude, η width, and volume of the near-side correlation in Au+Au collisions formed with all unique pairs of charged particles.
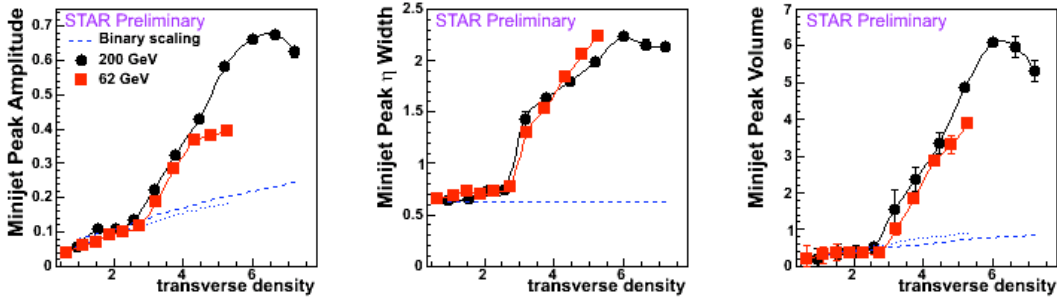

Figure 4-7: From left to right: amplitude, pseudorapidity width, and volume of the same-side Gaussian correlation component versus transverse particle density. Binary scaling predictions of minijet correlations in proton-proton collisions are indicated by the blue dashed curves.

Data from two collision energies are shown in Figure 4-7. For both energies, the abrupt transitions of amplitude and width occur at the same value of tranverse density. This is a non-trivial observation since these correspond to different N_{part} or N_{binary} values, indicating that N_{part} and N_{binary} are not relevant to the physical mechanism causing the abrupt change. Finding the correct scaling quantity can help to elucidate the mechanism responsible for the development of the correlation structure. With the two energies studied, there are still at least two possible scaling quanties consistent with the data; transverse density and Bjorken energy density. These variables differ by constants and a factor of $\langle m_T \rangle$. By carrying out a similar analysis at different beam energies corresponding to significantly different $\langle m_T \rangle$ values, we can better establish what mechanism leads to the abrupt transition in the peak width and volume. For example, is this related to the liberation of quark and gluon degrees of freedom at a particular energy density, or is it due to multiple scattering of minimum-bias partons? This is one example of an area in which the RHIC beam energy scan can provide important new insights into questions raised by studies at higher energies. It is estimated that these studies require 5-10 ~ million events at several center of mass energies between ~10 and ~40 GeV.

Proven Performance at Low Energies: An engineering study was undertaken by C-AD and the RHIC experiments at the end of the most recent run (Run 8). It is a major challenge to inject and collide ions at the low end of the desired energy range, since that is well below the design injection energy of RHIC, which corresponds to a center-of-mass energy of 19.6 GeV [60]. During this study, the goal of the C-AD accelerator physicists was to demonstrate the injection and collision of Au ions at energies of 9.2 and 5 GeV. The primary goal was trigger testing, but there was also a desire to perform preliminary physics studies. The peak luminosity achieved at 9.2 GeV was determined to be 3.2×10^{23} cm^{-2}s^{-1} and the average luminosity was 1.5×10^{23} cm^{-2}s^{-1}. These luminosity values are expected to improve by a factor of 2-10 for future runs.
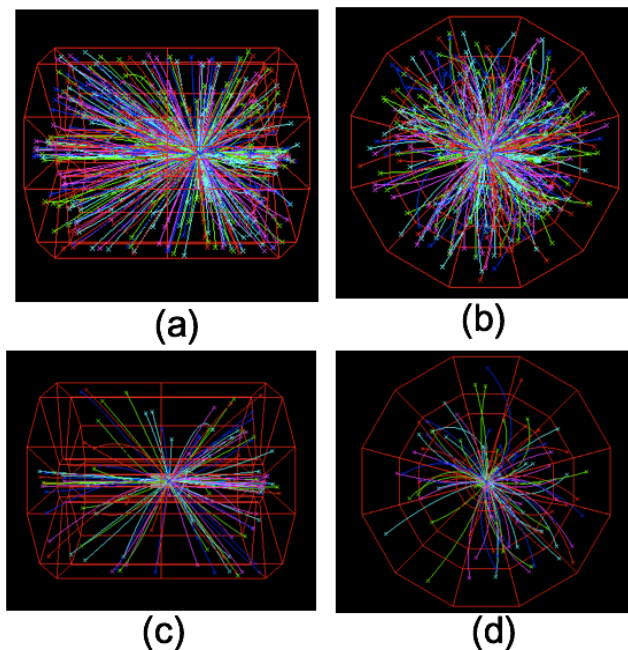

(a)

(b)

(c)

(d)

Figure 4-8: Event display of a high-multiplicity (upper panel) and a low-multiplicity (lower panel) Au+Au collision at 9 GeV.

Figure 4-8 shows the display of tracks in the STAR TPC for two events. The event shown in the top panel is for a typical high-multiplicity event and the one in the bottom panel is for a lower-multiplicity event. The reconstructed tracks clearly show the position of the vertex in the event display and will allow a precise extraction of the vertex position in off-line analysis. Figure 4-9 shows a preliminary distribution of the vertex spread in the beam (z) direction. The preliminary values of the transverse size of the beam are about 2 mm, which is only slightly larger than values found at higher energies. Detailed analysis is in progress to establish the beam characteristics more precisely and also to perform a variety of physics analyses. The STAR measures of various trigger rates will be combined with information from the accelerator physicists to establish a much more reliable estimate of the rates to be expected in the future energy scan.
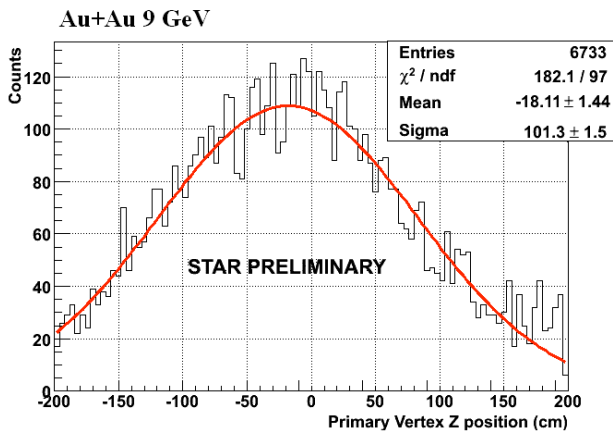

Figure 4-9: Vertex distribution for Au+Au collisions at 9 GeV.

4.2. Beam use request for Run 10

In establishing our request for Run 10, we have considered how to maximize the physics impact while keeping the duration of this initial low energy physics run within reasonable bounds. To start the beam energy scan program at RHIC, we request 14 weeks of Au+Au collisions dedicated to the energy scan. The goals that we can reasonably expect to accomplish are limited by the low event rates expected at the lower beam energies. These event rates can be improved through upgrades such as electron cooling in RHIC. However, these upgrades will not be available by Run 10.

We expect to gain new insight into the near-side correlations by gathering at least 5 million usable events at 12.3 and 17.3 GeV, and 10 million events at 28 and 39 GeV. It should be noted that the exact values of all beam energies used will depend on matching the RHIC RF frequency and harmonic number to optimize collisions at both PHENIX and STAR, and, at approximately 39 GeV, to avoid the transition energy in RHIC. These approximate values of the energy are selected in order to provide data near the critical point estimates suggested by Gavai and Gupta [61], and in order to gain at least two more energies where we expect to be able to resolve a near-side peak in the two-particle correlations. Possible trends

suggesting the disappearance of the near-side peak in p_T and number correlations can also be verified with these data sets.

In order to check for a discontinuity in the K/π ratio as suggested by NA49 data and to improve the precision of the K/π fluctuations, we also require at least one million events for energies at 6.1, 7.7 and 8.6 GeV. In most cases the SPS energies cannot be exactly matched due to accelerator limitations. These data sets will allow improvements to the K/π fluctuation measurements but may not allow for more differential analyses, which are useful for a more detailed interpretation of the measurements. Such analyses and the very lowest data points such as 5 GeV and 6 GeV must be revisited once better rates can be provided by RHIC. Towards this goal, we request about 7 days for an engineering run at 5 GeV during Run 10. The program as described above allows us to accomplish a significant fraction of our physics goals in a 14-week period, while taking into account the limitations of the RHIC facility. Greater statistics and significant event samples for energies near 5 and 6.GeV will need to be accomplished during future runs after accelerator upgrades. Figure 4-10 shows the expected uncertainty after the initial beam energy scan.
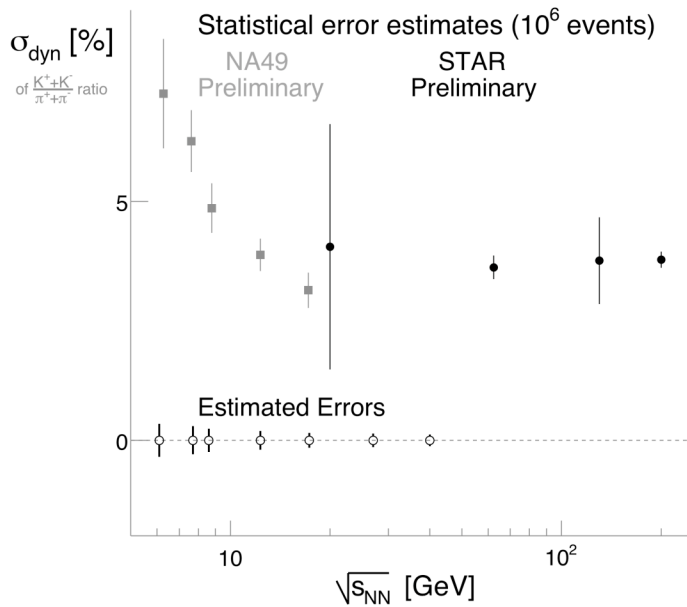

Figure 4-10: Current measurements of the dynamic width of the distribution of kaon to pion ratios along with the estimated errors from a Run 10 beam energy scan. Estimates are made for one million minimum bias events at each energy. Larger event samples requested will allow for more differential studies.

Table 5: Run plan for a 14 week physics +1 week commissioning beam energy scan.

$\sqrt{s_{NN}}$ [GeV]	μ_B [MeV]	Approximate Event Rate [Hz]	Goal [Events]	Duration [Days]
5.0	550	0.5	Testing	7
6.1	491	1.4	1M	23
7.7	410	2.7	2M	20
8.6	385	4	2M	15
12.3	300	10	5M	15
17.3	229	25	10M	12
27	151	30	10M	7
39	112	50	10M	6

Table 6: Run plan for a 12 week physics +1 week commissioning beam energy scan.

$\sqrt{s_{NN}}$ [GeV]	μ_B [MeV]	Approximate Event Rate [Hz]	Goal [Events]	Duration [Days]
5.0	550	0.5	Testing	7
6.1	491	1.4	1M	20
7.7	410	2.7	2M	20
8.6	385	4	1.5M	10
12.3	300	10	5M	15
17.3	229	25	5M	6
27	151	30	10M	7
39	112	50	10M	6

5. Heavy ion collisions at 200 GeV

5.1. Triggered probes and heavy flavor with heavy ions

With the luminosities available at RHIC, collision rates are too large for all events to be written to tape with the STAR DAQ. Therefore, triggers are needed to sample the events for rare probes, the most discriminating of which use the Barrel Electromagnetic Calorimeter in a number of ways. A simplified history of sampled luminosity is shown in Table 7, which compares by run and species the integrated luminosity sampled by the Barrel EMC High Tower trigger with the highest threshold, requiring all detectors to be read out. A comparison between species can be made based on the binary scaling hypothesis, in which the pp-equivalent luminosity in collisions between species A and B scales as A*B. This approximation is only roughly correct: for probes that are suppressed, such as hadrons at high p_T, the combination of suppression and centrality cuts can reduce the rates of triggered probes relative to this expectation by up to an order of magnitude. The integrated luminosity has been steadily progressing, so that we now have on the order of 10 pb^{-1} pp-equivalent integrated luminosity sampled in p+p, d+Au, and Au+Au collisions at 200 GeV.

Table 7: Integrated luminosity in highest threshold Barrel EMC high tower trigger with full detector readout. pp-equivalent luminosity for collisions between species A and species B is calculated as A*B*luminosity.

Run	System	Threshold [GeV]	Integrated Luminosity	pp-equivalent L [pb^{-1}]
3	d+Au	4.5	1.7 nb^{-1}	0.7
	p+p	4.5	0.17 pb^{-1}	0.17
4	Au+Au	3/sin(theta)	50 ub^{-1}	2
	p+p	4.6/sin(theta)	0.15 pb^{-1}	0.15
5	Cu+Cu	3.75	860 ub^{-1}	3.4
	p+p	4.2	2.8 pb^{-1}	2.8
6	p+p	5.4	11 pb^{-1}	11
7	Au+Au	5.5	0.5 nb^{-1}	20
8	d+Au	8.4	36 nb^{-1}	14
	p+p	4.3	3.1 pb^{-1}	3.1

Before Run 9, the STAR TPC has limited the luminosity that can be sampled, since it had linear deadtime that would rise with the rate of triggers that are written to tape. In practice, this led to a loss of 50-70% of the events that could be sampled by the trigger, since triggered programs competed with large samples of minbias and central events, and the size of the triggered datasets themselves also need to be considered. With DAQ1000 for Run 9

and beyond, this limitation has been largely removed, so that the triggered program can both easily coexist with the untriggered program and essentially double its efficiency in sampling the integrated luminosity delivered by the accelerator.

The next step is to increase these sampled luminosities by orders of magnitude. With stochastic cooling in RHIC II, in one RHIC year STAR can sample up to 20 nb^{-1} in Au+Au collisions. A strawman for the progression of luminosities is shown in Table 8. The following section will demonstrate a sample of the measurements that can be made within this scenario.

Table 8: Strawman for increase in integrated sampled luminosity at $\sqrt{s_{NN}} = 200$ GeV over the next five years.

Run	System	Total Integrated Sampled Luminosity	pp-equivalent Sampled Luminosity	Physics from run
9-10	p+p	50 pb^{-1}	50 pb^{-1}	Reference data for: First attempt at separation of Upsilon 1S from 2S+3S Further study of e-D from B J/Psi to high p_T
9-10	Au+Au	0.5 nb^{-1}	20 pb^{-1}	Electron spectra for R_{AA} with low material to resolve PHENIX/STAR discrepancy
11	p+p	100 pb^{-1}	100 pb^{-1}	Extension of reference data from Runs 9-10
12	Au+Au	5 nb^{-1}	200 pb^{-1}	High precision γ-hadron, Upsilon, J/Psi, e-D with HFT for bottom
13	p+p	200 pb^{-1}	200 pb^{-1}	Reference for Run 12
13+	Au+Au	20 nb^{-1}	800 pb^{-1}	High precision utilization of RHIC II luminosity

γ-hadron correlations: Correlations between a direct photon and a hadron have been termed a "golden probe" of parton energy loss in the medium. A direct photon does not interact with the medium, and so does not lose energy. RHIC sits at a sweet spot in terms of backgrounds, as the nearly exclusive source of coincident photons and hadrons in the relevant kinematic regime is QCD Compton scattering between a quark and a gluon. Photons from pion decay are subdominant, and Next-to-Leading-Order processes such as parton fragmentation into photons are expected to be small, on the order of 10%, as a first measurement from PHENIX indicates. From this clean process, both the identity and kinematics of the parent parton of the associated hadron are cleanly tagged. This allows for a precise measurement of the modification of the fragmentation function of a quark due to its interactions in medium.

The challenge with photon-hadron correlations is the low production rate. Figure 5-1 shows results to date, shown at QM2008, for measurements of direct photon-hadron correlations. While the results are within errors of theoretical predictions, the size of the uncertainties do not provide sufficient distinguishing power between different theoretical scenarios.
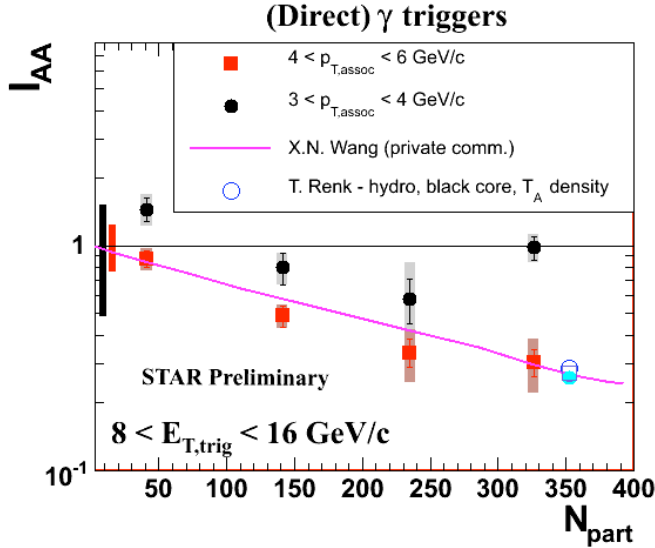

Figure 5-1: Suppression of away-side hadrons associated with direct photons from Run 7 Au+Au (0.5 nb^{-1}) and Run 6 p+p (9 pb^{-1}). Bars at the origin at unity denote uncertainty in the p+p reference, error bars indicate Au+Au statistical uncertainties, and grey bands denote systematic uncertainties.
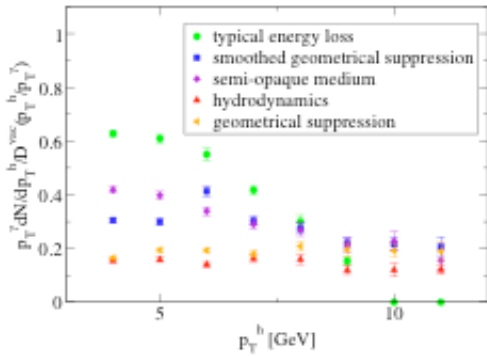

Figure 5-2: Prediction for sensitivity of suppression of γ-hadron away-side correlations to different scenarios, where E$_T^\gamma$ > 15 GeV. From T. Renk, Phys. Rev. C74 (2006) 034906.
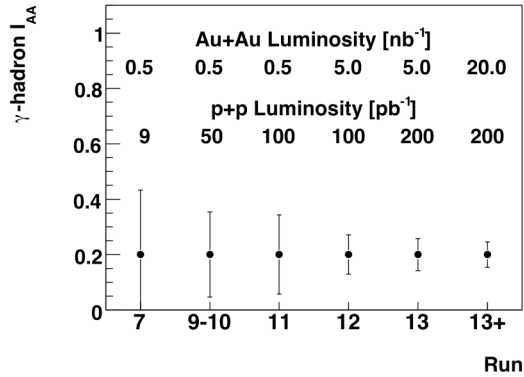

Figure 5-3: Projection for statistical uncertainties in γ-hadron suppression in a scenario of luminosity progression in different years. Projection is for E$_T^\gamma$> 15 GeV, associated particle p$_T$ from 4-6 GeV/c.

In order to make progress, more luminosity is needed. Figure 5-2 shows one set of predictions under different theoretical scenarios of the suppression pattern, for a somewhat higher trigger E$_T$, > 15 GeV, than STAR has measured to date. This higher trigger E$_T$ is needed to ensure that the associated hadron is both at relatively low fractional momentum with respect to the trigger photon and at high enough p$_T$ to be cleanly associated with jet

phenomena. Figure 5-3 shows a projection of the evolution of the uncertainties in a representative bin, 4-6 GeV/c associated particle p_T for one scenario of evolving luminosity sampled by STAR in the coming runs. This bin shows the largest deviation between theoretical scenarios, though the scenarios with the largest deviations are currently disfavored. As shown in the figure, incremental progress can be made over the next five years, as cooling in RHIC ramps up to the full luminosity of RHIC II. Beyond this, studies of suppression focusing on the orientation of the trigger with respect to the reaction plane, and for identified hadrons combining the full Barrel Time of Flight detector with dE/dx in the TPC, will be possible in certain kinematic regions. With RHIC II luminosities, precise determination of the modification of quark fragmentation functions in medium will be possible with these correlation measurements.
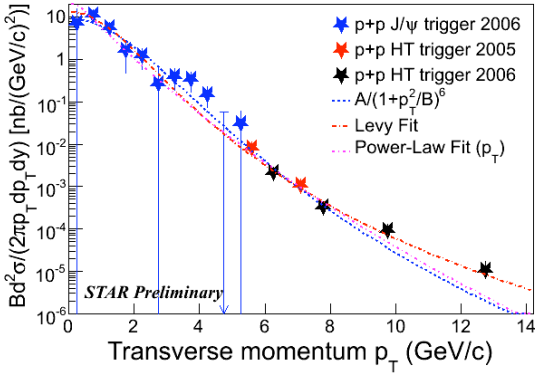

Figure 5-4: J/Psi differential cross section at mid-rapidity from p+p collisions at √s=200 GeV.

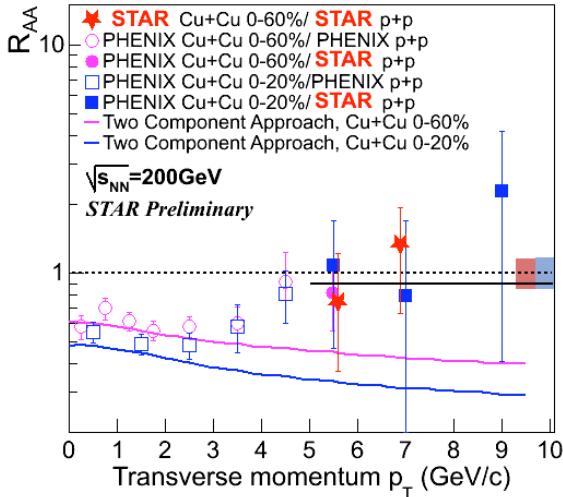**Figure 5-5: J/Psi R_{AA} in Cu+Cu collisions, as comparted to a theoretical expectation.**

Quarkonia: At Quark Matter 2008, STAR showed J/Psi spectra out to transverse momenta of 14 GeV/c from triggered data from p+p and Cu+Cu collisions in Runs 5 and 6, as shown in Figure 5-4. By comparing STAR data across species and with PHENIX data, it appears that J/Psi suppression decreases at high p_T and R_{AA} approaches unity, in contradiction to some theoretical expectations, see Figure 5-5. However, this statement is statistically limited, at approximately 2-sigma, so further measurements are sorely needed. Figure 5-6 shows a projection of statistical uncertainties after the integrated sampled luminosities proposed for Runs 9-10, assuming that the increased bandwidth of DAQ1000 allows the thresholds to remain constant as luminosity increases, and that R_{AA} is unity. Should J/Psi be suppressed at high p_T, uncertainties will increase accordingly. While such integrated luminosities would greatly extend the reach of J/Psi measurements at RHIC, precision measurements await the higher luminosities of RHIC II, as shown in Figure 5-7 for luminosities expected by Run 13. At lower p_T, the addition of the full Time of Flight barrel will greatly decrease backgrounds, and should enable significant measurements, though

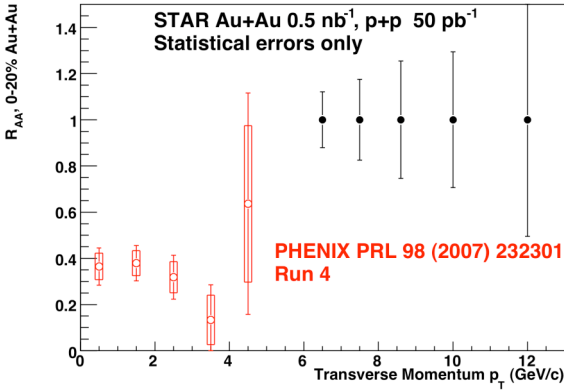effective triggering is still under study to understand the statistical significance that can be achieved.

Figure 5-6: Projection for statistical uncertainty in J/Psi R_{AA} at high p_T, assuming R_{AA}=1, from integrated sampled luminosity of 0.5 nb^{-1} in Au+Au collisions and 50 pb^{-1} in p+p collisions, as proposed in Runs 9-10.
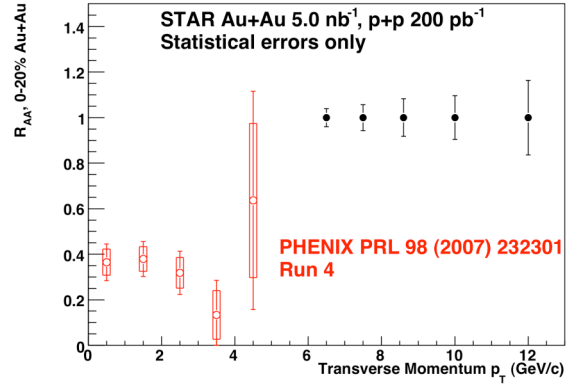
Figure 5-7: Projection for statistical uncertainty in J/Psi R_{AA} at high p_T, assuming R_{AA}=1, from integrated sampled luminosity of 5 nb^{-1} in Au+Au and 200 pb^{-1} in p+p collisions, as proposed to occur by the end of Run 13.

Upsilons remove many of the ambiguities that surround J/Psi suppression, since the b quark production cross-section is not large enough for recombination to be appreciable, and interactions between the Upsilon and co-moving hadrons are expected to be weak, leading to a cleaner signature of suppression at early times. Different states of Upsilon (1S, 2S, and 3S) are expected to be affected by the medium at different levels: the 1S state is expected to be unsuppressed, while the 2S and 3S will be successively more strongly suppressed. By studying the full pattern of suppression, one can place constraints on the temperature and/or energy density of the medium. STAR has begun the Upsilon program with Runs 6 and 7. Shown in Figure 5-8 and Figure 5-9 are mass peaks from p+p collisions in Run 6 and Au+Au collisions in Run 7, both peaks of which have significance of approximately 4-sigma. A comparable dataset was collected in d+Au collisions in Run 8.
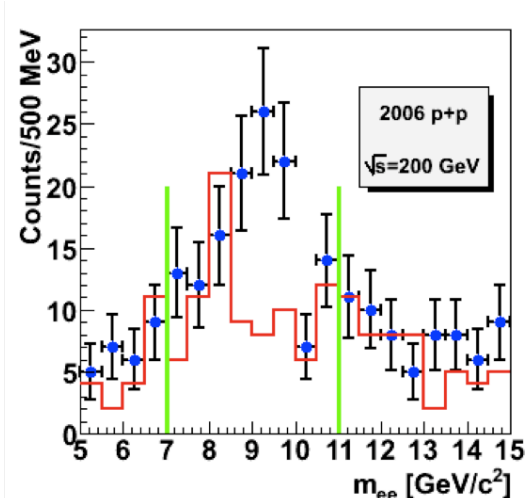
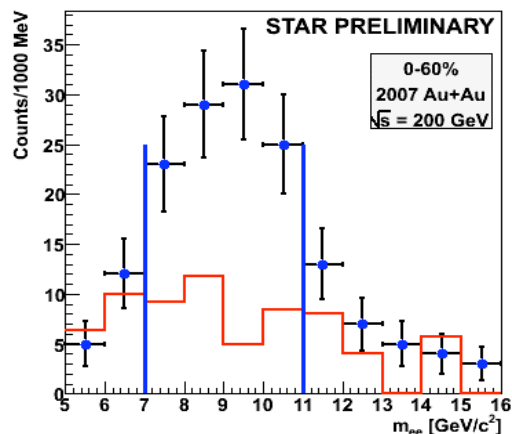**Figure 5-8: Upsilon (1S+2S+3S) mass peak from p+p run 6, 9 pb⁻¹.**

Figure 5-9: Upsilon (1S+2S+3S) mass peak from Au+Au Run 7, 0.3 nb⁻¹.

After Run 7, STAR removed the inner tracking detectors the SVT and SSD, which greatly reduce the amount of material seen by electrons, and so reduces the broadening in the mass resolution in the di-electron channel from Bremsstrahlung. Figure 5-10 shows the expected resolution from simulation in the current configuration. With this resolution, and 50 pb⁻¹ sampled integrated luminosity from p+p collisions in Run 9, a first measurement separating the 1S from the 2S and 3S states appears to be feasible. This will need to be followed up with later runs integrating larger sampled luminosity in both p+p and Au+Au.
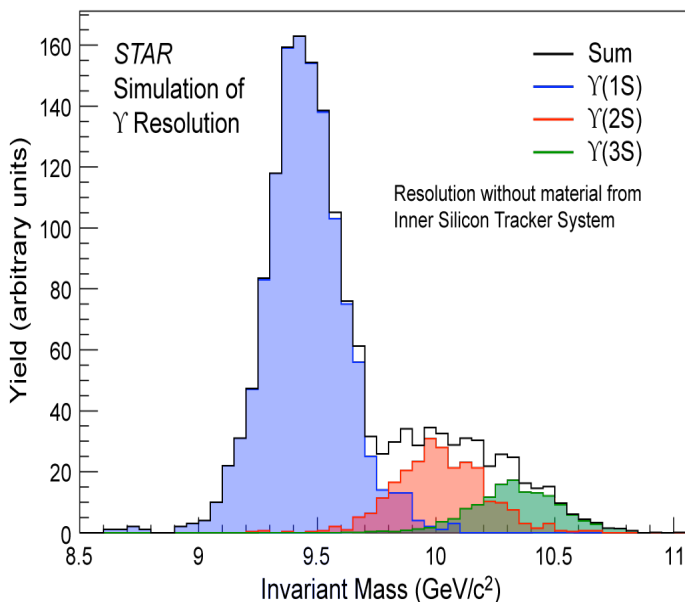

Figure 5-10: Expected mass resolution in Runs 8 and beyond, with no inner tracking detectors

The ultimate goal from RHIC II luminosity is shown in Figure 5-11, which shows expected uncertainties in Upsilon(1S) that can be achieved with 20 nb⁻¹ sampled integrated luminosity in Au+Au collisions and 100 pb⁻¹ sampled integrated luminosity in p+p

58

collisions. With this dataset, precision measurements of the dissociation of quarkonium states will be made possible.
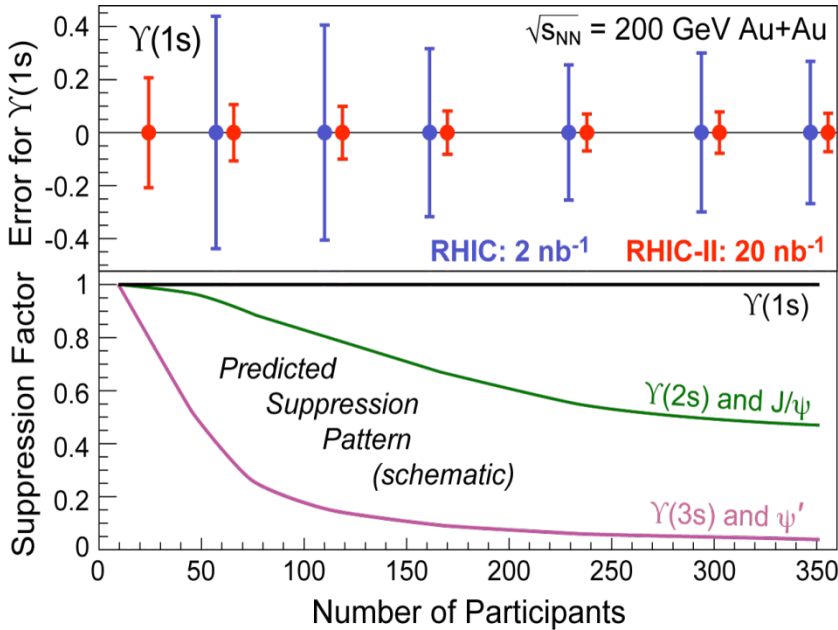

Figure 5-11: Projection of uncertainties in Upsilon(1S) R_{AA} for two sets of integrated luminosity.

Open Heavy Flavor: Energy loss of heavy quarks tests perturbative calculations of partonic energy loss in the medium in a way orthogonal to photon-hadron correlations. Non-photonic electrons, produced predominantly from decays of beauty and charm, are strongly suppressed, providing a strong challenge to these calculations. There are, however, a number of limitations to the measurements that cloud their interpretation.

First, as shown in Figure 5-12, the uncertainties on the spectrum of non-photonic electrons are quite large, and there is an apparent discrepancy between STAR and PHENIX (though R_{AA} is consistent between the experiments). Data from Run 8 will help to resolve these issues, since the sampled integrated luminosity increased by a factor of 30 relative to the published results, and without the SVT and SSD the backgrounds from conversion electrons in STAR are comparable to those in PHENIX.

The major limitation comes from the uncertainty in the relative contribution of charm and beauty to the non-photonic electrons. Energy loss calculations predict significant differences between the suppression of charm and beauty, but perturbative calculations cannot accurately predict the relative contribution of charm and beauty to these non-photonic electrons. Without measuring this fraction accurately, we are left with an unconstrained problem. First attempts at measuring this fraction in p+p collisions, using correlations between the electron and hadrons or fully reconstructed D's, are shown in Figure 5-13. The measurements are consistent with the most advanced calculation, a Fixed-Order Next-to-Leading-Log calculation, but the data do not strongly constrain the uncertainties in the calculation.
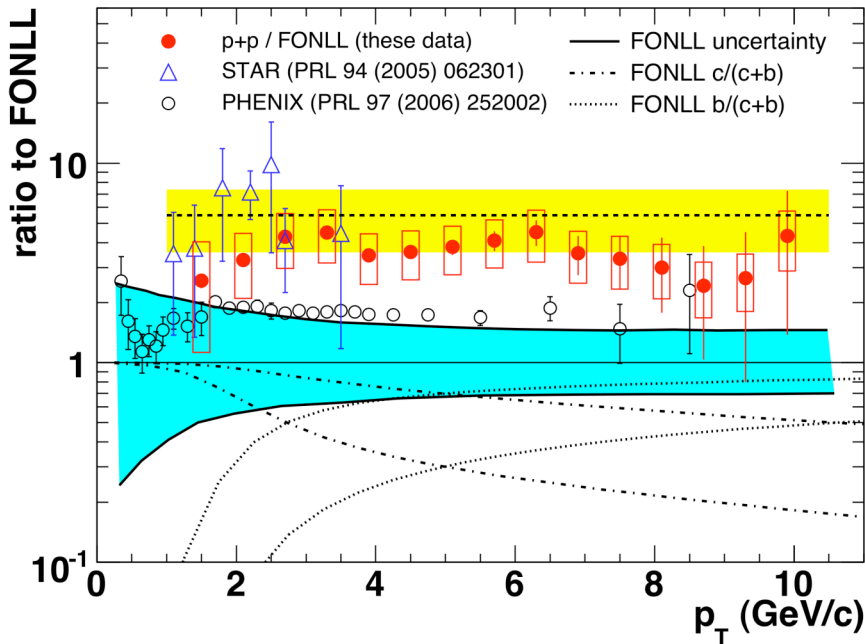
Figure 5-12: Ratio of non-photonic electron spectrum in p+p collisions at 200 GeV to a theoretical FONLL calculation. From a sampled integrated luminosity of 0.1 pb^{-1}.
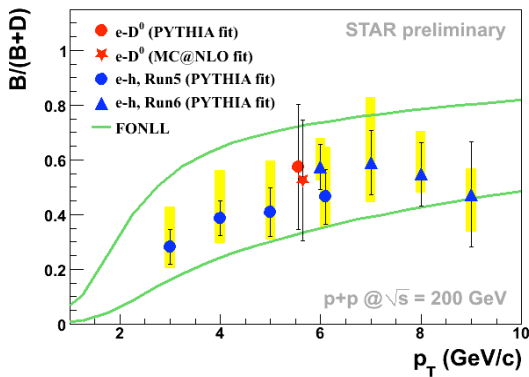
Figure 5-13: Relative contribution of beauty to non-photonic electrons, from correlation measurements, as compared to the uncertainty band from a FONLL calculation. Sampled integrated luminosity in Run 6 was 9 pb^{-1}.
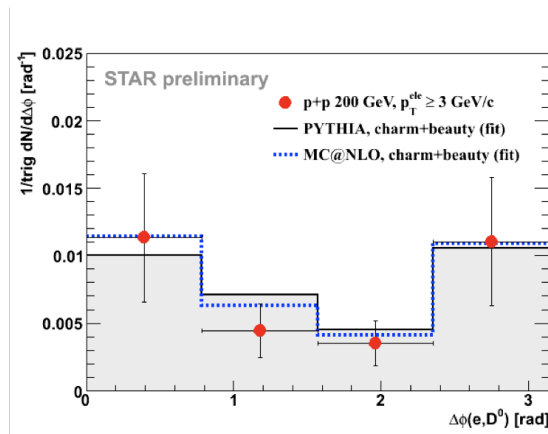
Figure 5-14: Per-trigger yields of reconstructed D mesons as a function of azimuth relative to a trigger non-photonic electron with p$_T$ between 4 and 8 GeV/c. From 9 pb^{-1} of p+p collisions in Run 6.

There are a number of future directions to constrain this situation. First, with larger untriggered datasets, and with the Heavy Flavor Tracker, direct D measurements out to high p$_T$ will be possible. With the TPC and TOF, with 200M events of any system D spectra can be measured with 3-sigma accuracy out to p$_T$ of 4-5 GeV. In p+p, with DAQ1000, this is

planned for Run 9. With the Heavy Flavor Tracker, D spectra and R_{AA} can be measured with high accuracy out to 10 GeV by Run 13.

In the triggered sector, correlations between electrons and fully reconstructed D mesons are the most promising, and the most starved for luminosity. Figure 5-14 shows the per-trigger yield of fully reconstructed D^0 mesons associated with a triggered non-photonic electron within 4-8 GeV/c. From simulations, the near side peak is almost exclusively from B decays, while the away-side peak is from a combination of B and D decays. With 50 pb^{-1} sampled integrated luminosity from p+p collisions in Run 9, a measurement of both the near and away side peak will be possible at the 20% level. Studies of these correlations are ongoing in the Cu+Cu and Au+Au datasets: precision measurements of the suppression of these correlations in medium will be possible in future years, aided greatly by the Heavy Flavor Tracker.
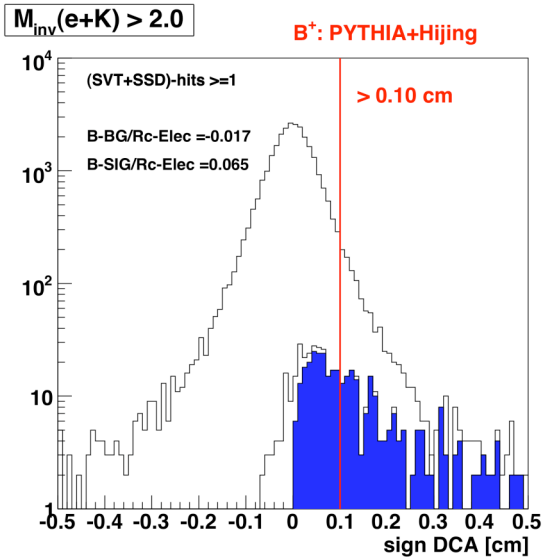
Figure 5-15: Signed DCA between secondary vertex of e and K candidates and the primary vertex for all particles, for injected B+, and the subtraction of negative from positive signed DCA (blue). From simulations with PYTHIA B decays injected into Hijing. Invariant mass between the e and K is required to be greater than 2 GeV to suppress D decays.
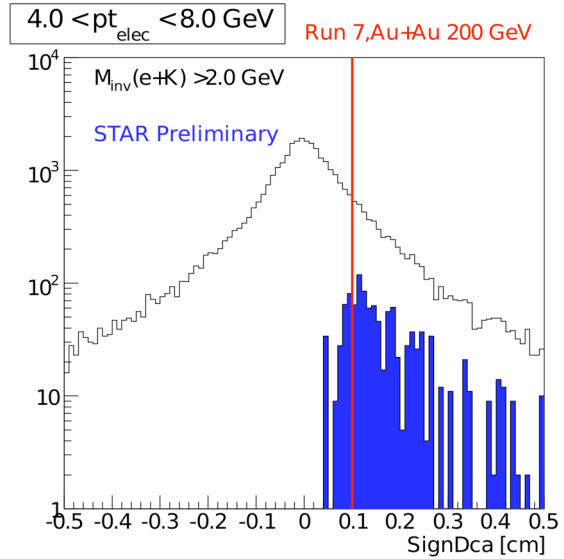
Figure 5-16: The same quantity as shown in Figure 5-15, only for Au+Au data taken during Run 7. Total sampled integrated luminosity, after vertex cut, was 50 ub^{-1}, leading to a signal of high significance, shown in blue.

A first step towards direct tagging of electrons from B decays, using e-K correlations at high invariant mass and secondary vertex reconstruction, was begun using the SVT and SSD in Run 7 Au+Au. The analysis follows a similar approach to that taken by CDF. Electrons, triggered with the Barrel Electromagnetic Calorimeter with $p_T > 4$ GeV, are paired with hadron candidates to form secondary vertices which approximate the decay vertex of a heavy (D or B) meson. Since the D mass is 1.8 GeV, a cut on the invariant mass

between the electron and hadron above 2 GeV strongly suppresses electrons from D decays. The signed distance of closest approach between the secondary and primary vertex, signed by $\cos(\theta)$ between the DCA vector and the hadron momentum vector, provides further discriminating power and the ability to measure backgrounds, since those pairs from B decay occur predominantly at positive values in this quantity. By subtracting the counts at negative signed DCA from positive signed DCA one obtains a clean signal for electrons from B decays, as shown in Figure 5-15 from simulation and Figure 5-16 from data. With the integrated luminosity sampled in Run 7, approximately 50 μb^{-1} after cuts on primary vertex position, a clear signal of high significance is seen in the data. Future measurements at much higher luminosity and vertex reconstruction precision will be possible with the HFT, allowing for precision study of the interaction of b quarks with the medium.

Heavy Flavor Tracker: Precision measurements of charm and beauty require the Heavy Flavor Tracker (HFT). The HFT is still a project in its early days, but is an important upgrade to STAR. In connection with the CD-0 review at BNL on February 25 and 26 the necessary beam conditions were outlined to fulfill the science milestones for the project. The actual year when the project will be ready to take data is of course uncertain, depending on funding and construction success. The technical driven plan presented at the CD-0 review have completion in time for the Run 12. It is, however, noted that the current planned start of construction funding in FY10 will imply a delayed schedule. Table 9 below is based on this technical schedule.

5.2. Triggered probes and heavy flavor beam use request

Table 8, in the previous section, provides a strawman plan for the year-by-year increase in luminosity towards the ultimate goal of RHIC II for triggered probes. In Runs 9-11, the main goals are to increase the statistical power of the reference in p+p collisions, and to make use of moderate amounts of integrated luminosity in Au+Au, in the time window between the removal of the SVT/SSD and the installation of the HFT, to make measurements in the electron sector that benefit from a low amount of material. Starting with Run 12, we expect to begin the precision program of RHIC II in earnest, with an order-of-magnitude increase in sampled integrated luminosity in Au+Au collisions and the installation of the Heavy Flavor Tracker. Specific needs for the Heavy Flavor tracker are described bellowed and surmised in Table 9.

Run 11: It is an important intermediate goal for the HFT upgrade to have the mechanical structures for the Pixel, and beam pipe in place for an engineering run. The Pixel would be instrumented with a few (2-3) ladders with sensors of the Phase-1 type. The primary purpose is to ensure the sensors and readout systems work in the RHIC environment, and gain experience with quality of data, alignment in preparation for the complete installation. The configuration will be chosen such that a partial measurement of directly identified D^0 spectrum is possible in a limited pt range.

Run 12: In the first run after completion of the HFT we anticipate taking 500M minimum bias events of Au+Au collisions at 200 GeV. This will allow us to measure v_2 of D^0 in the p_t range from 600 MeV/c up to a p_t of larger than 5 GeV/c. The absolute error on the measurement will be 0.009 for the p_t bin from 600 to 1000 MeV/c and 0.007 for the p_t bin from 3.75 to 4.25 GeV/c. This will address the question if the light quarks are thermalized. From the same 500M events we also will be able to measure the p_t dependence of R_{cp} of D^0 mesons in the p_t range from 1 GeV/c to 10 GeV/c. For the central events we take the 10% most central events and for the peripheral events we chose the centrality bin of 60 to 80%. R_{cp} will be determined to 5% in the p_t bin 1.75 to 2.25 GeV/c and to 16% in the p_t bin 7.5 to 8.5 GeV/c. The errors are for the case that the open charm suppression is the same as for light quark mesons. This measurement will further our understanding of the energy loss mechanism in the hot and dense medium created at RHIC. All errors are statistical only.

Run 13: In the second year we anticipate a long p+p run at 200 GeV. In a run of 3 months we expect to be able to record 2 billion minimum bias events, with which we will measure the p_t dependence of D^0 production and achieve a precision of 17% for the p_t bin between 7 and 8 GeV/c. The total D^0 production cross section will be measured with a precision of better than 15%. This is important input for pQCD calculations and the combination of p+p and Au+Au data will enable us to determine R_{AA}.

Run 14: In the third year we anticipate a high statistics Au+Au run. With 1,000M minimum bias events we will be able to perform impact parameter selected v_2 and R_{AA} measurements. In the centrality bin with the largest v_2 signal, $40 - 60\%$, the statistical error in the D^0 production will be less than 2.5% in each p_t bin, with $p_t = 0.5$ GeV/c, in the p_t range from 1 to 4 GeV/c. Finite reaction plane resolution will dominate the v_2 errors, the maximum error being about 10%. The systematic measurement of the centrality dependence will allow us to address the issue of light quark thermalization and determine the collective velocity of charm quarks. In the third year we will have accumulated a Λ_c spectrum with about 14,000 identified Λ_c in the p_t range of 2 to 10 GeV/c.

Table 9: Heavy Flavor Tracker Timeline and Beam Use Request

Installation/Run	FY	Physics	Request
Run 11	FY11	Commissioning	HFT engineering run (A+A at 200 GeV)
Run 12	FY12	v_2(pt) for D^0; R_{CP}	200 GeV Au+Au, 500M minbias
Run 13	FY13	D^0 reference spectrum to 10 GeV/c	200 GeV pp, 2,000M minbias
Run 14	FY14	Centrality-dependent v_2(pt) Λ_c spectrum	200 GeV Au+Au, 1,000M minbias

5.3. Non-triggered datasets at 200 GeV: Recent heavy ion physics results

Recent relativistic heavy ion physics results: A key strength of STAR is the ability to identify a wide variety of the hadron species produced in the collision. Stable charged particles are identified through dE/dx measurements and weakly decaying strange and multi-strange hadrons from their decay vertices. Various resonance peaks can be revealed by combining particles in pairs either without identification, or by using one or both of the identification techniques mentioned above. These capabilities have allowed us to address a variety of physics topics by measuring the yields and transverse momentum spectra of a wide range of particles. The other major advantage of the STAR detector is the large azimuthal acceptance, which has allowed many correlation and other event-by-event analyses to be made. RHIC has provided A+A collisions at several energies and with two species (Au and Cu). This has enabled detailed systematic studies as a function of system size, geometry and energy to be performed.

Results on Spectra and Yields: The recent progress in this area has been on two fronts. One is the use of the Run 5 Cu+Cu data from $\sqrt{s_{NN}}$ = 62 and 200 GeV collisions to explore the dependence of particle yields and spectra on the system size and, for systems with a similar number of participant nucleons (N_{part}), the geometrical shape. The strange particle yields as a function of N_{part} have long been of interest to further understand the origins of strangeness enhancement. Cu+Cu data covered a region in N_{part} where the uncertainty on N_{part}, determined from a Glauber model, for semi-peripheral Au+Au collisions is rather large. It is over this region (N_{part} < 100) that some of the largest changes in thermal fit parameters occur. Although the analysis is being finalized and the interpretation is not settled we can say that the enhancement for Cu+Cu and Au+Au at the same N_{part} is not identical, in that the enhancement in Cu+Cu is larger than in Au+Au collisions.[62]

This could be related to the energy density achieved if the collision is more compact or, more speculatively, could be due to a core-halo scenario where the ratio of core and halo contributions differs depending the shape (surface to volume effect). In a core-halo model, the independent collisions in the halo should be like p+p collisions. One of the weaknesses in our current data comes from the large errors on the p+p collision yields, in particular for Omega, where the fractional error is 80%[63]. A measurement using 600 M minimum bias p+p events would provide as accurate a mesurement for the Omega as the current Xi measurement made with 15 M events. It is expected that the TOF system will relax this target somewhat. This measurement would complete the program with strange particle yields at $\sqrt{s_{NN}}$ = 200 GeV.

The second area of progress is the extension of identified particle spectra to higher p_T. STAR reported on the nuclear modification factors (R_{AA}) of protons and pions, and showed that their partonic sources had similar energy loss[64]. This was contrary to initial expectations, as gluons are thought to favor baryon production and, due to the fundamental coupling strengths in QCD, gluons are expected to interact more strongly with the medium than quarks. We have begun to explore this finding with further analysis, the most recent being the extension to higher p_T of the rho measurement, presented at Quark Matter 2008. Clearly it would be of benefit to measure R_{AA} for further hadron species. The Run 5 Cu+Cu

and Run 4 Au+Au data sets are large enough to allow the strange particle spectra to be measured to above 7 GeV in p_T, and using the Run 7 data on tape can extend the latter dataset. There is, however, no suitable reference data. A large minimum bias p+p sample is required for this reference. Our estimates suggest that at least 300 M events would be required.

The biggest single improvement for future Au+Au running comes from the installation of the STAR TOF system. This will extend particle identification above the present limits from dE/dx at low p_T, where proton to pion and pion to kaon separation ceases to be possible at around $p_T \sim 1.2$ and 0.7 GeV, respectively. The TOF also provides clean electron and positron identification. The resonance program would benefit in a major way from minimum bias Au+Au collisions with the TOF. K* resonance production and v_2 measurements will be greatly improved. The measurement of phi by its decay to e^+e^- becomes possible, which provides reconstruction from particles decaying earlier in the collision process, the decay products of which will not be affected by the later hadron gas stage of the collision. It is estimated that a 10% error on the peak in the data integrated over all p_T can be made with 7 M minimum bias events, so a few hundred million events should be sufficient to obtain p_T spectra. The continuum di-lepton spectra below the mass peak can also be studied. Finally, we intend to search for U(1) symmetry restoration by looking at the eta meson [65]
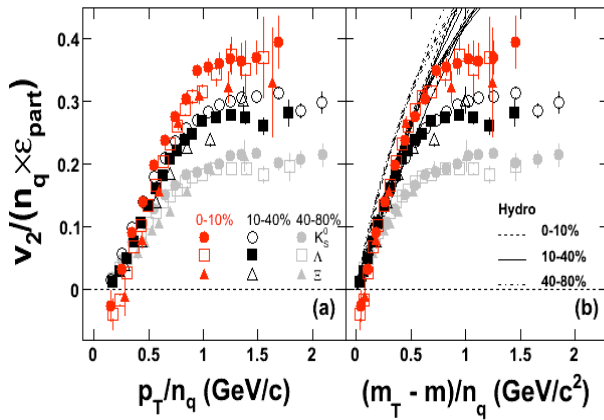
Figure 5-17: Preliminary $v_2/(n_q\varepsilon_{part})$ versus p_T/n_q and $(m_T-m)/n_q$ for various centralities in Au-Au collisions at 200 GeV.
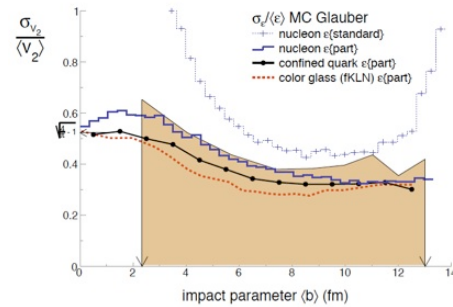
Figure 5-18: Preliminary measurements of the relative v_2 fluctuations compared to various models as a function of impact parameter.

Progress has also been made in our understanding of v_2 fluctuations. Most theories indicate that the magnitude of the momentum-space anisotropy (v_2) is driven by the spatial anisotropy of the initial state. However these calculations also show that this spatial anisotropy can vary significantly between events with the same impact parameter. Such

eccentricity fluctuations should result in fluctuations in v_2 that is preserved through the evolution of the system. Figure 5-18 shows STAR's measured relative v_2 fluctuations as a function of impact parameter. The brown shaded region indicates the upper limit of the measured relative fluctuation, while the curves indicate various theoretical calculations. STAR's data are consistently beneath those derived from a Glauber calculation using the standard eccentricity calculation. However, the data is consistent with the magnitude of the fluctuations calculated using the participant eccentricity and slightly above those predicted from a calculation invoking Color-Glass-Condensate initial conditions. In all cases the data rule out large fluctuations and correlations from sources other than event-by-event differences in geometry of the initial conditions.

Non-triggered Correlations Results: Also reported at QM2008 were STAR's new results on non-triggered two-particle correlations. In this analysis no transverse momentum requirement is placed on either of the two particles, so that the correlations are formed from all unique pairs of particles in an event. The resulting correlations will be sensitive to any process that induces relative momentum correlations between final state particle pairs in the acceptance. Such processes include, but are not limited to, elliptic flow, quantum statistics, resonances and, minijets. These minimum-bias jets with no a-priori p_T cut (though dominated by ~1 GeV/c hadrons) are the focus of this analysis. Each dynamical process generates a characteristic correlation structure on relative azimuth and pseudorapidity. It has been shown by STAR that the correlation data can be readily decomposed into a few analytic structures that can be related to the above sources.

Minijet correlations, measured as the same-side (relative $\varphi < \pi/2$) two-dimensional Gaussian correlation structure, are clearly observed in p+p collisions. One important application of this analysis is to study what happens to these correlation patterns in heavy-ion systems as the collision centrality increases. The null hypothesis is that, barring an increase in amplitude in proportion to the number of binary collisions, the minijet correlation will remain unchanged. While we observe an approximate binary scaling in Au+Au collisions from most peripheral to mid-central collisions, at about 55% and 40% centralities for the 200 and 62 GeV data, respectively, a sharp transition point is observed, as shown in Figure 4-7. For more central collisions the minijet structure changes dramatically. The peak amplitude grows rapidly and the relative η width broadens by a factor of 2-3, while the φ width (not shown) narrows significantly. This correlation structure becomes so large that it is estimated to include approximately one third of all produced particles in central collisions. STAR also observes that for both energies the same-side peak amplitude, η width, and correlation volume scale with transverse particle density, estimated as the number of final-state particles per unit rapidity per unit of initial collision overlap area, as shown in Figure 4-7. This non-triggered correlation analysis technique enables unprecedented access to the dynamics of low momentum particles and provides a sensitive probe of the physics affecting the majority of particles produced in heavy ion collisions. For example, these correlation measurements can provide new information about the degree of thermalization in RHIC collisions.

Hadron-Triggered Correlation Results: The ongoing heavy ion physics program with the STAR detector at RHIC has enabled remarkable advances in the study of hot strongly

interacting matter [66]. An extended reach in particle momentum with ongoing analysis of Run 4 Au+Au data as well as analysis of the base-line p+p data sets from Runs 2 through 6 allowed for further development of "hard probes" to study the behavior of the created medium that was difficult to access at lower collision energies. Data samples from lighter collided ions complement these developments by providing a better handle on system size variations. Use of penetrating probes is becoming increasingly sophisticated and is currently at the brink of new advances, both with hadron-triggered correlations in large non-triggered datasets, and, as has been discussed in an earlier section, with datasets triggered by the Barrel Electromagnetic Calorimeter. With the above-mentioned data sets STAR continues the exploration of fundamental properties of QCD matter, providing further constrains on theoretical models. Full capabilities for particle identification coupled with large acceptance of STAR have enabled advanced analyses of correlations and fluctuations, necessary for quantitative tests of QCD predictions on energy loss, jet fragmentation and hadronization in QGP medium. These capabilities have afforded a number of first "proof-of-principle" measurements, documenting STAR's ability to take advantage of planned upgrades and increased luminosity available at RHIC II. Here we summarize briefly recent advances of various correlations analyses and provide an outlook for the near term future and planning.

Identified Di-hadron Correlations: The suppression of hadron yields and back-to-back correlations has firmly established that jets are quenched by very strong interactions with the matter produced in central Au+Au collisions. The results are consistent with the effects of parton energy loss in traversing the dense medium, predicted before the data were available [67,68]. Those pQCD calculations appear to efficiently describe both the centrality- and p_T-dependence of the observed suppression if energy densities of about 2 orders of magnitude higher than normal nuclear density are assumed. Further explorations of the hadron suppression with identified particle species provided new challenges for the pQCD models. At intermediate p_T, as illustrated in Figure 5-19 and Figure 5-20 with proton and antiproton R_{CP}, all measured baryons show less suppression, with respect to binary scaling, than measured mesons (see, for example, charged pions R_{CP} in the same figure). As seen in the figure, the baryon/meson effects disappear at high p_T, where baryons and mesons show a common degree of suppression. The theoretical calculations[69,70] expect significant (factor of 3) differences in energy loss for quarks and gluons, which should appear in the nuclear modification factor for baryons and mesons due to differences in contributions from quark vs. gluon fragmentation.

Di-hadron correlations provide additional means to probe the medium. They permit the experimental observation of the energy lost by partons, which appears in the form of an excess of softer emerging hadrons. Measurement of particle spectra and ratios for associated hadrons in the jet cones could address this issue of color-charge dependence of energy loss explicitly. The current STAR program includes di-hadron correlations with a variety of identified particles. Such measurements test for the presence of meson/baryon effects at intermediate p_T, and explore the interplay between various hadronization mechanisms. Hyperon-hadron correlations, shown in Figure 5-20, show significant and similar, correlations for all species of hyperons up to and including the Omega, in apparent contradiction to predictions from a coalescence picture.
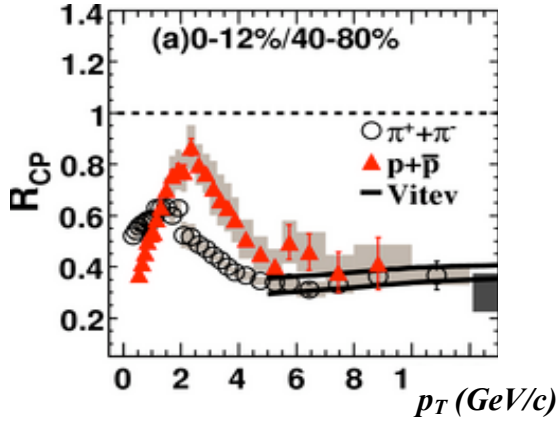
Figure 5-19: R_{CP} for $\pi^+ + \pi^-$ and $p + \bar{p}$ in 200 GeV Au+Au collisions[71]. The solid lines show jet quenching predictions for pions[72].
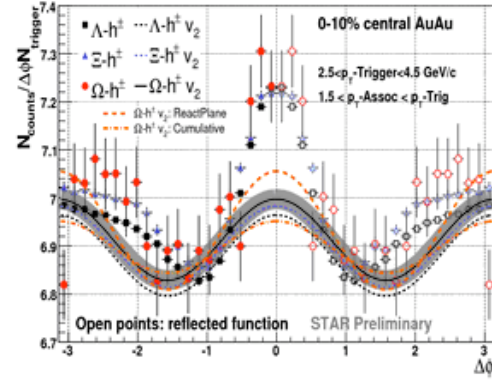
Figure 5-20: Hyperon-hadron azimuthal correlations in central Au+Au collisions at 200 GeV.

Higher statistics Au+Au data samples are required to address the constituent quark dependences of correlation structures, as well as to decompose the observed correlation peaks into spectral measurements.

Mechanisms of Jet-Medium Interactions: STAR is actively working on understanding the mechanisms of jet interactions with a hot and dense QCD medium via studies of jet-shape modifications in heavy ion collisions. As seen in the Figure 5-21, modifications of the correlation shapes are quite significant in the intermediate and soft sectors. For some particular kinematic selections of correlated particles the overall broadening of the away-side distribution is accompanied by the developing of a dip $\Delta\phi \sim \pi$. This shape of the away side distributions stirred many theoretical discussion and investigations [77,78,79,80]. In particular, shock wave induced conical flow ("sonic boom"), Čerenkov gluon radiation, and a "deflected jet" induced by interactions between the propagating partons and the flowing medium were proposed to explain the oserved modifications.

Preliminary STAR results on the three-particle azimuthal correlation analysis [81,82] are shown in Figure 5-22. The correlation surface reveals more details about the jet fragmentation and propagation through the medium. The elongation of away-side peak along the diagonal in the $\Delta\phi 1$-$\Delta\phi 2$ space is already observed in pp and d+Au data and is interpreted as possible effects of k_T broadening. This elongation becomes more pronounced in Au+Au collisions potentially indicating the presence of some additional mechanisms, such as for example deflected jets, contributing to shape of the observed correlation. Observation of off-diagonal peaks evident in more central Au+Au data is consistent with conical flow or Čerenkov radiation scenarios. More advanced studies, for example differential in p_T, are needed to provide the discriminating power between the two scenarios. Such studies require larger data samples.

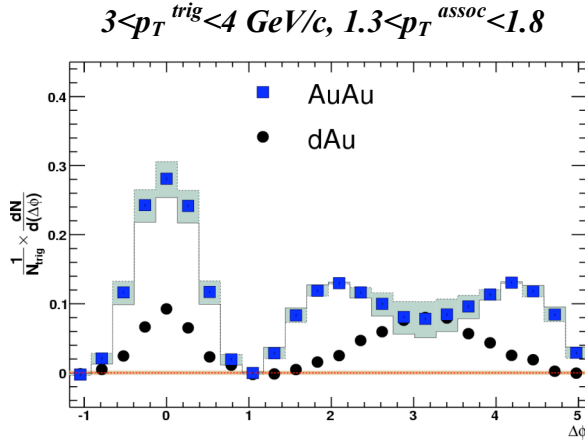$3<p_T^{trig}<4$ GeV/c, $1.3<p_T^{assoc}<1.8$

Figure 5-21: Comparison of the background-subtracted $\Delta\phi$ distributions for d+Au and central Au+Au data for the associated particles in the (1.3, 1.8) p_T range.
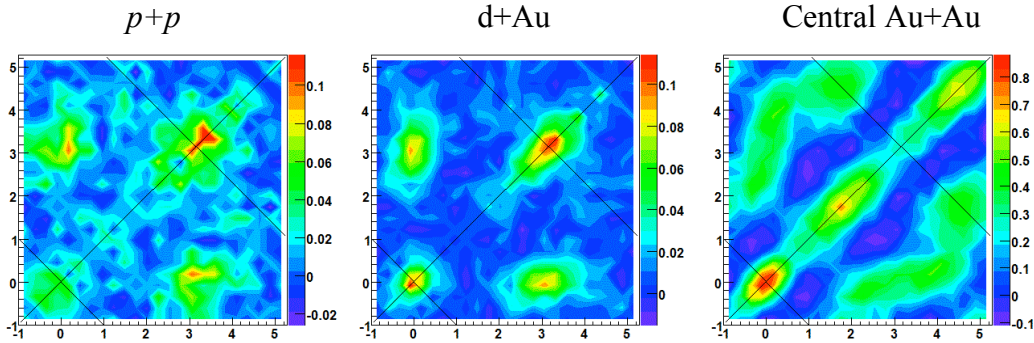

Figure 5-22: Background subtracted 3-particle azimuthal correlations for p+p (left), d+Au (center), and ZDC triggered 12% central Au+Au (right). Trigger particles are selected in the transverse momentum range of $3.0<p_T<4.0$ GeV/c, and the correlation function is build with hadrons with transverse momentum between $1.0<p_T<2.0$ GeV/c.

Another three-particle correlation technique has been recently explored by STAR to differentiate between various jet-medium interaction scenarios proposed to accommodate the data. We capitalize on earlier direct di-jet signatures, in which at high enough associated and trigger p_T, associated hadrons at the away-side in azimuth from the triggered hadron show a clear back-to-back jet-like peak. Assuming that the combination of trigger and hard away-side associated hadron determine a jet-axis, we correlate a third, softer, hadron with the axis. The comparisons of the $\Delta\phi$ projections of such tri-hadron (2+1) correlation for central Au+Au and d+Au data at RHIC top energy reveal no modification of shapes or suppression of yields for di-jets in the same kinematic range where a typical di-hadron analysis shows dramatic changes. For the first time for soft associated hadrons, the away-side correlation structure is also peaked in both $\Delta\eta$ and $\Delta\phi$, further confirming the di-jet nature of these events. Statistics available limit the ability to vary the away-side trigger threshold, necessary to further explore the geometric, fragmentation, and energy-loss fluctuation biases inherent in the theoretical explanation of these correlations.

Jets and Ridges in correlations at RHIC: The correlation structure of charged hadrons in Au+Au collisions are dramatically modified not only in $\Delta\phi$, but also in the $\Delta\eta$ direction compared to a simpler $p+p$ reference. Figure 5-23 shows the 2-dimensional correlation in $\Delta\phi$–$\Delta\eta$ space between a high p_T trigger hadron and a lower p_T associated hadron in $p+p$ (left) and central Au+Au collisions (right). The near-side peak, symmetric in $\Delta\phi$–$\Delta\eta$ in $p+p$ collisions, is substantially broadened in the $\Delta\eta$ direction in Au+Au collisions.

Within a two-component model, the structure appears to be composed of a "jet" with properties similar to those seen in $p+p$ collisions and a "ridge" with properties similar to those of the bulk. The origin of the ridge is still uncertain, but it has been speculated that the "ridge" may be due to redistribution of energy lost to the medium through some mechanism, such as expansion or unstable color modes, that breaks the symmetry in azimuth and pseudorapidity.
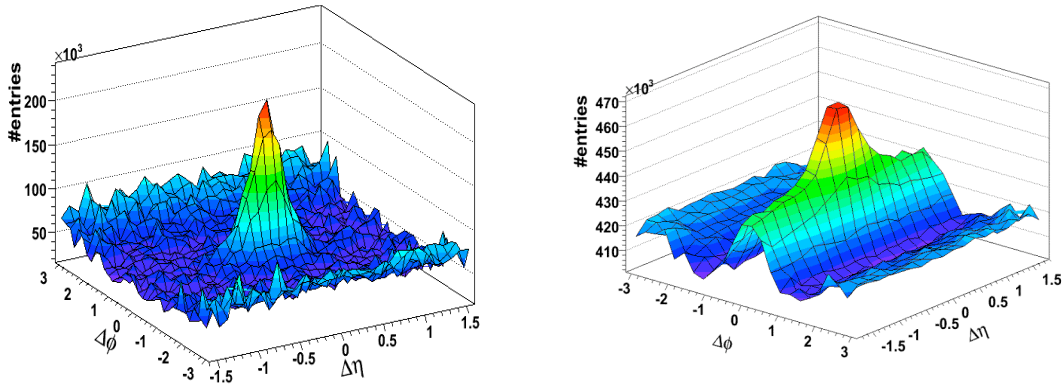

Figure 5-23: Di-hadron correlations in p+p (left) and central Au+Au collisions (right). Trigger particles are selected in the transverse momentum range of 3<p$_T$<4 GeV/c, while the correlation function is built with associated hadrons with transverse momentum greater than 2 GeV/c.

Of particular interest for multi-particle production models are di-hadron correlation studies with multi-strange triggers. Due to the quark mass difference it is expected that multi-strange hadron production will be dominated by thermal quark recombination in the momentum range accessible at RHIC. Di-hadron azimuthal correlations with multi-strange hadrons such as Ω, Ξ and φ will provide experimental constrains on the validity or the extent of recombination influence in hadronization at RHIC. Initially, parton recombination models predicted that no jet-like azimuthal correlations would exist for multi-strange baryons at the intermediate (2-4 GeV/c) p$_T$ region. STAR measurements of multi-strange hadron correlations in d+Au and Au+Au collisions, showing jet-like structures for all measured species with no variation in correlation strength based on strangeness content, has already rejected those models. The theoretical explanations that followed those results have suggested that observed azimuthal correlation signal is not a direct result of jet fragmentation, but rather expanding medium response to the propagating parton or

"phantom jet". Both scenarios preserve the correlation in azimuthal space, but in pseudorapidity space the latter scenario predicts a ridge-like structure. To advance our understanding of the nature of these correlations, extension of the correlation analysis into $\Delta\phi$-$\Delta\eta$ space for Ω and Ξ baryons is necessary, which is not possible with the limited statistics of our current datasample.

The details of hadro-chemistry of jet fragments can provide additional constraints for the models. Preliminary STAR results show significantly lower baryon/meson ratios in the jet-cone around a 4 GeV/c trigger particle, as compared to non-triggered distributions. At the same time, the ratios in the "ridge" part of the correlation structure suggest enhanced production of the baryons that might be related to the fragmentation of the gluons radiated of the hard-scattered quark resulted in trigger.
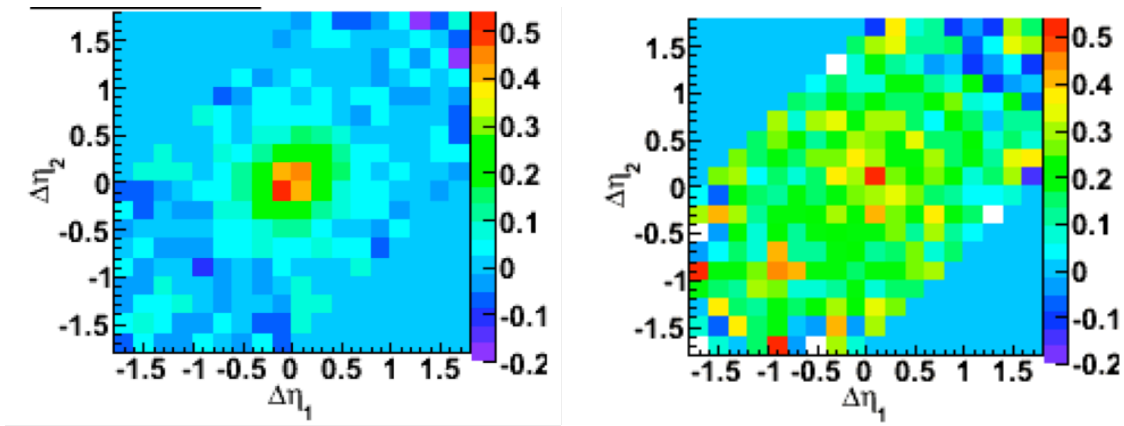

Figure 5-24: 3-particle correlations in $\Delta\eta$-$\Delta\eta$ for 200 GeV minimum bias d+Au (left) and central Au+Au collisions (right). The trigger particle is selected in transverse momentum range between 3–10 GeV/c and associated particle p_T range is between 1–3 GeV/c.

Further understanding of the source of the "ridge" can be provided by adding an additional particle, and moving to a 3-particle correlation analysis in $\Delta\eta$-$\Delta\eta$ space. Preliminary results, with unidentified hadrons, are presented in Figure 5-24 for minimum bias d+Au collisions (left) and central Au+Au collisions (right) at 200 GeV. A clear jet peak is observed in these correlations at $(\Delta\eta,\Delta\eta)\sim0$ for both d+Au and Au+Au collisions. In addition, a uniform overall excess of associated particles is observed in Au+Au collisions. This observation is contrary to most model predictions, which would lead to an excess of yield along the diagonals or strips across the $\Delta\eta_1=0$ and $\Delta\eta_2=0$. These early results from a statistics-starved analysis, consistent with jet fragmentation accompanied by an overall excess of associated yields with no further correlation among the associated particles, already provide more stringent constraints on the interpretation of ridge formation, and set high expectations for future higher statistics data samples.

Correlations Relative to the Reaction Plane: In addition to the above experimental observations in the near side from high p_T triggered di-hadron correlations, STAR has begun a study of the near side "jet" and "ridge" structures with respect to the reaction plane. The new analysis can study path-length effects in greater detail, by exploiting non-central collisions where the overlap region between the two colliding nuclei is anisotropic: the size in the reaction plane direction is shorter than that perpendicular. By selecting the trigger particle direction with respect to the event plane, $\varphi_S=|\varphi_T-\psi_{EP}|$, one selects different path-lengths of the medium the away-side parton traverses, providing more differential information than the inclusive jet-correlation measurements. STAR has previously performed an exploratory measurement of jet-correlations at high p_T with trigger particles in-plane ($|\varphi_T-\psi_{EP}| < \pi/4$) and out-of-plane ($|\varphi T-\psi_{EP}| > \pi/4$) in non-central Au+Au collisions[83], in which away-side particles correlated with out-of-plane trigger particles were found to be more suppressed than those correlated to in-plane trigger particles. We have extended these measurements to finer bins in $|\varphi_T-\psi_{EP}|$ and to lower associated and trigger p_T ranges. Minimum bias data from Run 4 provided approximately 20 million events for this analysis. The results discussed below are for the trigger particle p_T range of $3<p_T^{trig}<4$ GeV/c and centrality bin of 20-60%. Data from central ZDC triggered sample and the d+Au run have been used for comparison purposes.
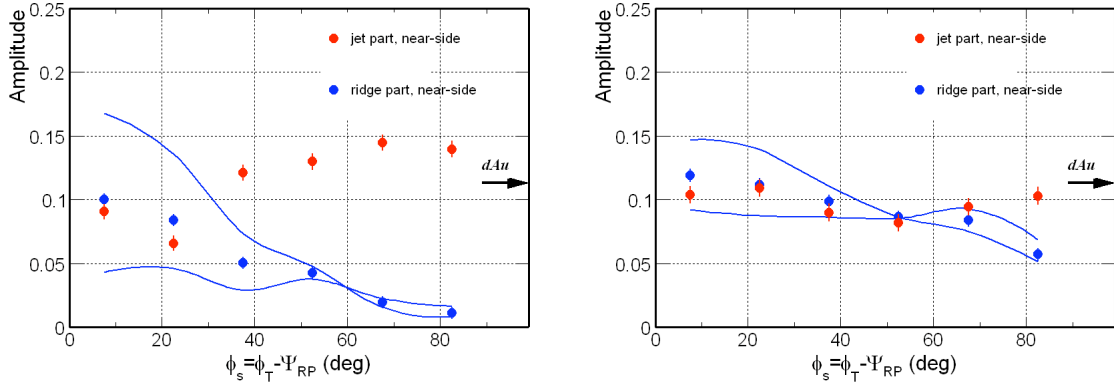

Figure 5-25: The near-side di-hadron correlation amplitudes ($|\Delta\phi|<0.35$) for jet part (red) and ridge part (blue) as a function of trigger particle azimuthal angle from the event plane, $\varphi_S =|\varphi_T-\psi_{EP}|$. The systematic uncertainties on the ridge amplitude are significant and indicated by the curves, while those on the jet data are small. The results are for $3<p_T^{trig}<4$ GeV/c and $1.0< p_T^{assoc}<1.5$ GeV/c in 20-60% (left panel) and top 5% (right panel) Au+Au collisions.

The away-side correlation broadens (and becomes double-peaked) with increasing trigger particle azimuthal angle from the reaction plane. In top 5% collisions, the away-side correlation is broader at small trigger particle angle, but at trigger particle angle of 90° from the reaction plane, little difference is found between the two centralities, perhaps consistent with the variations in the away-side medium path-length. The near-side jet component varies little with trigger particle angle from the reaction plane and generally agrees with that in d+Au. However, the ridge component decreases significantly with the trigger particle angle in collisions from 20-60% in centrality. The change is weaker in the most central 5%

collisions, consistent with the more spherical geometry. The near-side modifications are quantified in Figure 5-25, where the amplitudes of correlations are shown as function of φ_S for the "ridge" part (blue points) in the 20-60% centrality (left panel) and the top 5% centrality (right panel), respectively. The "jet" part amplitudes are shown in the same figure in red, for the 20-60% centrality (left panel) and the top 5% centrality (right panel), respectively.

The preliminary results of path-length effects studies suggest that the near-side jet in the reaction plane direction interacts with the medium, losing energy and generating a sizeable ridge over a long $\Delta\eta$ range. The near-side jet perpendicular to the reaction plane suffers minimal interaction with the medium, with no significant ridge and with the correlated multiplicity only slightly higher than that in d+Au. One should note that although the results are dominated by systematics, the systematic uncertainties are correlated, thus statistical precision is important, and a higher statistics sample is needed to assess the reliability of systematic uncertainty estimates, and to expand these studies as function of trigger p_T.

5.4. Future EM probes in STAR

Electromagnetic probes[84] uniquely provide direct access to the in-medium modifications of hadronic states (vector mesons $\rho(770)$, $\omega(782)$, $\varphi(1020)$) via dilepton invariant-mass spectra, which can illuminate the nature of hadron mass generation and thus the origin of ~ 98% of the visible mass in the universe (as well as related changes in the structure of the QCD vacuum including the restoration of chiral symmetry). In addition, at masses above ~1 GeV there exists the possibility of detecting novel nonperturbative (resonant) correlations in a sQGP. Electromagnetic probes are also unique in inferring the temperature of the system during its hottest phases via direct thermal radiation of photons and dileptons radiation; additional HBT interferometry of thermal photons offers the cleanest measurement of early system sizes.

At STAR electron identification is made possible by a combination of a measurement of the energy loss by charged particles due to ionization (dE/dx) of the Time Projection Chamber (TPC) gas and a velocity measurement with the TOF system[85]. The relativistic rise of the electron dE/dx separates electrons from hadrons, except where electrons cross with pions at momenta of ~0.2GeV/c, with kaons at ~0.6GeV/c, with protons at ~1.1GeV/c, and with deuterons at ~1.5GeV/c. A time-of-flight measurement, with the requirement that $|1 - \beta|$ <0.03, eliminates slow hadrons and cleans up the crossing regions. This results in clean electron identification[77]. In addition to direct measurements of open-charm hadrons (via Kπ decays), the STAR HFT [86] will serve as a powerful device to discriminate primordial electrons from background electrons, both from photonic sources such as conversions and from correlated decay of charm and beauty. Rejection of π^0 and η Dalitz decays by a factor of 3 (single track) can be achieved by measuring both electrons of the pair, which is possible due to the large acceptance of the STAR TPC. The large reduction in electron background will enable us to observe the electromagnetic signal from low-mass vector mesons and the radiation of intermediate-mass dileptons with a few hundred thousand central Au+Au events in STAR. With the upgrades we expect to detect 6K φ and 22K ω

decays in 200 Million recorded central Au+Au collisions[84,86]. These measurements will be of comparable accuracy to those presented by NA60 at QM05[87] in central In+In collisions, which consisted of signals ~ 6K for the ω and ~ 10K for the φ.

In the absence of HFT, and with 50% of the Barrel TOF, a possible configuration for Run 9, we expect that the electron background level will be similar to that of the PHENIX detector as presented in Ref.[88] From φ yields measured by STAR in the hadronic decay channel (φ→K$^+$K$^-$), we estimate that a signal with 25σ significance and signal-to-background ratio between 1:25 to 1:10 will be obtained in 300M minimum bias events. This is an example of the high quality measurements that can be made with electron pairs in such a configuration.

We also propose to place a 0.1 radiation length lead photon converter[88] - concentric with the beam pipe with a radius of approximately 43 cm - into STAR for portions of two upcoming runs, ideally Runs 10 and 12. The driving physics motivation is to make measurements of direct photon HBT in full energy Au-Au collisions, which could provide unique and extremely interesting information about all stages of the evolving collision system. The inclusion of a converter in STAR would give an increased efficiency for reconstructing photon pairs at low relative momentum by using pairs in which one photon converts and is reconstructed via its daughter tracks in the TPC and the other is reconstructed in the Barrel EMC. We envision a short (approximately 1 week, 50M central Au+Au collisions) time of running with the converter during Run 10. This would serve chiefly as a proof of principle for the photon HBT measurement although other physics topics would benefit from the increased photon efficiency. When this 1 week of running is complete, the converter would be withdrawn to a location that sits largely outside of the STAR acceptance. If the results of this trial run prove to be satisfactory, we would propose a significantly longer run with the converter during Run 12. The goal of this run would be to collect on the order of 10^9 full energy central Au-Au events with the converter in place and using this data, to expand the HBT measurement into the more interesting kinematic range and increase the detail of the measurement.

5.5. U+U collisions at RHIC

The Uranium nucleus is an oblate spheroid so central U+U collisions can be very asymmetric. The conversion of that spatial asymmetry to momentum space can test the validity of the zero mean-free-path limit which some believe has been achieved in central Au+Au collisions at RHIC. The new EBIS ion source, which will be commissioned in 2009, will allow RHIC to provide U+U collisions as early as 2011.

Grazing (non-central) collisions of spherical nuclei produce elliptic shaped overlap areas. The expansion of and radiation from the produced spatially asymmetric fireball yield asymmetries in momentum space. The momentum space anisotropy may probe the dynamics of the expanding system. For nearly central Au+Au collisions at 200 GeV, the momentum space anisotropy seems to reach the value predicted for a system with zero mean-free-path where a hydrodynamic description of the expansion may be valid. Figure 5-

26 shows heavy-ion data for the ratio of the momentum anisotropy to the intial spatial anisotropy (v_2/ε). The data at the right of the plot are for central 200 GeV Au+Au collisions where the transverse charged particle density (1/S dN/dy) is largest.

A central U+U collision is expected to reach densities 30% larger than central Au+Au. Due to the oblate shape of the Uranium nucleus, even very central U+U collisions will have a large initial spatial deformation. For these reasons, U+U collisions will allow RHIC to test for the presence of a hydrodynamic limit. The ratio v_2/ε may continue to rise, as the current trend indicates or it may begin to saturate. A leveling off of the trend would be a strong indicator of the attainment of a zero mean-free-path, hydrodynamic limit. These collisions will provide a stringent test of the models shown in the figure and lead to a significant extension to higher densities of the measurement of v_2/ε into previously unexplored territory.
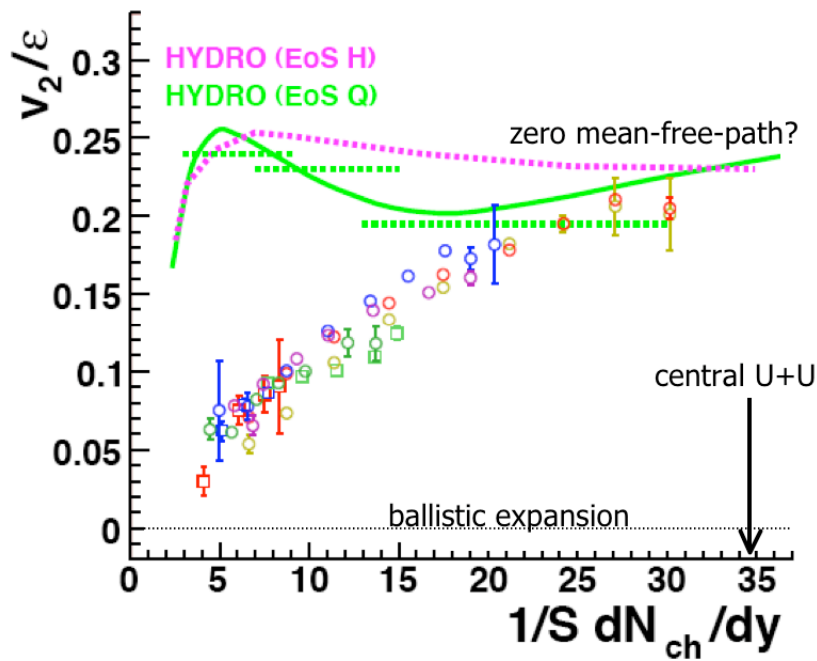
Figure 5-26: Heavy ion data on eccentricity scaled v_2 vs transverse particle density. A central U+U collision is expected to reach densities 30% larger than central Au+Au while the eccentricity is large.

5.6. Non-triggered probes at 200 GeV: Au+Au beam use request for Runs 9 and 10

The collection of ~300M minbias events combined with the improvement in particle identification via the ToF will allow for a significant improvement in the measured directed flow (v_1) of protons. If 600M minbias events can be recorded then a detailed study of both

directed, elliptic and v_4 can be made as a function of p_T and particle species including the Λ and K^0_s. With such a large minbias sample STAR will also be able to perform large $\Delta\eta$ correlation studies. Detailed measurements of all the Fourier harmonics (v_n) are important for furthering our understanding of the bulk dynamics of the matter created in RHIC collisions. For instance the observation of a "wiggle" in the v_1 measurement around mid-rapidity could indicate a change in the compressibility of the matter created. The higher order harmonics can be used as a more sensitive test of the initial conditions. Both the v_1 and v_4 results have been performed by STAR with limited statistics but finer granular rapidity measurements using PID are needed to further constrain models of both the initial conditions and the dynamical evolution of the system.

Systematic studies of the centrality dependence of jet-like correlation structures as function of trigger and associate hadron p_T in di-hadron and di-triggered (2+1) correlations should shed additional light on questions of the initial gluon density, parton thermalization, and QGP formation and subsequent hadronization. An increase of the minimum bias dataset by more than an order of magnitude will provide higher-p_T access for triggered di-hadron correlation studies with respect to reaction plane, and measurements more differential in centrality. While current trigger selections are limited to p_T of 3-4 GeV/c, a dataset of this size will shift the upper limit to 6 GeV/c. The current reaction-plane dependent analysis concentrates on a wide centrality bin from 20-60%, which can be binned more finely with such a larger dataset. Detailed exploration of qualitative features feasible at higher p_T should greatly enhance our leverage in disentangling some of the competing physics effects.

With a few hundred million minimum bias events and 50-100% of the TOF, STAR's two particle relative η, ϕ correlation analysis at low transverse momentum will be extended to explore identified (π, K, p) particle correlations, focusing on the flavor and baryon-to-meson content of the same-side correlations below and above the transition centrality point. In Run 10 it is desirable to have a dedicated Au+Au run at full energy with full barrel TOF and complete DAQ 1000. We would like as many events as practically possible, focusing (assuming prior fulfillment of our statistic requirements for minimum bias data) on utilizing both minimum bias, central and specialized rare probes triggers, including high tower triggers at 6 GeV and/or software trigger selecting high-p_T events of interest. The progress in physics analyses mentioned below requires a minimum factor of 10 increases in the statistics, which corresponds to approximately 200 M central-triggered events.

Many of the existing theoretical descriptions of final-state interactions at RHIC assume vacuum fragmentation of partons, which may be valid in the high-energy limit, when the fragmentation time exceeds the medium traversal time of the leading parton. It is therefore important to understand the features of fragmentation functions that may distinguish parton energy loss in a QGP from other possible sources of jet softening and broadening. It is necessary to employ the extended particle identification capabilities of STAR in the hard sector studies, addressing energy loss mechanisms and modification of jet fragmentation functions with both identified and unidentified angular correlations in $\Delta\eta$-$\Delta\phi$ space. Such measurements will enable the study of the transition between jet fragmentation dominant and multi-parton mechanisms of hadron formation. A new extended sample of central Au+Au data would allow quantitative studies of spectral distribution for associated hadrons

with identified (baryon/meson) triggers, as well as spectral measurements of identified species in jets and ridges. 3-particle correlation technique developed with the Run 4 data available would capitalize on the high statistics sample, providing systematic studies of correlation structures as function of trigger and associate hadron momenta.

Other physics topics that would become feasible with the requested sample include jet-induced Lambda polarization, resonance production in jets. Additionally, rare particle searches and resonance studies will become possible even in central Au+Au collisions, benefiting greatly from TOF availability.

As well as the pp2pp program discussed above, STAR plans to continue its ultra-peripheral collisions (UPC) program in Au+Au events. The Au+Au UPC analysis of STAR focuses on heavy vector mesons, in particular the J/ψ, ϕ production, and four-prong particle decays. The four-prong data will be used to improve the previous reported measurement of the parameters of the ρ' (~1450) and/or ρ' (1700) resonance, and a search for heavier resonances decaying to 4 pions. With 50 M minbias UPC triggered Au+Au events, the collection of which is made possible via DAQ1000, we expect to reconstruct ~1500 ρ' candidates. A search for the four-pronged KK$\pi\pi$ and, statistics permitting, KKKK final states will also be performed. With such high statistics a 6-prong final state study will also be feasible as will the first attempt to observe the two-photon production of the f_2(1270). Meanwhile the reconstruction of the J/ψ will enable the study of the gluon distribution functions around x=0.01 and Q^2=(1.5 GeV)^2. Finally multiple vector meson production in a single ion-ion collision is within reach with such a data set. Approximately 1 out of 1,000 ρ^0 should be accompanied by a second ρ^0. Quantum correlations in the production and in the decay can then be studied, for example with $\rho^0\rho^0$ with in the same quantum state, stimulated decay becomes a possibility.

5.7. Non-triggered probes: p+p beam use request for Runs 9 and 10

For the unbiased references for STAR spectral analyses and correlation studies it is necessary to collect at least 300 M minimum bias 200 GeV p+p events as part of proton physics run. With full implementation of DAQ1000 this can be achieved in a reasonable length of time. Reasonably low pile-up levels are optimal for those studies, and therefore a dedicated run is required for at least a significant portion of this dataset, which can be taken concurrently with the special, low luminosity conditions during the pp2pp run. The event estimates are driven by the high-p_T program requirements and the Omega baryon measurement. These data would afford reliable measurements of the omega-baryon yield, and extend p_T spectra reach for identified protons, pions and strange baryons into the fragmentation region from approximately 6-10 GeV/c. This limit corresponds to the maximum p_T reach achieved in Au+Au and Cu+Cu collisions, and would greatly aid in systematic studies of hadron suppression via nuclear modification factors. STAR's p+p data are also world-leading in the area of identified particle fragmentation functions. Any 500 GeV running would be useful to test these models tuned with the 200 GeV data.

STAR's femtoscopic analysis is also ongoing with data from p+p collisions. The analysis focuses on two main areas. The first topic is the continued investigation into the observation that the extracted radii from Au+Au events seem to scale linearly to those from p+p when pion pairs with the same mean m_T are selected. This is surprising since radial flow, which is expected to affect the HBT radii, in Au+Au events is very different to that in p+p. There are also unexplained long range correlations observed that need further study. Second a new analysis of HBT with respect to the jet axis has started. The goal of this analysis is to see if the presence of a jet affects the space-momentum correlations of the underlying event. The femtoscopic measurements as a function of m_T require several million minbias events. While there seem to be sufficient data at 200 GeV there is much interest in performing these measurements at 500 GeV, to see if the observed scaling is preserved at a different collision energy. The HBT analysis with respect to the jet, or thrust, axis needs several million high tower triggered data. This data set is requested for both 200 and 500 GeV collisions.

[1] Deep Inelastic Scattering, Madison, Wisconsin, April 2005 [hep-ex/0507013].
[2] W. Vogelsang and F. Yuan, PRD **72**, 054028 (2005).
[3] J. Adams et al. (STAR Collaboration), PRL **92**, 171801 (2004).
[4] D. Adams et al, (E704 Collaboration), PLB **261**, 201 (1991); PLB **264**, 462 (1991).
[5] J. Adams et al. (STAR Collaboration), PRL **97**, 152302 (2006).
[6] D. Sivers, PRD **41**, 83 (1990); PRD **43**, 261 (1991).
[7] J.C. Collins, NPB **396**, 161 (1993).
[8] J. Qiu and G. Sterman, PRD **59**, 014004 (1998).
[9] A.V. Efremov, V.M. Korotiyan and O.V. Teryaev, PLB **348**, 577 (1995).
[10] B.I Abelev et al., the STAR Collaboration, arXiv:0801.2990v1 [hep-ex]
[11] C. Kouvaris et al., hep-ph/0609238.
[12] U. d'Alesio and F. Murgia, private communications.
[13] B.I. Abelev, the STAR collaboration, PRL **99**, 142003 (2007).
[14] A. Airapetian et al, PRL **94**, 012002 (2005).
[15] D. Boer and W. Vogelsang, PRD **69**, 094025 (2004).
[17] K.H. Ackermann et al. (STAR Collaboration), NIM A**499**, 624 (2003).
[18] B.Jaeger, M. Stratmann and W. Vogelsang, PRD **70**, 034010 (2004).
[19] M. Stratmann and W. Vogelsang, PRD **70**, 034010 (2004).
[20] B.I. Abelev et al., (STAR Collaboration), PRL **97**, 252001 (2006).
[21] B.I. Abelev et al., (STAR Collaboration), arXiv:0710.2048.
[22] D. de Florian, R. Sassot and M. Stratmann, PRD **75**, 114010 (2007).
[23] W. He, for the STAR Collaboartation, BAPS **53**, 46 (2008).
[24] J. Webb, for the STAR Collaboration, SPIN 2006 proceedings.
[25] B.A. Kniehl, G. Kramer and B. Poetter, NPB **597**, 337 (2001).
[26] Q.H. Xu, Z.T. Liang and E. Sichtermann, PRD **73**, 077503 (2006).
[27] D. de Florian, M. Stratmann and W. Vogelsang, PRD **81**, 530 (1998).
[31] D. de Florian et al., arXiv:0804.0422.
[34] L.C. Bland, hep-ex/0002061.
[35] D. Sivers, PRD **41,** 83 (1990); **43,** 261 (1991).
[36] G.L. Kane, J. Pumplin, W. Rebko, PRL **41,** 1689 (1978).

[37] R.D. Klem *et al.*, PRL **36**, 929 (1976); W.H. Dragoset *et al.*, PRD **18**, 3939 (1978); S. Saroff *et al.*, PRL **64**, 995 (1990); B.E. Bonner *et al.*, PRD **41**, 13 (1990); B.E. Bonner *et al.*, PRL **61**, 1918 (1988); A. Bravar *et al.*, PRL **77**, 2626 (1996); D.L. Adams *et al.*, PLB **261**, 201 (1991).
[38] J. Collins, PLB **536**, 43 (2002).
[39] S.J. Brodsky, D.S. Hwang, I. Schmidt, PLB **596**, 99 (2001).
[40] A. Airapetian *et al.*, PRL **94**, 012002 (2005).
[41] E.S. Ageev *et al.* (COMPASS), NPB **765**, 31 (2007).
[42] J. Adams *et al.* (STAR), PRL **92**, 171801 (2004).
[43] C. Bourrely, J. Soffer, Eur. Phys. Journ. **C36**, 371 (2004).
[44] R. Seidl *et al.* (Belle collaboration), PRL **96**, 232002 (2006).
[45] M. Anselmino *et al.* PRD **72**, 094007 (2005).
[46] A. Airapetian et al., PRL **94**, 012002 (2005).
[47] A. Bacchetta, C. Bomhof, U. D'Alesio, P.J. Mulders and F. Murgia, PRL **99**, 212002 (2007).
[48] G. Bunce, N. Saito, J. Soffer, and W. Vogelsang, Ann. Rev. Nucl. Part. Sci. **50**, 525 (2000).
[49] RHIC SPIN collaboration, G. Bunce et al., BNL internal document, Status and Prospects of the RHIC Spin Physics Program.
[50] D. de Florian, G. A. Navarro, and R. Sassot, PRD **71**, 094018 (2005).
[51] M. Gluck, E. Reya, M. Stratmann, and W. Vogelsang, PRD **63**, 094005 (2001).
[52] T. Gehrmann and W. J. Stirling, PRD **53**, 6100 (1996).
[53] P. M. Nadolsky and C. P. Yuan, NPB **666,** 31 (2003).
[54] S. Bültmann et al., PLB **579**, 245 (2004).
[55] W. Guryn et al., RHIC Proposal R7 (1994) (unpublished).
[56] S. Bültmann et al., NIM A **535**, 415 (2004).
[57] E. Leader, *Spin in Particle Physics*, Cambridge University Press (2001), ISBN: 0521020778
[58] N. H. Buttimore, B. Z. Kopeliovich, E. Leader, J. Soffer, T. L. Trueman, PRD **59**, 114010 (1999).
[59] T. L. Trueman, PRD **77**, 54005 (2008).
[60] T. Satogata et al., ``RHIC challenges for low energy operations,'' In the Proceedings of Particle Accelerator Conference (PAC 07), Albuquerque, New Mexico, 25-29 Jun 2007, pp 1877.
[61] R. V. Gavai and S. Gupta, PRD **71**, 114014 (2005).
[62] Proceedings of "Strange Quark Matter 2007", J. of Phys. G 2008.
[63] B.I. Abelev et al. (STAR Collaboration), PRC **75**, 064901 (2007).
[64] B.I. Abelev et al. (STAR Collaboration), PRL **97**, 152301 (2006).
[65] Kapusta, Kharzeev, and McLerran, PRD **53**, 5028 (1996).
[66] J. Adams *et al*. (STAR Collaboration), NPA **757**, 102 (2005).
[67] I. Vitev and M. Gyulassy, PRL **89**, 252301 (2002).
[68] X.-N. Wang, PLB **595**, 165 (2004).
[69] M. Djordjevic *et al.*, PLB **632**, 81 (2006).
[70] S. Wicks *et al.*, NPA **784**, 426 (2007).
[71] B. Abelev *et al.* (STAR Collaboration), PRL **97**, 152301 (2006).
[72] I. Vitev, PLB **639**, 38 (2006).
[77] H. Stoecker, NPA **750**, 121 (2005).
[78] J. Casalderrey-Solana, E. Shuryak and D. Teaney, J. Phys. Conf. Ser. **27**, 22 (2005); NPA **774**, 577 (2006).
[79] J. Ruppert and B. Muller, PLB **618**, 123 (2005).
[80] V. Koch, A. Majumder and X. N. Wang, PRL **96**, 172302(2006).

[81] F. Wang, *nucl-ex*/0610027.

[82] J. Ulery, (STAR Collaboration), NPA **783**, 511 (2007).

[83] J. Adams *et al.* (STAR Collaboration), PRL **93**, 252301 (2004).

[84] G. David, R. Rapp and Z. Xu, arXiv: nucl-ex/0611009 v2

[85] M. Shao et al. NIMA **558**, 419 (2006).

[86] STAR HFT: http://rnc.lbl.gov/~wieman/hft_final_submission_version.pdf
    K. Schweda et al., NPA **774**, 907 (2006).

[87] E. Scomparin et al. (NA60 Collaboration), NPA **774**, 67 (2006).

[88] STAR Photon Converter Proposal:
    http://hepwww.physics.yale.edu/star/converter-proposal.pdf